AD-A241 464

DOCUMENTATION PAGE

Form Approved
OMB No. 0704-0188

1b. RESTRICTIVE MARKINGS

2a. SECURITY CLASSIFICATION AUTHORITY

3. DISTRIBUTION / AVAILABILITY OF REPORT
As it appears on the report

2b. DECLASSIFICATION / DOWNGRADING SCHEDULE

4 PERFORMING ORGANIZATION REPORT NUMBER(S)

5. MONITORING ORGANIZATION REPORT NUMBER(S)
AFOSR-TR- 91 0786

6a NAME OF PERFORMING ORGANIZATION
University of California
Mech., Aerospace & Nucl. Engrng.

6b. OFFICE SYMBOL (If applicable)

7a. NAME OF MONITORING ORGANIZATION
AFOSR

6c. ADDRESS (City, State, and ZIP Code)
46-127N Engr. IV
Los Angeles, CA 90024-1597

7b. ADDRESS (City, State, and ZIP Code)
AFOSR/NA
Bolling AFB DC 20332-6448

8a NAME OF FUNDING / SPONSORING ORGANIZATION
AFOSR

8b OFFICE SYMBOL (If applicable)
N/A

9. PROCUREMENT INSTRUMENT IDENTIFICATION NUMBER
F49620-87-K-0003

8c. ADDRESS (City, State, and ZIP Code)
Bolling Air Force Base
Washington, DC 20332-6448

10. SOURCE OF FUNDING NUMBERS

PROGRAM ELEMENT NO.	PROJECT NO.	TASK NO	WORK UNIT ACCESSION NO.
61102F	2302	B1	

11. TITLE (Include Security Classification)
Control Augmented Structural Optimization of Aeroelastically Tailored Fiber Composite Wings

12. PERSONAL AUTHOR(S)
Peretz P. Friedmann and Lucien A. Schmit, Jr.

13a. TYPE OF REPORT	13b. TIME COVERED	14. DATE OF REPORT (Year, Month, Day)	15. PAGE COUNT
FINAL	FROM 11/11/86 TO 9/30/90	1991, 18 August	

16. SUPPLEMENTARY NOTATION

17. COSATI CODES			18 SUBJECT TERMS (Continue on reverse if necessary and identify by block number)
FIELD	GROUP	SUB-GROUP	Aeroelasticity, Active Control, Structural Optimization, Transonic Flutter Suppression - Unclassified

19. ABSTRACT (Continue on reverse if necessary and identify by block number)

Under AFOSR Contract F49620-87-K-003 the problem of control augmented structural optimization of aeroelastically tailored fiber composite wings was addressed in a series of comprehensive studies. This research culminated in the first truly integrated, practical computer program capable of treating this multidisciplinary synthesis problem by simultaneously changing structural, aerodynamic and control type design variables for practical aircraft configura tions. The effectiveness and efficiency of this integrated aeroservoelastic optimization capability was displayed by applying it to an RPV type vehicle as well as the more complex F-16 and X-29 type airplane models.

In addition, within the framework of this research a digital adaptive controller capable of suppressing flutter in composite wings under time varying flight conditions in subsonic and transonic flow was developed. This efficient analysis can be used as the basis for structural optimization studies of actively controlled composite wings in transonic flow.

20. DISTRIBUTION / AVAILABILITY OF ABSTRACT
☒ UNCLASSIFIED/UNLIMITED ☐ SAME AS RPT. ☐ DTIC USERS

21. ABSTRACT SECURITY CLASSIFICATION
UNCLASSIFIED

22a NAME OF RESPONSIBLE INDIVIDUAL
Peretz P. Friedmann and L.A. Schmit, Jr.

22b TELEPHONE (Include Area Code)
(213)825-6041

22c OFFICE SYMBOL

DD Form 1473, JUN 86 Previous editions are obsolete. SECURITY CLASSIFICATION OF THIS PAGE

DR Spencer T. Wu 202-767-6902

Summary of Accomplishments - Final Report
November 1, 1986 - September 30, 1990
Air Force Office of Scientific Research
Contract No. F49620-87-K-0003

CONTROL AUGMENTED STRUCTURAL OPTIMIZATION OF AEROELASTICALLY TAILORED FIBER COMPOSITE WINGS

Principal Investigators:

Peretz P. Friedmann and Lucien A. Schmit, Jr.
Mechanical, Aerospace and Nuclear Engineering Department
University of California
Los Angeles, CA 90024-1597

Under AFOSR Contract F49620-87-K-0003 which was initially funded November 1, 1986 and completed on September 30, 1990, the problem of control augmented structural optimization of aeroelastically tailored fiber composite wings was addressed in a series of comprehensive studies. This research culminated in the first truly integrated, practical computer program capable of treating this multidisciplinary synthesis problem by simultaneously changing structural, aerodynamic and control type design variables for practical aircraft configurations such as the F-16 fighter.

The main line of this research program has been described in a substantial number of publications [1-9]. A brief description and summary of the contributions contained in these publications is provided below. A more detailed description of this research effort is summarized in Refs. 3, 4, 6 and 8 which are attached as Appendix A of this report.

Reference 1 is a detailed report describing the structural model used in this research activity and its implementation in a computer code. Using this structural model a complete airplane configuration can be efficiently modeled as an assembly of flexible lifting surfaces. Each lifting surface is modeled as an equivalent plate whose stiffness is controlled by contributions from thin cover skins (fiber composite laminates) and the internal structure

(spar and rib caps). Wing sections are connected to each other via stiff springs (representing hinge stiffnesses at attach points) and flexible springs (representing the stiffness of actuators and their backup structure). Each wing section can include several trapezoidal parts. Concentrated masses are used to model nonstructural items and balance masses.

Structural topology, shape and material properties are preassigned; however, skin layer fiber orientations are treated as design variables. Skin thicknesses are also indirectly represented as design variables. Concentrated masses and springs at preassigned locations can also be treated as design variables. It was demonstrated that this structural model is capable of capturing the important modes of an F-16 fighter wing, with accuracy comparable to a detailed finite element model, and at the fraction of the computational cost. This computational efficiency is a key ingredient in the success of the subsequent optimization studies, based upon this model.

Reference 3, which is an expanded and improved version of Ref. 2, presents the theoretical basis for the synthesis of an actively controlled composite wing as a multidisciplinary optimization problem. A unique integration of analysis techniques spanning the disciplines of structures, aerodynamics, and controls is described. A rich variety of behavior constraints can be treated including stress, displacement, control surface travel and hinge movement, natural frequency, aeroservoelastic stability, gust response, and handling quality constraints, as well as performance measures in terms of drag/lift coefficients, drag polar shape, required load factor or roll rate, and wing mass. The design space includes a simultaneous treatment of structural, aerodynamic, and control system design variables. The basis for multidisciplinary wing optimization is prepared by formulating the analysis capability together with the related behavior sensitivity analysis. Applicability of approximation concepts to this particular multidisciplinary optimization problem is examined by studying typical aeroservoelastic stability, gust response and performance-related constraints. The computational efficiency of the combined analysis and sensitivity, as well as the quality of key behavior constraint approximations, was shown to

be excellent. Thus the single-level optimization of composite, actively controlled practical wings, described in the subsequent references could be carried out.

The integrated multidisciplinary synthesis capability (described in Ref. 3) was used in Ref. 4 in a series of innovative exploratory design studies in which constraints from several disciplines are taken into account simultaneously and the design space is opened up to include structural, control system, and aerodynamic design variables. The effectiveness and the efficiency of the new capability are studied using a mathematical model of a remotely piloted vehicle (RPV). The emphasis in these studies was on active-control/structure interaction in the RPV wing design problem. These studies have demonstrated the successful adaptation of NLP/AC (nonlinear programming/approximation concepts) techniques to problems with important new types of constraints (aeroservoelastic stability, gust response) exhibiting greater complexity than those previously treated in pure structural synthesis problems.

In Ref. 6 the effectiveness and efficiency this integrated aeroservoelastic optimization capability is displayed by applying it to an RPV as well as more complex F-16 and X-29 type airplane models. Simplified handling quality constraints are added to the set of design requirements. The performance of several complex eigenvalue approximations was also examined. Effects of control law structure on the weight and robustness of the resulting aeroservoelastic design provide new insights into the complex multidisciplinary interactions involved.

In Ref. 7, aerodynamic constraints, represented by induced drag constraints are added to the previous set of constraints explored. New approximations for induced drag constraints are developed. Again the composite wing of an RPV is used for numerical experimentation with the new capability. Design studies with design variables and constraints that span the disciplines of structures, controls and aerodynamics are presented. It is demonstrated that the synthesis of actively controlled, fiber composite wings with modeling accuracy that is acceptable for preliminary design is both feasible and practical. Results of the new design

studies provide interesting and important new insights into the complex nature of multidisciplinary interactions present in wing design.

Reference 5 is Dr. Livne's landmark Ph.D. dissertation which incorporates both the analysis and the results discussed so far; in a single document. It is our intent to publish this document as a Air Force Technical Report with the assistance of the funding agency.

Recognizing that the description of the research activity provided above might be fragmented, we find it useful to provide, below, a concise overview of the principal research accomplishments described in Refs. 1-7. This research has produced a truly integrated comprehensive multidisciplinary wing synthesis capability which is the most advanced of its kind available to date. This capability which is depicted schematically in Fig. 1, integrates the disciplines of structures, aerodynamics, and controls. There is no comparable capability available in the academic, industrial, or research community.

The principal accomplishments are:

1. Fully coupled structural, aerodynamic and control system analyses.

2. Extended design space, where one can change simultaneously structural, aerodynamic and control type design variables.

3. Inclusion of a rich mix of behavior constraints and alternative objective functions.

4. Combination of analysis/sensitivity capability with approximation concepts and optimization algorithm.

5. Ability to deal with both maneuver and handling type of constraints.

6. Demonstration of the effectiveness of the new synthesis procedure by applying it to optimization of conventional wings, swept back wings and forward swept wings (RPV, F-16, X-29).

The unique features of this synthesis capability are:

1. Balanced high quality, yet computationally efficient analysis modeling.

2. Analytic sensitivity for all constraints with respect to all design variables.

3. It contains the first successful approximations of aeroservoelastic stability and gust response constraints in the design space.

4. The design space spans three disciplines simultaneously.

5. The formulation includes a more comprehensive set of constraints, design variables and alternative objective functions than structural synthesis programs such as TSO, FASTOP or ASTROS.

The effectiveness and computational efficiency of this synthesis capability when applied to the multidisciplinary optimization of a lightweight fighter is depicted in Fig. 2. For this case the computing times, number of design variables, and constraints are shown in Fig. 2. Such a problem has 40 design variables and over 3000 constraints. The combined computer time for one analysis, and sensitivity analysis is about 6 min of CPU time. The number of analyses for a converged optimal design N^* is between 10 and 20. Thus multidisplinary optimization of practical airplane fighter wings is feasible because it requires between one to two hours of CPU time.

The synthesis capability which has been described above, is limited to the subsonic flow regime. Another important contribution made in the course of this research contract

was the extension of the aeroservoelastic analysis capability to the transonic flow regime. Obviously such an analysis capability, which is computationally efficient, is a prerequisite for extending this synthesis capability to the transonic flow regime, in which all modern fighter aircraft must operate.

The description of a transonic adaptive aeroservoelastic analysis capability based approximate unsteady time domain aerodynamics is presented in Refs. 8 and 9.

References 8 and 9 describe the development of a digital adaptive controller capable of suppressing flutter in composite wings under time varying flight conditions in subsonic and transonic flow. The wing structure is modeled using the modeling capability such as that described in Ref. 1. A new transonic unsteady aerodynamic approximation methodology is developed which is computationally efficient and particularly suitable for transonic aeroservoelastic applications. This approximation is based on a combination of unsteady subsonic aerodynamics with a transonic correction procedure. The transient response of the aeroservoelastic system is obtained using Roger's approximation for converting frequency domain aerodynamics into the time domain, state transition matrices, and an iterative time marching algorithm. The aeroservoelastic system in the time domain is modeled using a deterministic ARMA model together with a parameter estimator. This approach enables one to compute the aeroelastic flutter boundaries in the time domain. This analysis capability was compared with experimental data, obtained at NASA Langley, and good agreement with experimental data was noted for the low transonic Mach number range.

The linear quadratic controller gain, for the digital flutter suppression system, at each time step is obtained using an iterative Riccati solver. The digital adaptive controller is robust with respect to the unknown external loads. Flutter and divergence instabilities are suppressed simultaneously using a trailing-edge control surface and displacement sensing. Acceleration sensing alone is inadequate for suppressing static instabilities such as divergence.

The most important accomplishments of this research [8,9] were:

1. This study represents the first application of adaptive optimal control methodology to active flutter suppressions in transonic flow.

2. Development of a computationally efficient aeroservoelastic analysis capability in transonic flow which is suitable for incorporation in a general integrated multidisciplinary wing design synthesis capability such as that described in Refs. 2 through 7.

During the course of this research contract two graduate students (Dr. Eli Livne and Dr. C. Pak), who were fully supported by the contract, have received their Ph.D. degrees.

It is evident from the forgoing that this research contract has been quite fruitful. In addition to the substantial productivity represented by published research results, this program has produced truly significant and original contributions to the state of the art. It has also provided intellectual stimulation and educational enrichment for the graduate students affiliated with the program. It is our earnest hope that the new ideas that have grown out of this research activity will significantly influence future design practice in the aerospace industry.

REFERENCES

1. Livne, E., Schmit, L.A., and Friedmann, P.P., "Design Oriented Structural Analysis for Fiber Composite Wings," UCLA Report UCLA-ENG-88-36, November 1988.

2. Livne, E., "An Integrated Approach to the Optimum Design of Actively Controlled Composite Wings," *Recent Advances in Multidisciplinary Analysis and Optimization*, NASA CP-3031, 1989, 897-918.

3. Livne, E., Schmit, L.A., and Friedmann, P.P., "Towards Integrated Multdisciplinary Synthesis of Actively Controlled Fiber Composite Wings," *Journal of Aircraft*, Vol. 27, No. 12, December 1990, pp. 979-992.

4. Livne, E., Schmit, L.A., and Friedmann, P.P., "Exploratory Design Studies Using an Integrated Multidisciplinary Synthesis Capability for Actively Controlled Composite Wings," AIAA Paper No. 90-0953-CP, Proceedings of AIAA/ASME/ASCE/AHS/ ACS 31st Structures, Structural Dynamics and Materials Conference, Long Beach, CA, April 1990, pp. 97-109 (modified version accepted for publication in the *AIAA Journal*, December 1991).

5. Livne, E., "Integrated Multidisciplinary Optimization of Actively Controlled Fiber Composite Wings," Ph.D. Dissertation, Department of Mechanical, Aerospace and Nuclear Engineering, University of California, Los Angeles, August 1990.

6. Livne, E., Friedmann, P.P., and Schmit, L.A., "Studies in Integrated Aeroservoelastic Optimization of Actively Controlled Composite Wings," AIAA Paper No. 91-1098-CP, Proceedings of AIAA/ASME/ASCE/AHS/ACS 32nd Structures, Structural Dynamics and Materials Conference, April 8-10, 1991, Baltimore, MD, pp. 447-461 (modified version submitted for publication to the *Journal of Guidance, Control and Dynamics*).

7. Livne, E., Schmit, L.A., and Friedmann, P.P., "Integrated Structure/Control/ Aerodynamic Synthesis of Actively Controlled Composite Wings," paper submitted to the *Journal of Aircraft*.

8. Pak, C., Friedmann, P.P., and Livne, E., "Transonic Adaptive Flutter Suppression Using Approximate Unsteady Time Domain Aerodynamics," AIAA Paper No. 91-0986-CP, Proceedings of AIAA/ASME/ASCE/AHS/ACS 32nd Structures, Structural Dynamics and Materials Conference, April 8-10, 1991, Baltimore, MD, pp. 1832-1854.

9. Pak, C., "Adaptive Active Flutter Suppression of Wings in Subsonic and Transonic Flight Regimes," Ph.D. Dissertation, Mechanical, Aerospace and Nuclear Engineering Department, University of California, Los Angeles, California, May 1991.

INTEGRATED OPTIMIZATION OF FIBER COMPOSITE, ACTIVELY CONTROLLED WING DESIGNS --
The Most Comprehensive Multidisciplinary Wing Synthesis Capability to Date

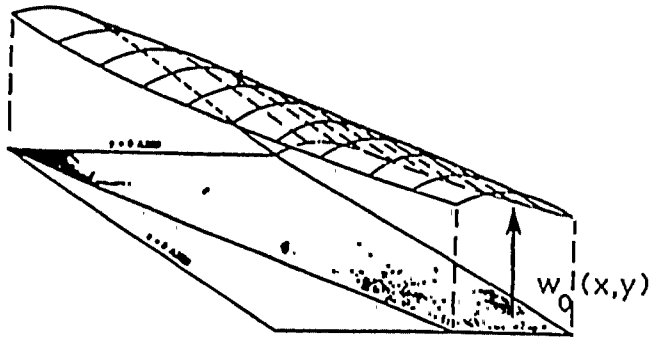

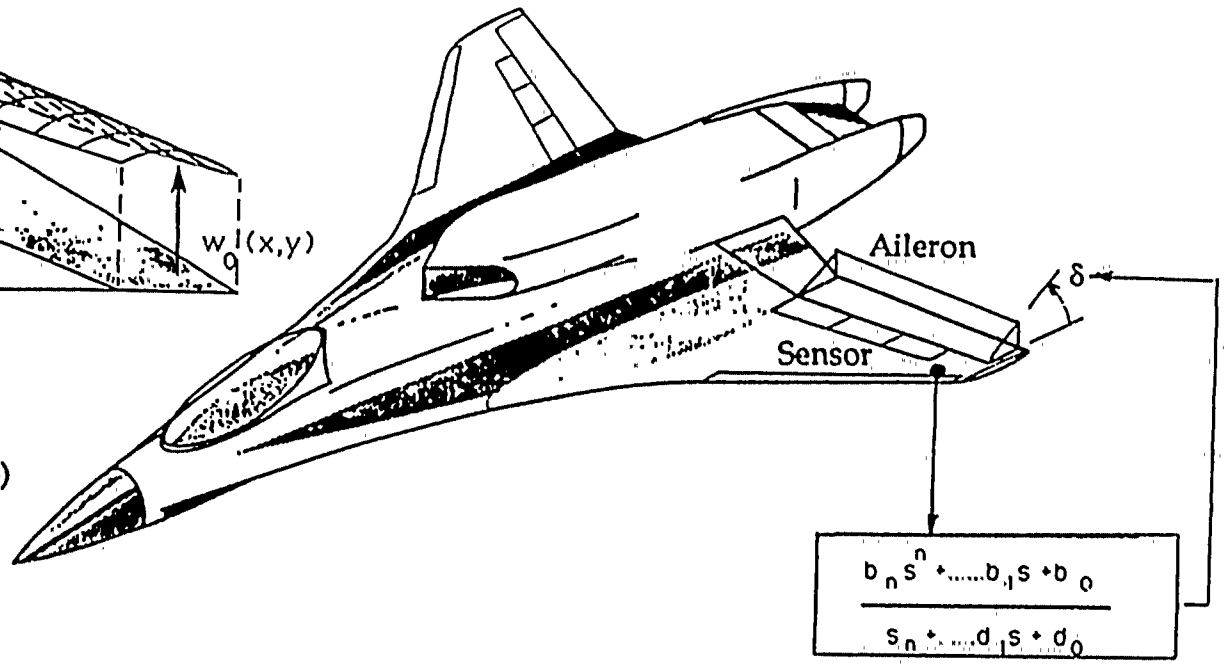

AERODYNAMIC
Design Variables: Camber
Constraints On: Drag
(Performance)

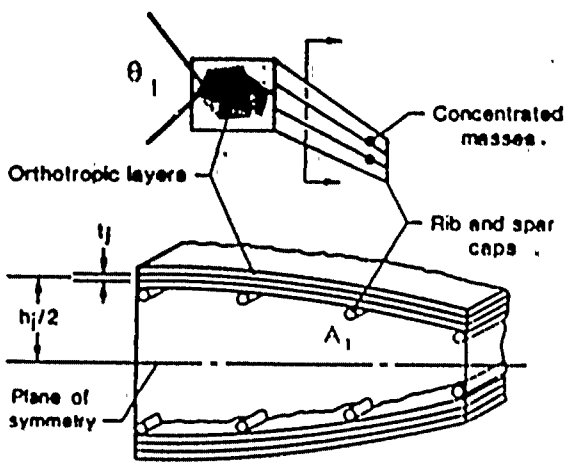

CONTROL System Design
Variables: b_1, d_1
Constraints on:
Aeroservoelastic Stability
Gust Response
Handling Qualities

STRUCTURAL
Design Variables: t_j, A_1, θ_1
Constraints on: Strength
Stiffness
Natural Frequencies

FIGURE 1

RUN TIME FOR LIGHT WEIGHT FIGHTER MULTIDISCIPLINARY ANALYSIS/SENSITIVITY ACHIEVED WITH CAPABILITY DEVELOPED UNDER THIS AFOSR CONTRACT

CPU Times on UCLA IBM 3090

Problem Size:	40 Design Variables 3222 Constraints	
Analysis Run Time:	40 secs	Total: 6.5 min
Sensitivity Analysis Run Time:	350 secs	

Optimization

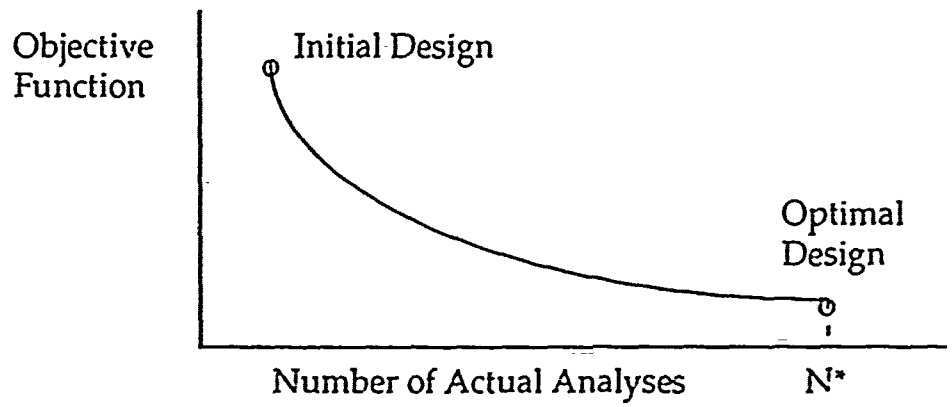

The Importance of Approximation Concepts

	Optimization Via Approximation Concepts	Optimization Via Conventional Math Programming
N*	10 → 20	4000 → 6000
CPU hours	1 → 2	433 → 650
Multidisciplinary Optimization	can be done	cannot be done

FIGURE 2

APPENDIX A
Detailed Summary of the Research Conducted

Note: This Appendix contains Refs. 3, 4, 6, and 8 cited in the body of the report

Ref. 3

Towards Integrated Multidisciplinary Synthesis of Actively Controlled Fiber Composite Wings

E. Livne,* L. A. Schmit,† and P. P. Friedmann‡
University of California, Los Angeles, Los Angeles, California 90024

The synthesis of actively controlled composite wings is formulated as a multidisciplinary optimization problem. A unique integration of analysis techniques spanning the disciplines of structures, aerodynamics, and controls is described. A rich variety of behavior constraints can be treated including stress, displacement, control surface travel and hinge moment, natural frequency, aeroservoelastic stability, gust response, and handling quality constraints, as well as performance measures in terms of drag/lift coefficients, drag polar shape, required load factor or roll rate, and wing mass. The design space includes a simultaneous treatment of structural, aerodynamic, and control system design variables. The paper sets the stage for multidisciplinary wing optimization by describing the capabilities and discussing the accuracy of the analysis and related behavior sensitivity analysis. Applicability of approximation concepts to the multidisciplinary optimization problem is examined by studying typical aeroservoelastic stability, gust response, and performance-related constraints. The computational efficiency of the combined analysis and sensitivity as well as the quality of key behavior constraint approximations indicate that single-level optimization of composite, actively controlled practical wings is within reach.

Nomenclature

$a_0, a_1 \ldots a_n$	= coefficients of the numerator polynomial in a sensor transfer function (see Fig. 3)
$[A],[B],[C],[D]$	= Linear time invariant (LTI) state space equation matrices
$[\bar{A}],[\bar{B}]$	= state space system matrices in standard form
b	= aerodynamic lag terms
b^G	= aerodynamic gust lag terms
b	= control law transfer function numerator coefficients
$c_0, c_1 \ldots c_n$	= coefficients of the denominator polynomial in a sensor transfer function (see Fig. 3)
$[C]$	= damping matrix
$[\hat{C}]$	= aerodynamically modified damping matrix in aeroservoelastic analysis
d_i	= transfer function denominator coefficients
$e_0, e_1 \ldots e_n$	= coefficients of the numerator polynomial in an actuator transfer function (see Fig. 3)
$[E],[F],[G],[H]$	= aeroelastic system matrices
$f_0, f_1 \ldots f_n$	= coefficients of the denominator polynomial in an actuator transfer function (see Fig. 3)
$F(X)$	= objective function
$[g]$	= vector of behavior constraint functions
G_A	= aileron gain (see Fig. 7)
$[K]$	= stiffness matrix
$[\hat{K}]$	= aerodynamically modified stiffness matrix in maneuver load analysis
$[\hat{K}]$	= aerodynamically modified stiffness matrix in aeroservoelastic analysis
$[M]$	= mass matrix
$[\hat{M}]$	= aerodynamically modified mass matrix in aeroservoelastic analysis
MS	= mean square value of response to gust
MS_0	= reference mean square value of gust response
n_{ACT}	= number of actuator states
n_{AER}	= number of aerodynamic added states
n_{CO}	= number of control law states
n_c	= number of control surface degrees of freedom (DOF)
n_G	= number of gust filter states
n_s	= number of structural DOF
n_{SE}	= number of sensor states
n_{SYS}	= number of aeroservoelastic states
N_l	= number of Roger lag terms
N_l^G	= number of Roger lag terms added for gust
p	= any design variable
$\{P\}$	= load vector
$[P_1]$-$[P_6]$	= minimum state or Roger approximation matrices
$\{q\}$	= generalized displacements
$\{q_c\}$	= control surface deflection
q_D	= dynamic pressure
$\{q(s)\}$	= the vector of Laplace transformed generalized displacements
$\{Q_G(s)\}$	= the Laplace transformed gust vector
$[Q(s)]$	= generalized aerodynamic force matrix
$[Q_w]$	= white noise intensity matrix
$\{r^A\}$	= aerodynamic added states
$\{r^G\}$	= aerodynamic gust added states
$s=\sigma+j\omega$	= Laplace variable
S	= reference area
t_1	= skin thickness term
$\{u\}$	= vector of control surface excitations [see Eq. (39)]
U_∞	= flight speed
w	= white noise input
w_G	= vertical gust velocity
$W_G(s)$	= the Laplace transformed vertical gust velocity

Presented as Paper 89-1268 at the 30th Structures, Structural Dynamics, and Materials Conference, Mobile, AL, April 3-5, 1989; received Aug. 9, 1989; revision received April 1, 1990; accepted for publication April 18, 1990.

*Graduate Research Assistant. Student Member AIAA.
†Professor of Engineering and Applied Science. Fellow AIAA.
‡Professor and Chairman. Associate Fellow AIAA.

$[U],[V],[W]$	= aeroservoelastic system matrices
$\{x\}$	= state vector
X	= vector of design variables
$[X]$	= state covariance matrix
y	= output
δ_i	= input command to an actuator
$[\Phi_0],[\Phi_1],[\Phi_2]$	= structural response transformation matrices
ζ	= equivalent viscous damping
ζ_0	= reference equivalent viscous damping

Subscripts

0	= reference value
ACT	= actuator
CO	= control law
c	= control surface
G	= gust
s	= structural DOF
SE	= sensor

Superscripts

G	= gust
L	= lower bound
U	= upper bound

Introduction

THE introduction of active control technology[1-6] and composite structural tailoring[7-11] to airplane wing design during the last 15 years requires a re-examination of the design practice followed in the past, which was based on a sequential, compartmented approach.

Using the sequential approach, undesirable interactions between disciplines, which were not taken into account properly during wing development, have resulted in expensive, sometimes lengthy, modifications and fixes.[12-16] At the same time there has been a growing recognition of the potential improvements possible when an integrated multidisciplinary design and synthesis approach is followed, in which all relevant disciplines are considered simultaneously.[17-19]

Three decades of extensive research and development have made optimization techniques widely accepted in every major discipline needed in wing design synthesis.[20] Structural synthesis has matured in the last decade and has already been used to size complex structures under various static and dynamic behavior constraints including flutter and static aeroelastic constraints.[21-38] Research carried out during the last 20 years on control system design, active flutter suppression, and gust alleviation has produced several alternative implementations of optimization to active control synthesis practices.[39-46] In the aerodynamic field, optimization has been used to synthesize wing camber, cross section, and planform to achieve desirable aerodynamic characteristics and performance.[47-58]

The growing confidence in modern analysis techniques and disciplinary optimization has led to a departure from conventional designs. It has become apparent that multidisciplinary interactions must be taken into account to prevent failure and to extract maximum benefits from the design freedom offered by a truly integrated approach. During the last decade, control augmented structural synthesis has emerged as an important research area.[59-66] Initial results, for wing design, have been recently reported emphasizing the multidisciplinary structural/aerodynamic synthesis of wings.[67-71] An initial study of the aeroservoelastic optimization problem, namely the simultaneous synthesis of wing structures and their active control systems, was also reported recently.[72] Methods for control law and control system performance sensitivity analysis with respect to structural and control system parameters have also been reported in recent years as a precursor to the application of multilevel decomposition techniques for design optimization.[73-75] An approach to the integrated handling qualities/aeroelastic stability design problem is given in Ref. 76. Parametric studies reported in Refs. 77 and 78 further highlight the importance of multidisciplinary design considerations for practical fighter wings. An integrated approach to the optimization of airplane configuration and control system was presented in Refs. 79 and 80 using simplified mathematical models. However, the application of modern optimization techniques to wing design involving a diverse mix of constraints based on analyses from several disciplines (structures, structural dynamics, aeroelasticity, aerodynamics, control, handling qualities) has not yet been treated in a comprehensive and realistic manner.

The purpose of this paper is to outline a unified framework for multidisciplinary wing synthesis. It contains a description of a set of techniques for analysis and behavior sensitivity analysis of actively controlled fiber composite wings, which will facilitate integrated design optimization. Several aspects of structural, aerodynamic, and control system modeling are discussed. Computational efficiency and accuracy of approximations for a rich variety of behavior constraints are examined. The paper lays the foundation for the application of approximation concepts and optimization techniques to practical control augmented aeroelastic wing design.

The Complexity and Multidisciplinary Nature of Wing Design

The set of wing design descriptors, whose elements consist of preassigned parameters and design variables,[22] is shown in Fig. 1. Discussion is limited to wings operating in the sub-

	STRUCTURES, STRUCTURAL DYNAMICS	AERODYNAMICS	CONTROL
SIZING DESIGN DESCRIPTORS (DESIGN VARIABLES OR PREASSIGNED PARAMETERS)	ELEMENT SIZE (AREA, THICKNESS)	CAMBER, LE/TE CONTROL SURFACE DEFLECTION	GAINS, TRANSFER FUNCTION COEFFICIENTS
CONFIGURATION DESIGN DESCRIPTORS	PLANFORM SHAPE (SWEEP, AR, TAPER RATIO), AIRFOIL CROSS SECTION, PLY ANGLE, RIB/SPAR LOCATIONS	PLANFORM SHAPE (SWEEP, AR, TAPER RATIO), AIRFOIL CROSS SECTION	ORDER OF TRANSFER FUNCTIONS
TOPOLOGICAL DESIGN DESCRIPTORS	NUMBER OF RIBS, SPARS, PLY ANGLES	NUMBER OF LE/TE CONTROL DEVICES	CONTROL SYSTEM STRUCTURE AND CONNECTIVITY

Fig. 1 Hierarchy of design descriptors in wing synthesis

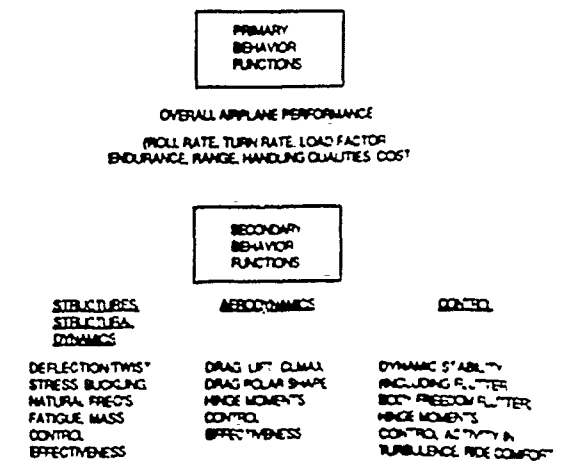

Fig. 2 Important behavior functions in multidisciplinary wing synthesis.

sonic to low-supersonic flight speeds, so that thermal effects can be neglected. A given set of design descriptors completely defines a particular wing design. Which of the descriptors will be preassigned parameters and which will be used as design variables depends on the level of application for optimization techniques in the hierarchy described in Ref. 22, namely, whether the design space includes sizing, configuration (geometry), or topological design variables. The set of behavior functions, from which constraints and objectives will be selected, can be divided into two categories (Fig. 2). Primary (system level) behavior functions are those performance measures that determine the overall quality and competitiveness of the wing. Secondary (subsystem level) behavior functions are the behavior functions that must be taken into account during the design to guarantee the prevention of failure in all possible failure modes and to introduce known constraints on subsystem performance. These are the means necessary to achieve the overall design goals and should ideally be "transparent" compared with real design objectives, although sometimes there can be strong correlation between a secondary behavior and a primary behavior function (e.g., mass and airplane performance).

The importance of multidisciplinary interactions in wing design is evident from Figs. 1 and 2. Structural topology, shape and sizing; control system topology, control law transfer function order, and gain values; as well as aerodynamic configuration layout, jig shape, and control surface deflections in maneuvers all interact to achieve desired wing performance while ensuring structural integrity, aeroservoelastic stability, ride comfort, and good handling qualities.[82-93]

The design synthesis problem can be cast in a mathematical programming form:

$$\min_{\{X\}} F(\{X\}) \tag{1}$$

$$s.t.\ \{g\} \le \{0\}$$

$$\{X^L\} \le \{X\} \le \{X^U\}$$

To overcome the inherent complexity and to address the computationally intensive nature of this problem, two approaches have been suggested in the literature. The first approach is based on the application of multilevel decomposition techniques combined with existing tools for detailed analysis and sensitivity analysis for each of the disciplines.[94,95] The second approach seeks to gain some insight into the nature of the problem by using highly simplified mathematical models or simple airplane configurations for structural, aerodynamic, and control system analysis.[72,79,80]

Modeling Considerations

Structural and Aerodynamic Modeling

In Ref. 20, Ashley points out that a considerable part of the research done on wing optimization has been based on models that are "a long way from the complicated, built up lifting surfaces of real aircraft with their multiple design criteria and constraints." He warns that "very undesirable consequences can result from the omission or careless handling of constraints," and this warning is particularly relevant for multidisciplinary synthesis, where only limited experience exists to guide the designer, and intuition may sometimes be misleading.

The prevalent structural beam/aerodynamic strip models used for basic research in aeroelasticity are often inadequate when it comes to synthesizing real wings.[96-98] More realistic models are needed. At the same time, detailed finite element models and Computational Fluid Dynamics (CFD) aerodynamic techniques are still computationally too expensive to use within the inner loop of a multidisciplinary synthesis approach. Thus, it is necessary to bridge the gap between the highly idealized and the very detailed modeling alternatives by introducing balanced analysis and design optimization models that capture essential behavior characteristics, without making the integrated multidisciplinary design optimization task intractable.

The integrated optimum design capability outlined here is based on modeling and analysis techniques for the required disciplines, which are consistent with each other in terms of accuracy and efficiency and, thus, lead to a balanced treatment of practical wings. In the structures area, a rather general equivalent plate analysis,[98] which builds on the basic ideas underlying the Aerodynamic Tailoring and Structural Optimization (TSO) computer code[7,28,29] and incorporates additional recent developments due to Giles,[99,100] is used. The equivalent plate approach for structural modeling of low aspect ratio wings has been known for many years. It was Giles, however, who showed that, using present day computers, a single high-order power series can be used for approximating displacements over wing planforms made of several trapezoidal segments to obtain accurate stress as well as displacement information. Stresses in spar and rib caps can be calculated in addition to composite skin stresses. Configurations made of several plate segments attached to each other via springs accounting for attachment stiffness and actuator stiffness can be analyzed to simulate wing/control surface configurations. The simplicity of manipulating simple power series leads to analytic rather than numerical integration for the mass and stiffness expressions. With the careful organization of computer storage space and ordering of calculations, major savings in computation times and core storage requirements can be achieved.

In the work described here, the equivalent plate structural analysis documented in Ref. 98 is integrated with the Piecewise Continuous Kernel Function Method (PCKFM) developed by Nissim and Lottati for lifting surface unsteady aerodynamics.[101-104] Lifting surface unsteady aerodynamics[105,106] has served as the basic aerodynamic modeling tool for the flutter analysis of airplanes since the 1960s. The PCKFM combines the power of the doublet lattice method in dealing with pressure singularities with the accuracy and speed of the kernel function method. Extensive numerical experimentation has demonstrated[101] that PCKFM is accurate and converges rapidly. For configurations involving control surfaces, it can take narrow gaps into account, is faster than lattice methods, and is more accurate in the calculation of control surface hinge moments. Thus, it is particularly suitable for calculating the generalized unsteady air loads (on lifting surfaces made up of wing and control surface elements) that are needed for active flutter suppression and gust alleviation studies.

The combination of modern equivalent plate structural modeling and PCKFM lifting surface aerodynamics is thought to be adequate for the preliminary design of airplane wings and for the exploratory venture into multidisciplinary practical wing synthesis. In addition to a reliable prediction of flutter results and static aeroelastic effects, useful hinge moment[106] and induced drag predictions[107,108] can be expected for subsonic and supersonic small angle-of-attack flight. The analysis is adequate for addressing flight stability and control problems of the elastic airplane.[109] Its aerodynamic predictions might be improved by using correction factor techniques if any measured data are available.

Finite-Dimensional State Space Modeling of Unsteady Aerodynamics

It is suggested in the literature that aeroservoelastic stability analysis can be successfully based on the p-k method using generalized aerodynamic force matrices computed for simple harmonic motion.[37,110] However, when the optimization of the design for aeroservoelastic stability is addressed and modern control techniques are to be implemented, it is necessary to cast the aeroelastic equations of motion in Linear Time Invariant (LTI) state space form. It then follows that some approximation of the unsteady aerodynamic loads in terms of rational functions of the Laplace variable is needed.

The method of Roger[111] has been widely used for finite-dimensional unsteady aerodynamic loads representation during the past decade. A series of aerodynamic stiffness, damping, apparent mass, and several lag terms is used to approximate elements of the generalized aerodynamic loads and gust force matrices over a range of reduced frequencies. A least-squares fitting procedure is carried out for each element of the matrices separately.

The minimum state method, developed by Karpel[112] and recently studied in Ref. 113, is found to be attractive because it has the potential for generating accurate approximations to unsteady generalized aerodynamic forces, while adding only a small number of states to the mathematical model of the aeroservoelastic system. It is based on an iterative fitting process in which all terms of the generalized aerodynamic load and gust force matrices are considered simultaneously. In comparison with other finite-state modeling techniques, the number of states needed in the minimum state method appears to be smaller for the same overall accuracy of approximation.[113] This leads to a state space model of lower order, thus reducing core requirements and computation time.

Considering the accumulated experience and fast generation of Roger approximations (resulting, however, in higher-order mathematical models of the aeroservoelastic system) vs the smaller-order mathematical models possible with the minimum state approach (with a relative lack of experience and time-consuming approximant generation as potential handicaps), it was decided to include both methods in the present capability as available alternatives.

Control System Modeling

The integrated aeroservoelastic system is modeled as an LTI system. Since the number of sensors and control surfaces is small in real airplanes, the complex, high-order laws generated by some multivariable control system design techniques are avoided at this stage. A schematic block diagram of the actively controlled aeroservoelastic system is shown in Fig. 3. Airplane motions (acceleration and angular rates) are measured by a set of sensors placed on the structure. The resulting signals are used as inputs to the control law block which commands control surface actuators. The control surface motions guarantee stability and desirable dynamic response of the complete system.

The control system is completely described by locations of sensors and control surfaces and by the transfer functions of the sensors, control laws, and actuators. Gain scheduling can be adopted by assigning different control laws to different flight conditions.

Optimization Considerations

Design Variables

Shape design variables have already received considerable attention in wing optimization studies.[67-71,79,80,85] However, in addition to a balanced approach to analysis in terms of the analysis techniques selected, we seek to keep a balance in level of optimization by focusing at present on sizing-type design variables in all disciplines considered (Fig. 1).

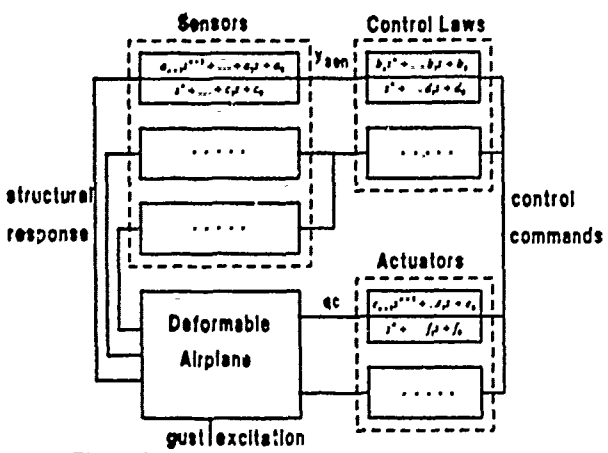

Fig. 3 Elastic airplane control system block diagram.

Structural Design Variables

Figure 4 shows an airplane modeled as an assembly of flexible lifting surfaces. Each lifting surface is modeled as an equivalent plate whose stiffness is controlled by contributions from thin cover skins (fiber-composite laminates) and the internal structure (spar and rib caps). Wing sections are connected to each other via stiff springs (representing hinge stiffness at attach points) and flexible springs (representing the stiffness of actuators and their backup structure). Each wing section can include several trapezoidal parts. Concentrated masses are used to model nonstructural items and balance masses.

The vertical displacement w of each wing section is approximated by a Ritz polynomial series of the form

$$w(x,y,t)=\sum_{i=1}^{N_w} q_i(t)x^{m_i}y^{n_i} \tag{2}$$

where x and y are chordwise and spanwise coordinates respectively. The exponents m_i and n_i define the specific polynomial series used. It can be a complete polynomial in x and y or a product of polynomials in x and y (see Ref. 98).

The depth of a wing section is given by a polynomial

$$h(x,y)=\sum_{i=1}^{N_h} H_i x^{r_i}y^{s_i} \tag{3}$$

where the H_i are preassigned parameters.

Thickness distribution of a typical skin layer is represented by

$$t(x,y)=\sum_{i=1}^{N_t} T_i x^{k_i}y^{l_i} \tag{4}$$

Rib and spar cap areas are allowed to vary linearly along their length η

$$A(\eta)=A_0+A_1\eta \tag{5}$$

Wing stiffness and mass matrix elements are linear combinations of certain area integrals over the planform, line integrals over spar/rib length, and polynomial terms evaluated at points where concentrated masses are located or springs are attached.[98] The present equivalent plate modeling capability[98] makes it possible to efficiently analyze combined wing box/control surface configurations. A wing assembly and a canard or horizontal tail may be attached to a fuselage (modeled as a flexible beam or a flexible plate) to simulate complete airplane configurations. The level of modeling detail can be selected independently for each section. Therefore, the degree of detail used to model control surfaces for analysis and synthesis is not limited, as is the case of the TSO code.

At the present stage of research, structural topology, shape, and material properties are preassigned; however, skin-layer fiber orientations are available as design variables. For skin-

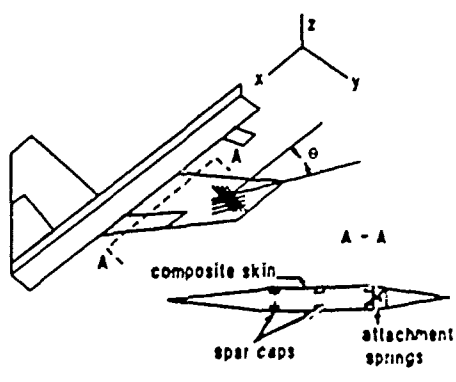

Fig. 4 Airplane as an assembly of equivalent plates.

layer thicknesses [Eq. (4)] the coefficients of the thickness power series serve as design variables. This guarantees smooth thickness variation for each layer. For spar and rib cap areas [Eq. (5)], two coefficients are used as design variables for each spar or rib. Concentrated masses at preassigned locations and spring constants for linear and rotational springs can also be treated as design variables.

Aerodynamic and Control System Design Variables

Wing cross section, aerodynamic planform, and topology are preassigned here. Performance and loads in quasistatic maneuvers can be influenced by designing the jig shape (initial camber) of the wing and by proper deflection of leading-edge and trailing-edge control surfaces. The initial camber of the wing is given by a series

$$w^0(x,y,t)=\sum_{i=1}^{N_w} q_i^0(t)\, x^{m_i} y^{n_i} \tag{6}$$

where the powers m_i and n_i are identical to those in Eq. (2), and any subset of the coefficients q_i^0 can serve as design variables. The deflections of control surfaces for each distinct maneuver point are also available as separate design variables.

The control system design variables at the lowest level in the hierarchy (analogous to sizing) are the coefficients of numerator and denominator of control law transfer functions. Control surface locations, sensor locations, topology of the control system, and order of numerator and denominator polynomials in the transfer functions are preassigned. It is also assumed that sensor and actuator transfer functions are preassigned, although the formulation is sufficiently general so as to allow the treatment of their numerator and denominator coefficients as additional design variables.

The set of design variables treated spans three disciplines, namely structures, aerodynamics, and control. The design space is thus opened up to include sizing level design variables from all three disciplines simultaneously.

Behavior Functions

In order to provide for a rich variety of constraints and alternative objective functions, the following analysis capabilities are included.

1) Static "maneuver load" analysis (static aeroelastic deflection and stress calculations for the elastic airplane in maneuver). maneuvers include symmetric pull-ups (defined by Mach number, altitude, and load factor) or steady rolling maneuvers (defined by Mach number, altitude, and roll rate). In addition to elastic deflections and stresses, the control surface deflections and hinge moments needed for the maneuvers are calculated.

2) Static "given loads" analysis (static deflection and stress calculations for the cantilevered wing under a set of prescribed loads). the loads are assumed independent of the structural design and do not change in the course of wing synthesis. This option is important for cases where linear aerodynamic theory is inadequate, forcing the use of experimental data.

3) Natural frequency and mode shape analysis. natural frequencies and mode shapes are obtained for different sets of boundary conditions (this facilitates generation of separate symmetric or antisymmetric modes).

4) Aeroservoelastic stability analysis. poles of the control-augmented airplane are calculated for different level flight conditions (defined by specifying Mach number and altitude).

5) Gust response analysis. root-mean-square (rms) values of control surface rotations and rates and rms values of selected sensor measurements due to continuous atmospheric turbulence are calculated for different flight conditions.

6) Drag analysis. induced drag is calculated for the elastic lift distribution during maneuvers. Drag values assuming either full leading-edge suction (fully attached flow) or no leading-edge suction (separated flow at the leading edge) or a combination of these[29,33] are available.

With the integrated analysis capability that has been developed, the following behavior functions can be evaluated. elastic displacements; elastic twist, spar/rib cap stresses, skin combined stress failure criteria[114]; natural frequencies, real and imaginary parts of aeroservoelastic poles; rms values of random control surface rotations and rates due to gust; rms values of sensor measurements in gust; total mass; lift and drag coefficients; control surface rotations; and hinge moments in maneuvers. It should also be noted that roll rate or load factor at a particular altitude and Mach number can be treated as design variables; therefore, they can be maximized or constrained.

Control surface effectiveness is not addressed directly at this stage. The synthesis emphasizes sustaining a desired roll rate or load factor while keeping hinge moments, control surface deflections, and stresses within allowable bounds.

Aeroservoelastic stability is guaranteed by providing adequate damping at each flutter critical aeroservoelastic pole throughout the flight envelope.[115] Handling qualities can be preliminarily addressed via inequality constraints on the aeroservoelastic pole locations (e.g., short-period root placement) and pilot-seat acceleration due to atmospheric turbulence.[86,89] The control surface deflection needed for trim and overall performance in a given maneuver and its rms activity due to gusts can be combined to ensure that no saturation occurs.[91,92]

Any of the behavior functions or their combinations can serve as objective functions. Possible alternatives are mass, drag (to be minimized), steady roll rate, lift-to-drag ratio (to be maximized), or a combination of these.

The present analysis capability offers a rich variety of behavior functions for wing design synthesis Thus, the interaction among structure, control, aerodynamics, handling qualities, and airplane performance can be taken into account in an integrated manner.

Approach to Integrated Optimization

Once the preassigned parameters, design variables, failure modes, load conditions, and objective function are selected, the integrated optimization problem can be cast as a nonlinear programming problem having the form of Eq (1)

The nonlinear programming approach combined with approximation concepts (NLP/AC approach) has proven to be an effective method for solving structural synthesis problems,[21,22] and here it will be adapted to the multidisciplinary design optimization task. In this method relatively few detailed analyses are carried out during optimization. Each analysis and the associated behavior sensitivity analysis serve as a basis for constructing approximations to the objective and constraint functions in terms of the design variables. Thus, a series of explicit approximate optimization problems is solved converging to an optimal design.

The main advantage of the NLP formulation is its generality. No a priori assumptions have to be made about the set of active constraints at the optimum Given an initial design, a local optimum is sought using mathematical programming techniques. Thus, it is especially suitable for multidisciplinary optimization, where the problem is large and complicated and past experience does not provide much intuitive guidance However, for the NLP approach to be practical, it is crucial to avoid too many detailed analyses. Success in this regard depends on efficient analysis/sensitivity calculations and on making the explicit approximations of objective and constraint functions robust yet simple enough for efficient solution.

The use of analytic behavior sensitivities and the construction of robust approximations for behavior functions in terms of the design variables are at the heart of the NLP AC approach. During the past two decades, approximation techniques for static deflection, stress, and natural frequency con

straints have been studied extensively and are now well established. Several methods for divergence and flutter constraint treatment have been developed, but no experience has been reported with the aeroservoelastic poles of an actively controlled airplane, the rms of the response to random gusts, or hinge moments of a flexible control surface on an elastic wing. It should be pointed out that in maneuver load analysis the loads acting on the airplane are functions of the design variables via static aeroelasticity as well as through inertial effects. The right side $\{P\}$ of the matrix equation

$$[\bar{K}]\{q\} = \{P\} \tag{7}$$

(where $\bar{K}$ is a stiffness matrix modified by aerodynamic terms corresponding to structural and control surface motions) thus depends on the structural design variables, whereas in the classical given loads analysis, the right side $\{P\}$ is fixed. Thus, the success of approximations using reciprocal variables (Ref. 116) for stress and static deflection in static analysis is not guaranteed in maneuver load analysis, and alternative approximations have to be carefully examined.

Some aspects of maneuver load and drag analysis have already been discussed in the literature within the framework of integrated wing optimization.[29,33,67,68,70] In the following we will, therefore, focus on the aeroservoelastic and gust response analysis and behavior sensitivity calculations.

Aeroservoelastic Analysis

As pointed out in Ref. 117, all time-dependent phenomena of the elastic airplane are governed by a universal set of equations of motion, wherein only the right side (representing the input) varies in proceeding from one phenomenon to the next. Indeed a measure of multidisciplinary integration of analysis techniques, concepts, and terminology is needed even before multidisciplinary optimization is addressed.

Several steps in this direction have been taken in the past.[118-121] However, almost 20 years after the publication of Ref. 118, still no particular approach to the dynamics of the deformable airplane is universally accepted. The analysis here for time-dependent problems is based on the widely used set of linearized equations for small perturbations of elastic airplane motion with respect to constant speed, level flight.[122-127] Although perturbations in the longitudinal direction are not taken into account at this stage, the analysis is adequate for addressing basic stability and control as well as aeroservoelastic problems of highly augmented airplanes in the context of preliminary design.[89]

Aeroelastic Model

Assuming small perturbations from a steady level flight, the Laplace transformed equations of motion for the elastic airplane are

$$\{[M]s^2 + [C]s + [K]\}\{q(s)\} - q_D S[Q(s)]\{q(s)\} = q_D S\{Q_G(s)\}\frac{w_G(s)}{U_\infty} \tag{8}$$

The vector of displacements can be expressed in terms of n_s structural response DOF and n_c control surface deflections:

$$\{q\} = \begin{Bmatrix} q_s \\ q_c \end{Bmatrix} \tag{9}$$

and the equations of motion corresponding to the structural DOF are partitioned accordingly to yield

$$\{[M_{ss}]s^2 + [C_{ss}]s + [K_{ss}]\}\{q_s\} + \{[M_{sc}]s^2 + [C_{sc}]s + [K_{sc}]\}\{q_c\} - q_D S[Q_{ss}(s)]\{q_s\} - q_D S[Q_{sc}(s)]\{q_c\} = \frac{q_D}{U_\infty} S\{Q_{Gs}(s)\}w_G(s) \tag{10}$$

The finite-dimensional approximation to the Laplace transformed generalized unsteady loads using the Roger approach[111,113] is of the form

$$[Q(s)] = s^2[P_1] + s[P_2] + [P_3] + \sum_{l=1}^{l=N_l} \frac{s}{(s+b_l)}[P_{l+3}] \tag{11}$$

In the minimum state method,[112,113] the functional dependence of the generalized aerodynamic force matrix on the Laplace variable is approximated by a rational expression of the form

$$[Q(s)] = [P_1]s^2 + [P_2]s + [P_3] + [P_4]\left[s[I] - [P_5]\right]^{-1}[P_6]s \tag{12}$$

The finite-dimensional Roger approximation of the Laplace transformed generalized unsteady gust loads used is of the form

$$[Q_G(s)] = s[P_2^G] + [P_3^G] + \sum_{l=1}^{l=N_l} \frac{s}{(s+b_l^G)}[P_{l+3}^G] \tag{13}$$

The minimum state approximation used for the gust load vector is

$$[Q_G(s)] = [P_2^G]s + [P_3^G] + [P_4^G]\left[s[I] - [P_5^G]\right]^{-1}[P_6^G]s \tag{14}$$

(Note that the notation $[P]$ is used to denote matrices associated with unsteady aerodynamics finite-dimensional state space approximations. However, the matrices $[P_l]$ and $[P_l^G]$ ($l \geq 4$) have different meanings depending on whether the Roger or minimum state approximation is used.)

Partitioning the aerodynamic matrices associated with structural DOF according to Eq. (9) leads to a Roger approximation of the form

$$[Q^{ss}(s), Q^{sc}(s)] = s^2[P_1^{ss}, P_1^{sc}] + s[P_2^{ss}, P_2^{sc}] + [P_3^{ss}, P_3^{sc}] + \sum_{l=1}^{l=N_l} \frac{s}{(s+b_l)}[P_{l+3}^{ss}, P_{l+3}^{sc}] \tag{15}$$

and to a minimum state partitioned approximation of the form

$$[Q^{ss}(s)] = [P_1^{ss}]s^2 + [P_2^{ss}]s + [P_3^{ss}] + [P_4^s][sI - P_5]^{-1}[P_6^s]s \tag{16}$$

$$[Q^{sc}(s)] = [P_1^{sc}]s^2 + [P_2^{sc}]s + [P_3^{sc}] + [P_4^s][sI - P_5]^{-1}[P_6^c]s \tag{17}$$

In the above expressions, $[P_1^{ss}], [P_2^{ss}], [P_3^{ss}]$ are aerodynamic apparent mass, damping, and stiffness matrices, respectively. Their dimensions are $(n_s \times n_s)$. $[P_1^{sc}], [P_2^{sc}], [P_3^{sc}]$ are aerodynamic apparent mass, damping, and stiffness matrices, respectively, associated with the coupling terms between control surface and structural motion. Their dimensions are $(n_s \times n_c)$.

Aerodynamic states are now introduced as follows. For the Roger approximation

$$\{r_l^A(s)\} = \frac{s}{(s+b_l)}[P_{l+3}^{ss}, P_{l+3}^{sc}]\begin{Bmatrix} q_s \\ q_c \end{Bmatrix} \tag{18}$$

$$\{r_l^G(s)\} = \frac{s}{(s+b_l^G)}\{P_{l+3}^G\}w_G(s) \tag{19}$$

Aerodynamic states for the minimum state method are introduced as

$$\{r_s^A(s)\} = \left[s[I] - [P_5]\right]^{-1}[P_6^s\ P_6^c]s\begin{Bmatrix} q_s(s) \\ q_c(s) \end{Bmatrix} \tag{20}$$

$$\{r_s^G(s)\} = \left[s[I] - [P_5^G]\right]^{-1}[P_6^G]w_G(s) \tag{21}$$

Thus, in the Roger approximation, the state space equations for the added aerodynamic states associated with structural deflection are

$$s\{r_i^A(s)\} = -b_l\{r_i^A(s)\} + [P_{i+3}^{ss}]s\{q_s\} + [P_{i+3}^{sc}]s\{q_c\} \quad (22)$$

and in the minimum state approximation

$$s\{r_s^A(s)\} = [P_5]\{r_s^A(s)\} + [P_6^s]s\{q_s(s)\} + [P_6^c]s\{q_c(s)\} \quad (23)$$

Two vertical wind gust state space models are available in the literature for random gust response calculations. These are the Dryden[5,6] model and any rational approximation to the von-Karman[128,129] model. In both cases a gust filter, represented by a strictly proper transfer function, is used to transform a Gaussian zero mean white noise input w into the vertical gust speed w_G with a given power spectral density and rms. A state space description of the gust input is thus of the form

$$s\{x_G\} = [A_G]\{x_G\} + \{B_G\}w \quad (24)$$

$$w_G(s) = [C_G]\{x_G\} \quad (25)$$

$$s\,w_G(s) = [C_G][A_G]\{x_G\} + [C_G]\{B_G\}w \quad (26)$$

If aerodynamically augmented mass, damping, and stiffness matrices are now introduced in the form

$$\hat{M}_{ss} = M_{ss} - q_D S P_1^{ss} \quad (27)$$

$$\hat{C}_{ss} = C_{ss} - q_D S P_2^{ss} \quad (28)$$

$$\hat{K}_{ss} = K_{ss} - q_D S P_3^{ss} \quad (29)$$

$$\hat{M}_{sc} = M_{sc} - q_D S P_1^{sc} \quad (30)$$

$$\hat{C}_{sc} = C_{sc} - q_D S P_2^{sc} \quad (31)$$

$$\hat{K}_{sc} = K_{sc} - q_D S P_3^{sc} \quad (32)$$

(K_{sc} and C_{sc} are zero)

and five subvectors of the state vector $\{x\}$ are defined as

$$\{x_1\} = \{q_s\} \quad (33)$$

$$\{x_2\} = s\{q_s\} \quad (34)$$

$$\{x_3\} = \{x_G\} \quad (35)$$

$$\{x_4\} = \{r^A\} \quad (36)$$

$$\{x_5\} = \{r^G\} \quad (37)$$

then after substitution of Eqs. (11-32) into Eq. (10), the structural and unsteady aerodynamic part of the integrated equations of motion can be written in matrix form as

$$s[E]\{x\} = [F]\{x\} + [G]\{u\} + \{H\}w \quad (38)$$

where $\{u\}$ is a vector of control surface excitations

$$\{u\} = \begin{Bmatrix} q_c \\ sq_c \\ s^2q_c \end{Bmatrix} \quad (39)$$

while $[E]$,$[F]$,$[G]$, and $\{H\}$ are matrices whose elements depend on structural, aerodynamic, and gust filter terms. Equations (38) are the Laplace transformed equations for the structural and aerodynamic states. To complete the state space formulation of this problem, the feedback expression relating the control surface motion $\{q_c(s)\}$ to the structural motions $\{q_s(s)\}$, $\{sq_s(s)\}$, $\{s^2q_s(s)\}$ is used to close the control loops.

Control System

The actual displacements, velocities, and accelerations at a set of points on the structure are given by

$$\{y_{STR}(s)\} = \{[\Phi_0] + [\Phi_1]s + [\Phi_2]s^2\}\{q_s(s)\} \quad (40)$$

The matrices Φ_0, Φ_1, Φ_2 are determined by the location of measurement points on the structure. Actual structural responses are measured by a set of sensors whose output signals serve as input to control laws. These control laws generate input commands $\{\delta\}$ to the actuators. The n_c commands, δ_i, are synthesized to serve as input to n_c actuators.

A typical control law transfer function is given by

$$\frac{\delta_i}{y_{SEi}} = \frac{b_n s^n + b_{n-1}s^{n-1} + \ldots + b_0}{s^n + d_{n-1}s^{n-1} + \ldots + d_0} \quad (41)$$

where y_{SEi} is the input signal to the control element. The state equations for a single control law are given by

$$s\{x_{CO}\} = \begin{bmatrix} 0 & 0 & . & -d_0 \\ 1 & 0 & . & -d_1 \\ 0 & 1 & . & -d_2 \\ . & . & . & . \\ . & . & . & . \\ . & . & . & . \\ 0 & 0 & . & -d_{n-1} \end{bmatrix}\{x_{CO}\} + \left\{ b_n \begin{bmatrix} d_0 \\ d_1 \\ . \\ . \\ . \\ d_{n-1} \end{bmatrix} - \begin{bmatrix} b_0 \\ b_1 \\ . \\ . \\ . \\ b_{n-1} \end{bmatrix} \right\} y_{SEi} \quad (42)$$

$$\delta_i = \{0\,0\,0 \cdots -1\}\{x_{CO}\} + b_n\, y_{SEi} \quad (43)$$

where d_i and b_i are the transfer function denominator and numerator coefficients. When all control laws are assembled, the multi-input multi-output control block controlling several actuators is represented by

$$s\{x_{CO}\} = [A_{CO}]\{x_{CO}\} + [B_{CO}]\{y_{SE}\} \quad (44)$$

$$\{\delta\} = [C_{CO}]\{x_{CO}\} + [D_{CO}]\{y_{SE}\} \quad (45)$$

Sensor and actuator transfer functions are assumed to have denominators of higher order than their numerators. When several sensors are present, the state space model relating the sensor states $\{x_{SE}\}$, the sensor outputs $\{y_{SE}\}$, and the actual structural response $\{y_{STR}\}$ is

$$s\{x_{SE}\} = [A_{SE}]\{x_{SE}\} + [B_{SE}]\{y_{STR}\} \quad (46)$$

$$\{y_{SE}\} = [C_{SE}]\{x_{SE}\} \quad (47)$$

The state space model relating the sensor states $\{x_{SE}\}$, the sensor outputs $\{y_{SE}\}$, and the actual response $\{y_{STR}\}$ is [see Eqs. (33), (34), (40), and (47)].

$$s\{x_{SE}\} = [A_{SE}]\{x_{SE}\} + [B_{SE}]([\Phi_0]\{x_1\} + [\Phi_1]\{x_2\} + [\Phi_2 s]\{x_2\}) \quad (48)$$

The state space model of the actuators is given by

$$s\{x_{ACT}\} = [A_{ACT}]\{x_{ACT}\} + [B_{ACT}]\{\delta\} \quad (49)$$

$$\{q_c\} = [C_{ACT}]\{x_{ACT}\} \quad (50)$$

where $\{q_c\}$ is the control surface deflection (assuming reversible surfaces). The matrices $[A_{CO}]$, $[B_{CO}]$, $[D_{CO}]$, $[C_{SE}]$, $[B_{SE}]$, $[A_{ACT}]$, and $[B_{ACT}]$ depend on the design variables associated with the control system through relations such as Eqs. (42) and (43). Using Eqs. (44–50), the control surface excitation vector $\{u\}$ [see Eq. (39)] can now be expressed in terms of structural, aerodynamic, and control system states as follows:

$$\{q_c\} = [C_{ACT}]\{x_{ACT}\} \quad (51)$$

$$s\{q_c\} = [C_{ACT}][A_{ACT}]\{x_{ACT}\} + [C_{ACT}][B_{ACT}][C_{CO}]\{x_{CO}\} + [C_{ACT}][B_{ACT}][D_{CO}][C_{SE}]\{x_{SE}\} \quad (52)$$

$$s^2\{q_c\} = [C_{ACT}][B_{ACT}][D_{CO}][C_{SE}][B_{SE}] \times ([\Phi_0]\{q_s\} + [\Phi_1]s\{q_s\} + [\Phi_2]s^2\{q_s\}) + [C_{ACT}][A_{ACT}]^2\{x_{ACT}\} + [C_{ACT}]([A_{ACT}][B_{ACT}][D_{CO}][C_{SE}] + [B_{ACT}][C_{CO}][B_{CO}][C_{SE}] + [B_{ACT}][D_{CO}][C_{SE}][A_{SE}]) \times \{x_{SE}\} + [C_{ACT}]([A_{ACT}][B_{ACT}][C_{CO}] + [B_{ACT}][C_{CO}][A_{CO}])\{x_{CO}\} \quad (53)$$

Complete System

The state vector of the whole system is partitioned into eight subvectors. The following subvectors are added to the five which have been already defined in Eqs. (33–37).

$$\{x_6\} = \{x_{ACT}\}(n_{ACT} \times 1) \quad (54)$$

$$\{x_7\} = \{x_{SE}\}(n_{SE} \times 1) \quad (55)$$

$$\{x_8\} = \{x_{CO}\}(n_{CO} \times 1) \quad (56)$$

Assembly of the state space models of the structure, sensors, actuators, control block, and approximate unsteady load and gust aerodynamics leads to the closed-loop state space equations of the complete system:

$$s[U]\{x(s)\} = [V]\{x(s)\} + \{W\}w \quad (57)$$

The order of the system is given by

$$n_{SYS} = 2n_s + n_{ACT} + n_{SE} + n_{CO} + n_G + n_{AER} \quad (58)$$

When N_l lag terms are used, then in the case of Roger approximation

$$n_{AER} = N_l n_s + N_l^G$$

and in the case of minimum state approximation

$$n_{AER} = N_l + N_l^G$$

The considerable saving in terms of added aerodynamic states with the minimum state approach is now evident, since with the Roger approximation the number of added states is a product of the number of lag terms used to fit the data [Eq. (11)] times the number of structural DOF used.

Dependence of System Matrices on the Design Variables

Examine the $[E]$, $[F]$, $[G]$, and $[H]$ matrices of Eq. (38). When augmented by the control system state space equations for the control system states [Eqs. (44), (48), and (49)] and if full-order structural matrices are used (no modal reduction), then each of these matrices is a linear combination of structural, aerodynamic, and products of control system terms. The transformation matrix relating system states $\{x\}$ to control excitations $\{u\}$ [Eqs. (51–53)] depends only on control system parameters (no modal reduction). Substitution of Eqs. (51–53) into Eq. (38) shows that the elements of the $[U]$, $[V]$, and $\{W\}$ matrices of Eq. (57) are of the form

$$(S1)_{ij} + (A1)_{ij} + (C1)_{ij} + (S2)_{ij}(C2)_{ij} + (A2)_{ij}(C3)_{ij} \quad (59)$$

The structural mass and stiffness terms $S1$, $S2$ depend only on structural design variables, whereas the control system matrices $C1$, $C2$, $C3$ depend only on control system design variables via the state space models of actuators, sensors, and control laws. Since wing cross section and planform shape are preassigned at present, when full-order stiffness and mass matrices are used, the aerodynamic terms associated with generalized unsteady loads and gust forces do not change with a change in design variables. When modal reduction is used to reduce the order of the system matrices, then a fixed modes approach is adopted here[130] resulting in fixed aerodynamic terms for the modally reduced models also. Modal reduction is further discussed in the next section.

Full-Order and Reduced-Order Models

With the equivalent plate approach, the structural model may include a relatively small number of DOF when compared to conventional finite element models. These are generalized displacements associated with the Ritz polynomials. The generalized aerodynamic matrices are calculated for the same set of Ritz polynomials used in Eq. (2). Thus, the aeroservoelastic stability analysis can be done with a full order model, including the full-order mass, stiffness, and aerodynamic matrices or by order reduction based on a small number of normal modes.

If a Roger or a minimum state approximation can be found that will accurately fit the full-order aerodynamic matrices with a small number of lag terms, then these approximation matrices can be used in the aeroservoelastic stability analysis even with modal reduction. They just have to be premultiplied and postmultiplied by the generalized mode shapes in order to have the approximation to the modally reduced aerodynamic matrices. Although the number of structural DOF might differ significantly between full-order and modal analysis, the number of aerodynamic states is the same when both approaches are based on the same minimum state approximation to the full-order aerodynamic matrices. If the Roger approximation is used, the number of added aerodynamic states increases with any increase in the number of modes used for reduction. This produces very large models when many modes or a full-order analysis are used. Another possibility is first to modally reduce the frequency-dependent unsteady aerodynamic matrices using modes that are periodically updated after a given number of analysis/sensitivity optimization cycles. Then it might be possible to fit these reduced matrices using fewer lag terms than the number needed to fit the full-order matrices. If a smaller number of lag terms can thus be used, this will reduce the dimensions of the U, V matrices in Eq. (57), compared to their dimensionality in a modal approach, which uses pregenerated full-order aerodynamic matrices. However, rather than preparing the full-order aerodynamic approximantes only once before any synthesis starts, in the latter case it would be necessary to generate aerodynamic approximants each time the set of modes used as a basis

for modal reduction is changed during the synthesis. All of the modal reduction/unsteady aerodynamic approximation alternatives described so far have been included in the present capability. However, their comparative assessment is beyond the scope of this paper.

When full-order aerodynamic matrices are used, they are generated once for the Ritz functions employed in the structural analysis, and they are invariant with respect to changes in either structural sizing or control system design variables. When modal reduction is used, the mode shapes are periodically updated after a given number of analysis steps and so are the aerodynamic matrices and their finite-dimensional rational approximations. Nevertheless, in eigenvalue sensitivity calculations, the derivatives of all reduced-order matrices are determined using a fixed-mode approach.[130] This might require the use of more modes in order to obtain good sensitivity information. In summary, the derivatives of the aerodynamic matrices with respect to structural or control system design variables are zero for the full-order case, and they are assumed zero for the reduced-order case.

The derivatives $\partial U/\partial p$, $\partial V/\partial p$ can be calculated analytically for either structural or control system design variables (p) by differentiating Eq. (59). The gust load vector $\{W\}$ depends only on gust filter and aerodynamic design variables, and therefore its partial derivative with respect to p vanishes.

Stability is examined by computing the eigenvalues of the generalized eigenvalue problem:

$$\lambda[U(p)]\{\phi\} = [V(p)]\{\phi\} \tag{60}$$

Sensitivity of eigenvalues with respect to structural and control system design variables is given by

$$\frac{\partial \lambda}{\partial p} = \frac{\psi^T\left[\lambda\frac{\partial U}{\partial p} - \frac{\partial V}{\partial p}\right]\phi}{\psi^T V \phi} \tag{61}$$

where ψ and ϕ are left and right eigenvectors, respectively.

Gust Response Analysis and Sensitivity

In addition to several publications addressing it in the context of active control technology,[5,6,39] airplane response to random atmospheric turbulence has already been discussed in the context of structural optimization.[131,132] Here, attention is focused on the rms values of control surface rotations $\{q_c\}$, rates $\{\dot{q}_c\}$, and sensor measurements $\{y_{SE}\}$.

The state space equations [Eq. (57)] are transformed into standard form

$$s\{x(s)\} = [\tilde{A}]\{x(s)\} + \{\tilde{B}\}w(s) \tag{62}$$

Since only $\{q_c\}$, $s\{q_c\}$, and $\{y_{SE}\}$ are considered, [Eqs. (47), (51), and (52)], it follows that each output considered y_k is given by

$$y_k = \{C_k\}^T\{x\} \tag{63}$$

where $\{C_k\}$ is either constant or a function of control system design variables.

The state covariance matrix is a solution of a Lyapunov's matrix equation[133] in the form

$$[\tilde{A}][X] + [X][\tilde{A}]^T = -\{\tilde{B}\}[Q_w]\{\tilde{B}\}^T \tag{64}$$

where $[Q_w]$ is the intensity matrix of the Gaussian white noise w. Sensitivity of the covariance matrix $[X]$ with respect to a design variable p is calculated by differentiating Eq. (64):

$$[\tilde{A}]\left[\frac{\partial X}{\partial p}\right] + \left[\frac{\partial X}{\partial p}\right][\tilde{A}]^T = -2\{\tilde{B}\}[Q_w]\left\{\frac{\partial \tilde{B}}{\partial p}\right\}^T - [X]\left[\frac{\partial \tilde{A}}{\partial p}\right]^T - \left[\frac{\partial \tilde{A}}{\partial p}\right][X] \tag{65}$$

and finally the derivative of the (rms)^2 of y_k is calculated by differentiation of the covariance expressions based on Eqs. (47), (51), and (52). It should be noted that

$$[\tilde{A}] = [U]^{-1}[V] \tag{66}$$

$$\{\tilde{B}\} = [U]^{-1}\{W\} \tag{67}$$

and

$$\frac{\partial [U]^{-1}}{\partial p} = [U]^{-1}\left[\frac{\partial U}{\partial p}\right][U]^{-1} \tag{68}$$

from which it follows that

$$\left[\frac{\partial \tilde{A}}{\partial p}\right] = [U]^{-1}\left[\frac{\partial V}{\partial p} - \frac{\partial U}{\partial p}\tilde{A}\right] \tag{69}$$

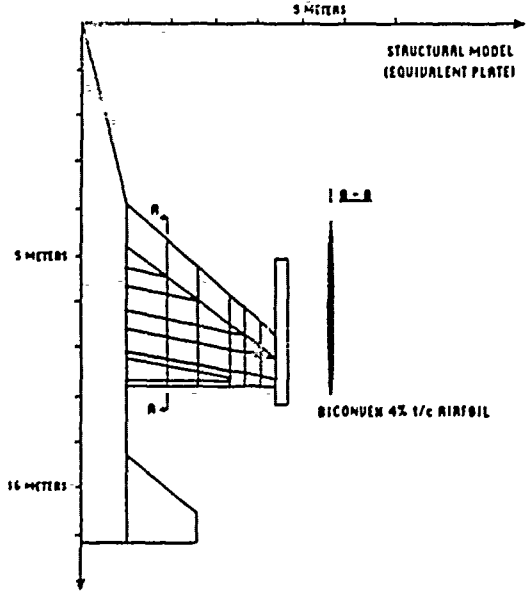

Fig. 5 Lightweight fighter structural model.

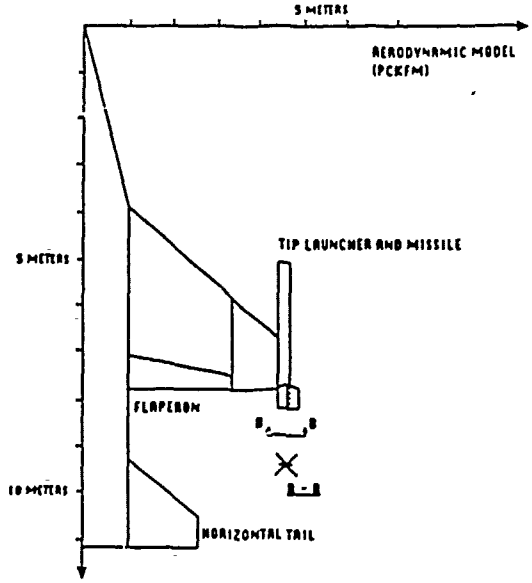

Fig. 6 Lightweight fighter aerodynamic model.

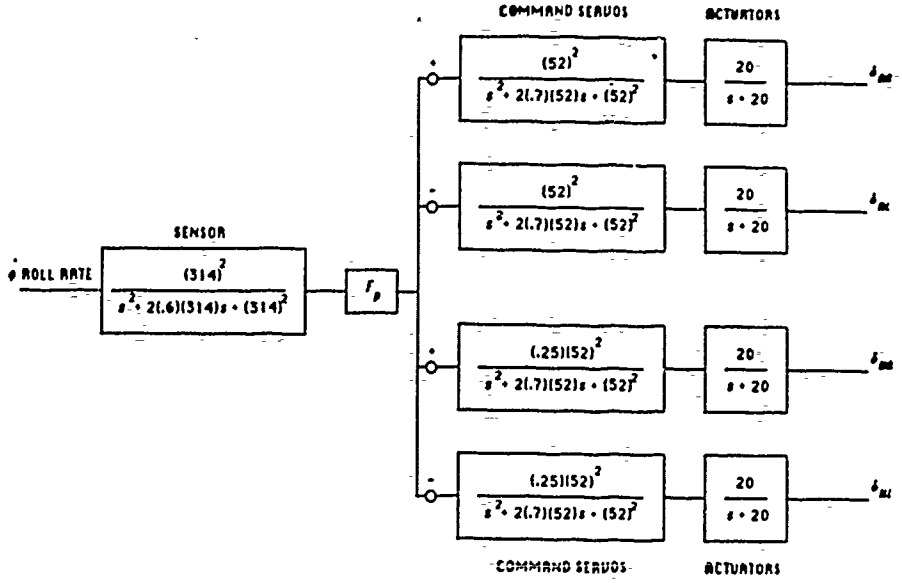

Fig. 7 Lightweight fighter control system roll channel.

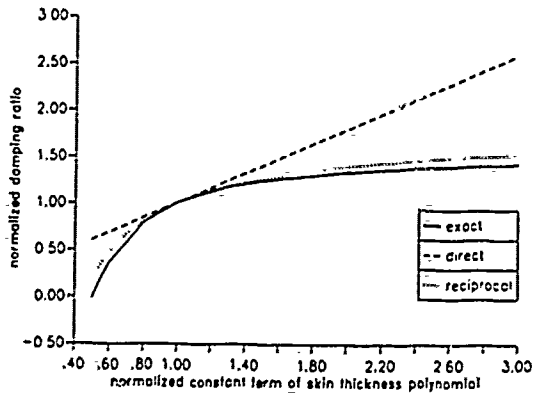

Fig. 8 Approximations of missile pitch root damping (variable wing thickness).

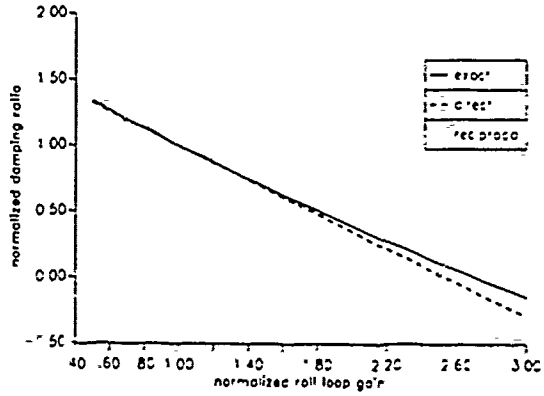

Fig. 9 Approximations of missile pitch root damping (variable roll loop gain).

and

$$\left\{\frac{\partial \bar{B}}{\partial p}\right\} = [U]^{-1}\left[\frac{\partial W}{\partial p} - \frac{\partial U}{\partial p}\bar{B}\right] \tag{70}$$

The Hessenberg-Schur method of Ref. 134 is used to solve both Eqs. (64) and (65). Note that after the analysis is carried out, the matrices $[\bar{A}]$, $[\bar{A}]^T$ are already reduced to Hessenberg and Schur forms. Therefore, the sensitivity calculations of Eq. (65) are equivalent to adding right sides to Eq. (64).

Numerical Examples

Actively Controlled Lightweight Fighter Test Model

Structural and aerodynamic models of a lightweight fighter airplane are shown in Figs. 5 and 6. The airplane is similar to the YF-16, and the construction of its mathematical model was guided by Refs. 29, 135, and 136. It is different than an actual YF-16. Vertical tail and ventral fins are not included. The fuselage and horizontal tail are assumed rigid. There is no leading-edge flap. The wing has a biconvex (about 4% thickness-to-chord ratio) airfoil. It is made of aluminum skins and an array of spars and ribs. A flexible aileron and a rigid tip launcher/missile assembly are attached to the wing using springs. The configuration analyzed weighes 20,000 lb and is statically unstable.

The roll channel of the flight control system is shown in Fig. 7. It is based on the YF-16 roll channel (Refs. 12, 135, and 136). The lightweight fighter model used here is intended to illustrate the well-known YF-16 aeroservoelastic roll instability (Refs. 12, 13, and 135). Lack of sufficient data precluded a more refined simulation of the YF-16. However, the model used here is representative of a typical fighter airplane and is quite complex in its detail.

Two mechanisms of instability, similar to those encountered in the YF-16, exist here. As the aileron gain F_p (Fig. 7) is increased, a 6.5 Hz instability appears associated with a missile pitch mode. With a further increase of F_p, a second instability appears at 3.5 Hz associated with the rigid-body roll mode. Mach 0.9 aerodynamics for antisymmetric motion at 20,000 ft is used in the stability calculations. Since the original airplane is unstable at this point, it is artifitially stabilized here by reducing the gain F_p and adding inherent damping. Stability of the model is necessary for studying gust response approximations.

Results

The multidisciplinary wing analysis/synthesis capability described here has been extensively tested. Structural, aerodynamic, aeroelastic, and aeroservoelastic results have been compared with analysis/test data available from other sources, and overall good correlation was found. The analytic behavior sensitivities were verified by finite-difference sensitivity checks. Here we emphasize some of the basic issues associated with the feasibility of applying the NLP/AC approach to truly integrated multidisciplinary wing synthesis.

These are the computational speed of analysis/sensitivity calculations and the robustness of behavior function approximations.

Parametric studies of the effects of design variable variations on aeroservoelastic poles are presented in Figs. 8 and 9. Figure 8 shows the variation of the damping ratio ζ of the missile pitch mode with a typical structural thickness design variable. In Fig. 9 the damping varies with a typical control system design variable, the gain (F_p) (Fig. 7). In both figures the design variable is varied over a wide range of values. In practical optimization, move limits will be imposed on design variables to ensure accuracy of behavior function approximations. When move limits of 30% are used, both direct and reciprocal Taylor series representations[116] yield reasonable approximations. Thus, hybrid approximations seem adequate for explicit representations of aeroservoelastic pole constraints.

Figure 10 shows the variation of the aileron mean square deflection due to atmospheric turbulence when the gain F_p is varied. As the missile pitch mode is destabilized (Fig. 9), the gust response increases sharply. Away from the stability boundary, the mean square (ms) aileron deflection is well-approximated by either a linear or reciprocal approximation with 30% move limits. Tighter move limits might be needed near the stability boundary as damping ratios approach zero. It is expected that any optimization procedure will respond to a decrease in damping and an increase in gust response by driving the design away from damping and gust response constraint violations.

Constraints associated with maneuver loads are evaluated next to determine the quality of approximations [see Eq. (7)]. The thickness of the skin on the wing inboard box is varied over a wide range of values. The variation of the aileron hinge moment needed to sustain a desired steady-state roll at sea level, $M = 0.9$, is shown in Fig. 11. A stress constraint for a point on the skin in a 9 g symmetric pull-up in terms of a quadratic stress failure criterion[114] is illustrated in Fig. 12. The aileron hinge moment increases as aileron effectiveness is lost due to a decrease in wing skin thickness in Fig. 11. Again, with move limits of 30%, both linear and reciprocal approximations work quite well. Based on the examples presented here, it is expected that robust approximations can be constructed for constraints associated with a) deflection, stress, control surface trim angle, and hinge moment in given pull-up and roll maneuvers and b) aeroservoelastic stability and gust response limitations in given level flight conditions. Similar considerations can be expected to apply to deflection and stress constraints in "given-load" load conditions as well as natural frequency constraints based on the extensive study of these constraints within the framework of structural synthesis [116].

Typical CPU times for execution of an analysis/sensitivity cycle on the lightweight fighter are given in Table 1. In this example, three maneuver load cases and one given-load case, symmetric and antisymmetric modes are calculated, and aeroservoelastic stability and gust response are included for one level flight condition. The wing is covered by a grid of 81 points for deflection and stress calculations. A total of 3222 constraints and all of their sensitivities with respect to 40 structural, aerodynamic, and control system design variables are calculated in about 7 min. The constraints include a comprehensive mix of gauge, slope, displacement, stress, natural frequency, aeroservoelastic pole, gust response, drag, hinge moment, and control surface travel constraints. As Table 1 shows, the major part of the computation time in one analysis/sensitivity cycle is spent on the behavior sensitivity calculations. Constraint deletion[22] strategies will reduce this time considerably by retaining only a small subset of critical and potentially critical constraints as drivers in each approximate problem formulation. Only sensitivities of the retained constraints are needed, and CPU time for one detailed analysis/sensitivity/approximate problem generation stage will be reduced considerably. Thus, if about 10-15 detailed analyses are

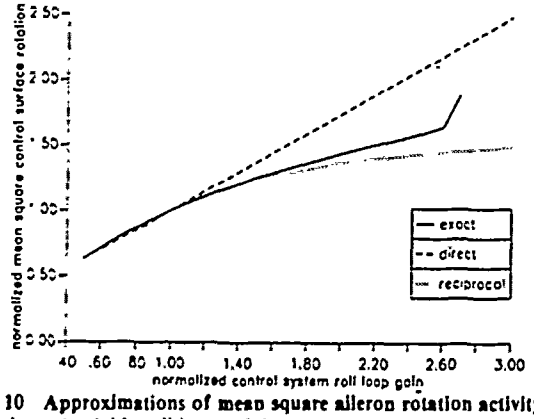

Fig. 10 Approximations of mean square aileron rotation activity in turbulence (variable roll loop gain).

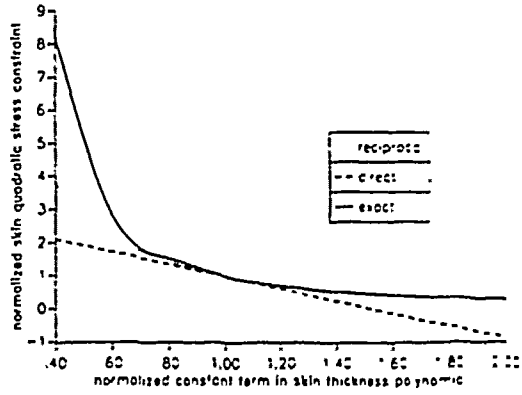

Fig. 12 Approximations of skin quadratic stress failure criterion in a 9 g symmetric pull-up maneuver (variable wing thickness).

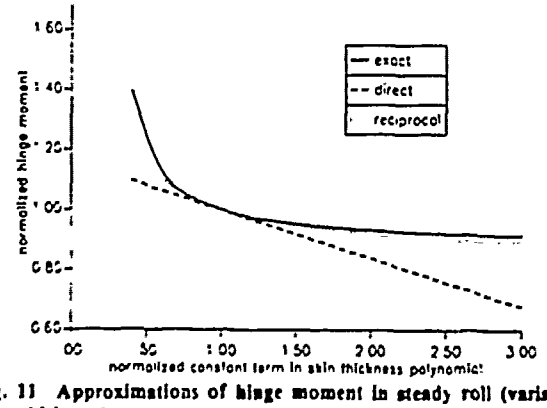

Fig. 11 Approximations of hinge moment in steady roll (variable wing thickness).

Table 1 Typical computation times, seconds

Generate M, K, and $[P]$	5.4
Given-load solution	0.09
Maneuver load solutions	0.35
Drag calculations	0.07
Natural modes	4.8
Generate A, B matrices	1.53
Aeroservoelastic stability analysis	15.58
Gust response analysis	11.44
Deflection, stresses calculations	0.86
Total analysis	40.12
Stess, deflection sensitivities	295.15
Natural frequency sensitivities	1.47
Aeroservoelastic pole sensitivities + gust response sensitivities	53.15
Total sensitivity	349.77

needed for optimization based on approximation concepts (Ref. 22), it can be anticipated that between 40–60 CPU min will be needed on the UCLA IBM 3090 Model 200 for integrated multidisciplinary optimization of practical wings.

Concluding Remarks

A general framework for wing optimization has been developed, highlighting the multidisciplinary nature of the problem. A balanced multidisciplinary wing analysis and behavior sensitivity analysis capability has been described. Emphasis was placed on various aspects of the aeroservoelastic problem formulation as well as integration and testing of the aeroelastic elements of the new method. Promising results in terms of approximation accuracy and computation times indicate that the integrated multidisciplinary optimization of practical actively controlled, fiber composite wings is within reach.

Acknowledgment

This research was supported by AFOSR Contract F49620-87-K-0003.

References

[1]Hwang, C., and Kesler, D. F., "Aircraft Active Controls – New Era in Design," *Astronautics & Aeronautics*, June 1983, pp. 70–85.

[2]Hanson, P. W., "An Aeroelastician's Perspective of Wind Tunnel and Flight Experiences with Active Control of Structural Response and Stability," NASA TM-85761, April 1984 (available from NTIS as N84-23924).

[3]Newsom, J. R., Adams, W. M., Mukhopadhyay, V., Tiffany, S. H., and Abel I., "Active Controls: A Look at Analytical Methods and Associated Tools," *Proceedings of the 14th Congress of the International Council of the Aeronautical Sciences*, Toulouse, France, 1984, ICAS Paper 84-42.3.

[4]Nissim, E., "Design of Control Laws for Flutter Suppression Based on the Aerodynamic Energy Concept and Comparisons with Other Design Methods," AIAA Paper 89-1212, April 1989.

[5]Liebst, B. S., Garrard, W. L., and Farm, J. A., "Design of a Multivariable Flutter Suppression/Gust Load Alleviation System," *Journal of Guidance, Control and Dynamics*, Vol. 11, No. 3, May–June 1988, pp. 220–229.

[6]Schmidt, D. K., and Chen, T. K., "Frequency Domain Synthesis of a Robust Flutter Suppression Control Law," *Journal of Guidance, Control and Dynamics*, Vol. 9, No. 3, May–June 1986, pp. 346–351.

[7]Lynch, R. W., and Rogers, Q. A., "Aeroelastic Tailoring of Composite Materials to Improve Performance," *Proceedings of the 16th AIAA Structures, Structural Dynamics and Materials Conference*, 1975, pp. 61–68.

[8]McCullers, L. A., "Automated Design of Advanced Composite Structures," *Mechanics of Composite Materials*, edited by Z. Hashin, Pergamon Press, New York, 1983.

[9]Lansing, W., Lerner, E., and Taylor, R. F., "Applications of Structural Optimization for Strength and Aeroelastic Design Requirements," AGARD-R-664, London, 1978.

[10]Shirk, M. H., Hertz, T. J., and Weisshaar, T. A., "Aeroelastic Tailoring—Theory, Practice, Promise," *Journal of Aircraft*, Vol. 23, No. 1, Jan. 1986, pp. 6–18.

[11]Weisshaar, T. A., "Aeroelastic Tailoring—Creative Uses of Unusual Materials," AIAA Paper 87-0976-CP, April 1987.

[12]Peloubet, R. P., "YF16 Active Control System/Structural Dynamics Interaction Instability," AIAA Paper 75-823, May 1975.

[13]Felt, L. R., Huttsell, J., Noll, T. E., and Cooley, D. E., "Aeroservoelastic Encounters," *Journal of Aircraft*, Vol. 16, No. 7, July 1979, pp. 477–483.

[14]Brinks, W. H., "F/A-18 Full Scale Development Test," *The Society of Experimental Test Pilots 24th Symposium Proceedings*, Lancaster, CA, Dec. 1980, p. 38.

[15]Swaim, R. L., "Aeroelastic Interactions with Flight Control," AIAA Paper 83-2219, Aug. 1983.

[16]Freyman, R., "Interactions Between an Aircraft Structure and Active Control Systems," *Journal of Guidance, Control and Dynamics*, Vol. 10, No. 5, Sept.–Oct. 1987, pp. 447–452.

[17]Tolson, R. H., and Sobieszczanski-Sobieski, J., "Multidisciplinary Analysis and Synthesis: Needs and Opportunities," AIAA Paper 85-0584.

[18]Sobieszczanski-Sobieski, J., and Haftka, R. T., "Interdisciplinary and Multilevel Optimum Design," *Computer Aided Optimal Design: Structural and Mechanical Systems*, edited by C. A. Mota Soares, Spring-Verlag, Berlin, 1987.

[19]Weisshaar, T. A., Newsom, J. R., Zeiler, T. A., and Gilbert, M. G., "Integrated Structure/Control Design—Present Methodology and Future Opportunities," 1986 Conference of the International Council of the Aeronautical Sciences, London, England, 1986, ICAS Paper 84-4.8.1.

[20]Ashley, H., "On Making Things the Best—The Aeronautical Uses of Optimization," *Journal of Aircraft*, Vol. 19, No. 1, Jan. 1982, pp. 5–28.

[21]Schmit, L. A., "Structural Analysis—Precursor and Catalyst," *Recent Experiences in Multidisciplinary Analysis and Optimization*, NASA CP-2327, Pt. 1, 1984, pp. 1–17.

[22]Schmit, L. A., "Structural Optimization—Some Key Ideas and Insights," *New Directions in Optimum Structural Design*, edited by E. Atrek, R. H. Gallagher, K. M. Ragsdell, O. C. Zienkiewicz, John Wiley and Sons, 1984.

[23]Hornlein, H. R. E. M., "Takeoff in Optimum Structural Design," *Computer Aided Optimal Design: Structural and Mechanical Systems*, edited by C. A. Mota Soares, Springer-Verlag, Berlin, 1987.

[24]Wilkinson, K., Markowitz, J., Lerner, E., George, D., and Batill, S. M. "FASTOP—A Flutter and Strength Optimization Program for Lifting Surface Structures," *Journal of Aircraft*, Vol. 14, No. 6, June 1977.

[25]Markowitz, J., and Isakson, G., "FASTOP3—A Strength, Deflection and Flutter Optimization Program for Metallic and Composite Structures," Air Force Flight Dynamic Lab, Wright Aeronautical Laboratories, Dayton, OH, AFFDL-TR-78-50, May 1978.

[26]Isakson, G., Pardo, H., Lerner, E., and Venkayya, V. B., "ASOP3—A Program for Optimum Structural Design to Satisfy Strength and Deflection Constraints," *Journal of Aircraft*, Vol 15, No. 7, July 1978, pp. 422–428.

[27]Lerner, E., "The Application of Practical Optimization Techniques in the Preliminary Structural Design of a Forward–Swept Wing," *The Second International Symposium on Aeroelasticity and Structural Dynamics*, Aachen, W. Germany, April 1985, DGLR-Bericht 85-02.

[28]Love, M., and Bohlman, J., "Aeroelastic Tailoring and Integrated Wing Design," *Recent Advances in Multidisciplinary Analysis and Optimization*, NASA CP-3031, Pt. 1, 1989, pp. 431–444.

[29]Lynch, R. W., Rogers, W. A., and Braymen, W. W., "Aeroelastic Tailoring of Advanced Composite Structures for Military Aircraft," AFFDL-TR-76-100, Vol. 1, April 1977.

[30]Triplett, W. E., "Aeroelastic Tailoring Studies in Fighter Aircraft Design," *Journal of Aircraft*, Vol. 17, No. 7, July 1980, pp 508–513.

[31]Triplett, W. E., "Flutter Optimization in Fighter Aircraft Design," *Recent Experiences in Multidisciplinary Analysis and Optimization*, NASA CP-2327, 1984, pp. 47–63.

[32]Haftka, R. T., "Automated Procedure for Design of Wing Structures to Satisfy Strength and Flutter Requirements," NASA TN D-7264, 1973.

[33]Haftka, R. T., "Optimization of Flexible Wing Structures Subject to Strength and Induced Drag Constraints," *AIAA Journal*, Vol. 15, No. 8, 1977, pp. 1101–1106.

[34]Starnes, J. H., Jr., and Haftka, R. T., "Preliminary Design of Composite Wings for Buckling, Strength and Displacement Constraints," *Journal of Aircraft*, Vol. 16, No. 2, 1979, pp. 564–570.

[35]Haftka, R. T., "Structural Optimization with Aeroelastic Constraints: A Survey of US Applications," *International Journal of Vehicle Design*, Vol. 7, No. 3–4, 1986, pp. 381–392.

[36]Lecina, G., and Petiau, C., "Advances in Optimal Design with Composite Materials," *Computer Aided Optimal Design: Structural and Mechanical Systems*, edited by C. A. Mota Soares, Springer-Verlag, 1987.

[37]Neill, D. J., Johnson, E. H., and Canfield, R., "ASTROS—A Multidisciplinary Automated Structural Design Tool," AIAA Paper 87-0713, April 1987.

[38]Venkayya, V. B., "Recent Developments in Large Scale Structural Optimization," *Recent Advances in Multidisciplinary Analysis and Optimization*, NASA CP-3031, 1989, pp. 1521–1540

[39]Nissim, E., and Abel, I., "Development and Application of an Optimization Procedure for Flutter Suppression Using the Aerodynamic Energy Concept," NASA TP-1337, Feb. 1978.

[40]Mayne, D. Q., Polak, E., and Sangiovanni-Vincentelli, A., "Computer Aided Design via Optimization," *Proceedings of the IFAC Workshop on Control Applications of Nonlinear Programming*, Denver, CO, June 1979.

[41]Gangsaas, D., Bruce, K. R., Blight, J. D., and Ly, U. L., "Appli-

cation of Modern Synthesis to Aircraft Control: Three Case Studies," *IEEE Transactions on Automatic Control*, Vol. AC-31, No. 11, Nov. 1986, pp. 995-1013.

[42]Gordon, V. C., and Collins, D. J., "Multi-Input Multi-Output Automatic Design Synthesis for Performance and Robustness," *Journal of Guidance, Control and Dynamics*, Vol. 9, No. 3, May-June 1986, pp. 281-287.

[43]Stimler, D. M., and Polak, E., "Nondifferentiable Optimization in Worst Case Control System Design: A Computational Example," *Proceedings of the IEEE Third Symposium on Computer-Aided Control System Design*, Arlington, VA, Sept. 1986, pp. 102-109.

[44]Mukhopadhyay, V., "Stability Robustness Improvement Using Constrained Optimization Techniques," *Journal of Guidance, Control and Dynamics*, Vol. 10, No. 2, March-April 1987, pp. 172-177.

[45]Mukhopadhyay, V., "Digital Robust Control Law Synthesis Using Constrained Optimization," *Journal of Guidance, Navigation and Control*, Vol. 12, No. 2, March-April 1989, pp. 175-181.

[46]Adams, W. M., and Tiffany, S. H., "Application of Optimization Techniques to the Design of a Flutter Suppression Control Law for the DAST ARW-2," *Recent Experiences in Multidisciplinary Analysis and Optimization*, NASA CP-2327, Pt. 1, 1984, pp. 279-295.

[47]Thwaites, B., *Incompressible Aerodynamics*, Oxford Univ. Press, Dover edition, New York, 1987, Chap. 8.

[48]Jones, R. T., "Three Dimensional Wings of Minimum Pressure Drag," *Theory of Optimum Aerodynamic Shapes*, edited by A. Miele, Academic Press, New York, 1965, Chap. 8.

[49]McDonald, J. W., and Stevens, J. R., "Optimized Design of Subsonic Lifting Surfaces," *Journal of Aircraft*, Vol. 7, No. 5, Sept.-Oct. 1970, pp. 442-447.

[50]Hicks, R. M., Murman, E. M., and Vanderplaats, G. N., "An Assessment of Airfoil Design by Numerical Optimization," NASA TM-X-3092, July 1974.

[51]Feifel, W. M., "Optimization and Design of Three-Dimensional Aerodynamic Configurations of Arbitrary Shape by a Vortex Lattice Method," *Vortex Lattice Utilization*, NASA SP-405, 1976, pp. 71-88.

[52]Lamar, J. E., "Minimum Trim Drag Design for Interfering Lifting Surfaces using Vortex-Lattice Methodology," *Vortex Lattice Utilization*, NASA SP-405, 1976, pp. 89-111.

[53]Hicks, R. M., and Henne, P. A., "Wing Design by Numerical Optimization," *Journal of Aircraft*, Vol. 15, July 1978, pp. 407-412.

[54]Vanderplaats, G. N., "Efficient Algorithm for Numerical Airfoil Optimization," *Journal of Aircraft*, Vol. 16, No. 12, Dec. 1979, pp. 842-847.

[55]Rajeswri, B., and Prabhu, K. R., "Optimum Flap Schedules and Minimum Drag Envelopes for Combat Aircraft," *Journal of Aircraft*, Vol. 24, No. 6, June 1987, pp. 412-414.

[56]Gupta, S. C., "GENMAP—Computer Code for Mission Adaptive Profile Generation," *Journal of Aircraft*, Vol. 25, No. 8, Aug. 1988, pp. 766-768.

[57]McGeer, T., "Wing Design for Minimum Drag with Practical Constraints," *Journal of Aircraft*, Vol. 21, No. 11, Nov. 1984, pp. 879-886.

[58]Lan, C. E., "Application of CONMIN to Wing Design Optimization with Vortex Flow Effect," *Recent Experiences in Multidisciplinary Analysis and Optimization*, NASA CP-2327, Pt. 1, 1984, pp. 297-308.

[59]Bodden, D. S., and Junkins, J. L., "Eigenvalue Optimization Algorithms for Structure/Controller Design Iterations," *Journal of Guidance, Control and Dynamics*, Vol. 8, Nov.-Dec. 1985, pp. 697-706.

[60]Lust, R. V., and Schmit, L. A., "Control-Augmented Structural Synthesis," *AIAA Journal*, Vol. 26, No. 1, Jan. 1988, pp. 86-95.

[61]Onoda, J., and Haftka, R. T., "An Approach to Structure/Control Simultaneous Optimization for Large Flexible Spacecraft," *AIAA Journal*, Vol. 25, No. 8, Aug. 1987, pp. 1133-1138.

[62]Haftka, R. T., "Optimum Control of Structures," *Computer Aided Optimal Design: Structural and Mechanical Systems*, edited by C. A. Mota Sores, Springer-Verlag, Berlin Heidelberg, 1987, pp. 381-388.

[63]Khot, N. S., "Minimum Weight and Optimal Control Design of Space Structures," *Computer Aided Optimal Design: Structural and Mechanical Systems*, edited by C. A. Mota Soares, Springer-Verlag, Berlin Heidelberg, 1987.

[64]Gilbert, M. G., and Schmidt, D. K., "Integrated Structure/Control Law Design by Multilevel Optimization," AIAA Paper 89-3470-CP, Aug. 1989.

[65]Junkins, J. L., and Rew, D. W., "Unified Optimization of Structures and Controllers," *Large Space Structures Dynamics and Control*, edited by S. N. Atluri and A. K. Amos, Springer-Verlag, Berlin Heidelberg, 1988.

[66]Thomas, H. L., and Schmit, L. A., "Control Augmented Structural Synthesis with Dynamic Stability Constraints," AIAA Paper 89-1216, April 1989.

[67]Grossman, B., Gurdal, Z., Strauch, G. J., Eppard, W. M., and Haftka, R. T., "Integrated Aerodynamic/Structural Design of a Sailplane Wing," *Journal of Aircraft*, Vol. 25, No. 9, Sept. 1988, pp. 855-860.

[68]Haftka, R. T., Grossman, B., Eppard, W. M., and Kao, P. J., "Efficient Optimization of Integrated Aerodynamic-Structural Design," *Proceedings of the International Conference on Inverse Design Concepts and Optimization in Engineering Sciences—II*, University Park, PA, Oct. 1987.

[69]Haftka, R. T., Grossman, B., Kao, P. J., Polen, D. M., and Sobieszczanski-Sobieski, J., "Integrated Aerodynamic-Structural Design of a Forward-Swept Transport Wing," *Recent Advances in Multidisciplinary Analysis and Optimization*, NASA CP-3031, 1989, pp. 445-463.

[70]Barthelemy, J. F. M., and Bergen, F. D., "Shape Sensitivity Analysis of Wing Static Aeroelastic Characteristics," *Journal of Aircraft*, Vol. 26, No. 8, Aug. 1989, pp. 712-717.

[71]Kapania, R., Bergen, F., and Barthelemy, J., "Shape Sensitivity Analysis of Flutter Response of a Laminated Wing," AIAA Paper 89-1267, April 1989.

[72]Zeiler, T. A., and Weisshaar, T. A., "Integrated Aeroservoelastic Tailoring of Lifting Surfaces," *Journal of Aircraft*, Vol. 25, No. 1, Jan. 1988, pp. 76-83.

[73]Gilbert, M. G., "Sensitivity Method for Integrated Structure-Active Control Law Design," *Sensitivity Analysis in Engineering*, NASA CP 2457, 1987.

[74]Karpel, M., "Sensitivity Derivatives of Flutter Characteristics and Stability Margins for Aeroservoelastic Design," AIAA Paper 89-3467, Aug. 1989.

[75]Gilbert, M. G., "Results of an Integrated Structure/Control Law Design Sensitivity Analysis," *Recent Advances in Multidisciplinary Analysis and Optimization*, NASA CP-3031, 1989, pp. 727-745.

[76]Gilbert, M. G., Schmidt, D. K., and Weisshaar, T. A., "Quadratic Synthesis of Integrated Active Controls for an Aeroelastic Forward Swept Wing Aircraft," *Journal of Guidance, Control and Dynamics*, Vol. 7, March-April 1984, pp. 190-196.

[77]Sensburg, O., Schmidinger, G., and Fullhas, K., "Integrated Design of Structures," *Journal of Aircraft*, Vol. 26, No. 3, March 1989, pp. 260-270.

[78]Schweger, J., Sensburg, O., and Berns, H., "Aeroelastic Problems and Structural Design of a Tailless CFC Sailplane," *2nd International Symposium on Aeroelasticity and Structural Dynamics*, Aachen, W. Germany, April 1985.

[79]Morris, S., and Kroo, I., "Aircraft Design Optimization with Multidisciplinary Performance Criteria," *Recent Advances in Multidisciplinary Analysis and Optimization*, NASA CP-3031, 1989, pp. 1219-1235.

[80]Morris, S., and Kroo, I., "Aircraft Design Optimization with Multidisciplinary Performance Criteria," AIAA Paper 89-1265, April 1989.

[81]Livne, E., "An Integrated Approach to the Optimum Design of Actively Controlled Composite Wings," *Recent Advances in Multidisciplinary Analysis and Optimization*, NASA CP-3031, 1989, pp. 897-918.

[82]Sharpe, W. E., and Newton, J. B., "Examples of Static Aeroelastic Effects on Present Combat Aircraft Projects," *Static Aeroelastic Effects on High Performance Aircraft*, AGARD CP-403, 1987.

[83]Schmidinger, G., and Sensburg, O., "Static Aeroelastic Considerations in the Definition of Design Loads for Fighter Airplanes," *Static Aeroelastic Effects on High Performance Aircraft*, AGARD CP-403, 1986.

[84]Booker, D., "Aeroelastic Tailoring for Control and Performance—Are Requirements Compatible?" *Combat Aircraft Maneuverability*, AGARD CP-319, 1981.

[85]Weisshaar, T. A., and Nam, C., "Aeroservoelastic Tailoring for Lateral Control Enhancement," *Recent Advances in Multidisciplinary Analysis and Optimization*, NASA CP-3031, 1989, pp. 803-814.

[86]Moynes, J. F., and Gallagher, J. T., "Flight Control System Design for Ride Qualities of Highly Maneuverable Fighter Aircraft," *Guidance and Control Design Considerations for Low Altitude and Terminal Area Flight*, AGARD CP-240.

[87]Swaim, R. L., and Yen, W. Y., "Effects of Dynamic Aeroelasticity on Aircraft Handling Qualities," *Journal of Aircraft*, Vol. 16, No. 9, Sept. 1979, pp. 635-637.

[88]Swaim, R. L., and Poopaka, S., "An Analytical Pilot Rating

Pof.4

EXPLORATORY DESIGN STUDIES USING AN INTEGRATED MULTIDISCIPLINARY SYNTHESIS CAPABILITY FOR ACTIVELY CONTROLLED COMPOSITE WINGS*

E. Livne*, L.A. Schmit** and P.P. Friedmann***

Mechanical, Aerospace and Nuclear Engineering Department
University of California
Los Angeles, California 90024

Abstract

Analysis and synthesis techniques used in a newly developed multidisciplinary control augmented fiber composite wing optimization capability are reviewed. Structural, aerodynamic and control system mathematical models that are suitable for the preliminary design of real airplanes are used in an integrated manner to synthesize improved designs of wings and their active control systems. Optimization techniques developed for structural synthesis are adapted to the integrated multidisciplinary wing synthesis problem, in which constraints from several disciplines are taken into account simultaneously and the design space is opened up to include structural, control system and aerodynamic design variables. The effectiveness and efficiency of the new capability are studied using a mathematical model of a remotely piloted vehicle (RPV).

Introduction

Multidisciplinary interactions have always been at the heart of airplane wing design. The introduction of active control technology[1-3] and composite structural tailoring[3-6] during the last fifteen years have made these interactions more complex and more important. Recent experience has shown that not accounting properly for multidisciplinary interactions during the design process can lead to dangerous consequences[7-8]. At the same time the benefits of multidisciplinary integration have become widely recognized motivating extensive research and influencing design[9-11].

* This research was supported by AFOSR Contract F49620-87-K-0003.

* Graduate Research Assistant, Student Member AIAA.

** Professor of Engineering and Applied Science, Fellow AIAA, ASCE, Member ASME

*** Professor and Chairman, Associate Fellow AIAA, Member AHS,ASME

Still the design practice of the past, which was based on a sequential, compartmented approach, is followed today. True, advanced analysis and testing tools have been developed to address multidisciplinary interaction. Active flutter suppression, maneuver load control, gust alleviation and ride smoothing techniques are utilized, to mention a few examples. Optimization techniques are used for control system synthesis, aerodynamic design and aeroelastic tailoring. Structural wing synthesis subject to structural, aeroelastic and aerodynamic performance constraints has successfully followed in the footsteps of structural synthesis[12-13] using a variety of computer codes and techniques[14-18].

However, the application of optimization techniques is still done one discipline at a time. True integration in design, namely the synthesis of wings subject to a set of multidisciplinary constraints addressing design variables from several disciplines simultaneously, has not been carried out.

Especially complex and difficult is the integrated synthesis of wing structure and its active control system. In the few cases where integrated synthesis was studied[19-21] the mathematical models used were so simplified that they did not provide an assessment of the techniques needed to optimize realistic wings, and the accumulation of practical design experience was not possible. Thus, the application of modern optimization techniques to wing design involving a diverse mix of constraints and design variables based on analyses from several disciplines (structures, structural dynamics, aeroelasticity, control, handling qualities) has not yet been treated in a comprehensive and realistic manner.

Reference 22 describes a synthesis capability for actively controlled fiber composite lifting surfaces. It discusses structural, aerodynamic and control system modeling techniques adopted and modified to challenge the formidable computational task of carrying out analysis and behavior sensitivity calculations for this problem with computer resources that will make optimization practical and with accuracy that is sufficient for preliminary design. It is based on the generalization of the nonlinear programming

approximation concepts (NLP/MC)[12-13] approach from structural synthesis to multidisciplinary optimization.

The present paper reports first results of wing control augmented structural synthesis achieved using the new capability. The applicability of approximation concepts to the control augmented structural synthesis of wings is studied. Examination of optimization convergence as influenced by including approximations of new constraints (especially aeroservoelastic stability and gust response constraints) guides identification of effective move limits, convergence criteria and approximation types to be used. Examples of integrated optimization of realistic wings and their active control systems with structural and control system design variables subject to gage, stress, aeroservoelastic stability and gust response constraints offer an improved understanding of this complex synthesis problem.

Review of Mathematical Modeling Techniques

Structural Modeling

The integrated optimum design capability is based on approximate analysis techniques for the required disciplines, which are consistent with each other in terms of accuracy and efficiency and thus lead to a balanced treatment of practical wings. In the structures area, a rather general equivalent plate analysis[23], which builds on the basic ideas underlying the TSO computer code[14] and incorporates additional recent developments proposed by Giles[24], is used. High order simple power series are used for approximating displacements over wing planforms made of several trapezoidal segments to obtain accurate stress as well as displacement information. Stresses in spar and rib caps can be calculated in addition to composite skin stresses. Configurations made of several plate segments attached to each other via springs (accounting for attachment stiffness and actuator stiffness) can be analyzed to simulate wing/control surface configurations.

Aerodynamics

The equivalent plate structural analysis documented in Ref. 23 is integrated with the PCKFM (Piecewise Continuous Kernel Function Method) developed by Nissim and Lottati for lifting surface unsteady aerodynamics[25-28]. This method is particularly suitable for calculating the generalized unsteady air loads (on lifting surfaces made up of wing and control surface elements) that are needed for active flutter suppression and gust alleviation studies.

When the optimization of the design for aeroservoelastic stability is addressed and modern control techniques are to be implemented, it is necessary to cast the aeroelastic equations of motion in LTI (Linear Time Invariant) state space form. It then follows that some approximation of the unsteady aerodynamic loads in terms of rational functions of the Laplace variable is needed.

The method of Roger[29] has been widely used for finite dimensional unsteady aerodynamic loads representation for quite a while. The Minimum State Method, developed by Karpel[30] and recently studied in Ref. 31, is found to be attractive because it has the potential for generating accurate approximations to unsteady generalized aerodynamic forces, while adding only a small number of augmented states to the mathematical model of the aeroservoelastic system. Both methods are available in the present capability.

Control System

The integrated aeroservoelastic system is modeled as a Linear Time Invariant (LTI) system. Since the number of sensors and control surfaces is small in real airplanes, the complex, high order control laws generated by multivariable control system design techniques are avoided at this stage. A block diagram of the actively controlled aeroservoelastic system is shown in Figure 1. Airplane motions (acceleration and angular rates) are measured by a set of sensors placed on the structure. The resulting signals, y_{SE}, are used as inputs to the control law block which commands control surface actuators The control surface motions, q_c, guarantee stability and desirable dynamic response of the complete system.

The control system is completely described by the location of sensors and control surfaces and by the transfer functions of the sensors,control laws and actuators. Gain scheduling can be adopted by assigning different control laws to different flight conditions.

Modeling Capabilities

The combination of modern equivalent plate structural modeling and PCKFM lifting surface aerodynamics is assumed to be adequate for this exploratory venture into multidisciplinary practical wing synthesis. In addition to a reliable prediction of deformations, stresses, flutter results and static aeroelastic effects, quite good hinge moments[32] and induced drag[33,34] can be expected for subsonic and supersonic small angle of attack flight The analysis is adequate for addressing flight stability and control problems of the elastic airplane[35]. Its aerodynamic predictions might be improved by using correction

factor techniques if any measured data are available. As to control system modeling, the techniques used here make it possible to properly model real flight control or active flutter suppression tems. Effects of real actuators and sensors on trol system performance are automatically taken into account through their given transfer functions.

Design Variables

Ref. 22 sets forth a framework for multidisciplinary wing synthesis and describes a hierarchy of design variables consisting of sizing type design variables at the lowest level, followed by shape and then toplogical type design variables. This classification applies to design variables spanning structures,control and aerodynamics. Here, in addition to a balanced approach to behavior prediction in terms of the analysis techniques selected, a balance is maintained in level of optimization by focusing on sizing type design variables for all disciplines considered.

Structural Design Variables

Figure 2 shows an airplane modeled as an assembly of flexible lifting surfaces. Each lifting surface is modeled as an equivalent plate whose stiffness is controlled by contributions from thin cover skins (fiber composite laminates) and the internal structure (spar and rib caps). Plate sections are connected to each other via stiff springs (representing hinge stiffness at attach points) and flexible springs (representing the stiffness of actuators and their backup structure). Each wing section can be made of several trapezoidal parts. Concentrated masses are used to model nonstructural items and balance masses.

The vertical displacement, w, of each wing section is approximated by a Ritz polynomial series of the form

$$w(x,y,t) = \sum_{i=1}^{N_w} q_i(t)\, x^{m_i}\, y^{n_i} \qquad (1)$$

where x and y are chordwise and spanwise coordinates respectively. m_i and n_i are powers reflecting the type of polynomial series used. It can be a complete polynomial in x and y or a product of polynomials in x and y (Ref. 23). The depth of a wing section is given by a polynomial

$$h(x,y) = \sum_{i=1}^{N_h} H_i\, x^{r_i}\, y^{s_i} \qquad (2)$$

where the H_i are preassigned parameters. Thickness distribution of a typical skin layer is represented by

$$t(x,y) = \sum_{i=1}^{N_t} T_i\, x^{k_i}\, y^{l_i} \qquad (3)$$

Rib and spar cap areas are allowed to vary linearly over their length η

$$A(\eta) = A_0 + A_1\, \eta \qquad (4)$$

The present equivalent plate modeling capability[23] makes it possible to efficiently analyze combined wing box/control surface configurations. A wing assembly and a canard or horizontal tail may be attached to a fuselage (modeled as a flexible beam or a flexible plate) to simulate complete airplane configurations. The level of modeling detail can be selected independently for each section. Therefore the degree of detail used to model control surfaces for analysis and synthesis is not limited, as is the case in the TSO code.

At the present stage of research structural topology, shape and material properties are preassigned. Skin layer fiber orientation are available as design variables. For skin layer thicknesses (Eq. 3) the coefficients of the thickness power series serve as design variables. This guarantees smooth thickness variation for each layer. For spar and rib cap areas (Eq. 4) two coefficients are used as design variables for each spar or rib. Concentrated masses at preassigned locations and spring constants for linear and rotational springs can also be treated as design variables.

Aerodynamic Design Variables

Wing cross section or aerodynamic planform topology are preassigned here. Performance and loads in quasi-static maneuvers can be influenced by the jig shape (initial camber) of the wing and by proper deflection of leading edge and trailing edge control surfaces. The initial camber of the wing is given by a series

$$w^0(x,y,t) = \sum_{i=1}^{N_w} q_i^0(t)\, x^{m_i}\, y^{n_i} \qquad (5)$$

where the powers m_i and n_i are identical to those in Eq. 1 and any subset of the coefficients q_i^0 can serve as design variables. The deflections δ_i of control surfaces (for each maneuver point seperately) are also available as design variables.

Control System Design Variables

The control system design variables of the sizing type consist of the values of coefficients in the numerator and denominator of control law transfer

factor techniques if any measured data are available. As to control system modeling, the techniques used here make it possible to properly model real flight control or active flutter suppression systems. Effects of real actuators and sensors on control system performance are automatically taken into account through their given transfer functions.

Design Variables

Ref. 22 sets forth a framework for multidisciplinary wing synthesis and describes a hierarchy of design variables consisting of sizing type design variables at the lowest level, followed by shape and then toplogical type design variables. This classification applies to design variables spanning structures,control and aerodynamics. Here, in addition to a balanced approach to behavior prediction in terms of the analysis techniques selected, a balance is maintained in level of optimization by focusing on sizing type design variables for all disciplines considered.

Structural Design Variables

Figure 2 shows an airplane modeled as an assembly of flexible lifting surfaces. Each lifting surface is modeled as an equivalent plate whose stiffness is controlled by contributions from thin cover skins (fiber composite laminates) and the internal structure (spar and rib caps). Plate sections are connected to each other via stiff springs (representing hinge stiffness at attach points) and flexible springs (representing the stiffness of actuators and their backup structure). Each wing section can be made of several trapezoidal parts. Concentrated masses are used to model nonstructural items and balance masses.

The vertical displacement, w, of each wing section is approximated by a Ritz polynomial series of the form

$$w(x,y,t) = \sum_{i=1}^{N_w} q_i(t)\, x^{m_i}\, y^{n_i} \qquad (1)$$

where x and y are chordwise and spanwise coordinates respectively. m_i and n_i are powers reflecting the type of polynomial series used. It can be a complete polynomial in x and y or a product of polynomials in x and y (Ref. 23). The depth of a wing section is given by a polynomial

$$h(x,y) = \sum_{i=1}^{N_h} H_i\, x^{r_i}\, y^{s_i} \qquad (2)$$

where the H_i are preassigned parameters. Thickness distribution of a typical skin layer is represented by

$$t(x,y) = \sum_{i=1}^{N_t} T_i\, x^{k_i}\, y^{l_i} \qquad (3)$$

Rib and spar cap areas are allowed to vary linearly over their length η

$$A(\eta) = A_0 + A_1\,\eta \qquad (4)$$

The present equivalent plate modeling capability[21] makes it possible to efficiently analyze combined wing box/control surface configurations. A wing assembly and a canard or horizontal tail may be attached to a fuselage (modeled as a flexible beam or a flexible plate) to simulate complete airplane configurations. The level of modeling detail can be selected independently for each section. Therefore the degree of detail used to model control surfaces for analysis and synthesis is not limited, as is the case in the TSO code.

At the present stage of research structural topology, shape and material properties are preassigned. Skin layer fiber orientation are available as design variables. For skin layer thicknesses (Eq. 3) the coefficients of the thickness power series serve as design variables. This guarantees smooth thickness variation for each layer. For spar and rib cap areas (Eq. 4) two coefficients are used as design variables for each spar or rib. Concentrated masses at preassigned locations and spring constants for linear and rotational springs can also be treated as design variables.

Aerodynamic Design Variables

Wing cross section or aerodynamic planform topology are preassigned here. Performance and loads in quasi-static maneuvers can be influenced by the jig shape (initial camber) of the wing and by proper deflection of leading edge and trailing edge control surfaces. The initial camber of the wing is given by a series

$$w^0(x,y,t) = \sum_{i=1}^{N_w} q_i^0(t)\, x^{m_i}\, y^{n_i} \qquad (5)$$

where the powers m_i and n_i are identical to those in Eq. 1 and any subset of the coefficients q_i^0 can serve as design variables. The deflections δ_i of control surfaces (for each maneuver point seperately) are also available as design variables.

Control System Design Variables

The control system design variables of the sizing type consist of the values of coefficients in the numerator and denominator of control law transfer

analyses (e.g. 3). Finite dimensional state space unsteady aerodynamic approximations can be generated for the full order aerodynamic matrices at the start of optimization, or directly for modally reduced aerodynamic matrices during optimization whenever the modal basis is changed[22].

Gust Response Analysis

The RMS (root mean square) values of control surface deflections and rates as well as RMS values of selected sensor measurements due to continuous atmospheric turbulence are calculated for different flight conditions. Both Dryden and rational approximations for the Von-Karman turbulence spectra are implemented. The relevant quantities are RMS values of control surface deflections $\{q_c\}$, rates $\{\dot{q}_c\}$ and sensor measurements $\{y_{SE}\}$.

The state space equations (Eq. 8) are transformed into standard form

$$s\{x(s)\} = [\tilde{A}]\{x(s)\} + \{\tilde{B}\}\hat{w}(s) \tag{9}$$

Since only $\{q_c\}$, $s\{q_c\}$ and $\{y_{SE}\}$ are considered[22] the output, y_k, is given by

$$y_k = \{C_k\}^T\{x\} \tag{10}$$

where $\{C_k\}$ is either constant or a function of control system design variables.

The state covariance matrix is a solution of a Lyapunov's matrix equation[39] in the form

$$[\tilde{A}][X] + [X][\tilde{A}]^T = -\{\tilde{B}\}[Q_w]\{\tilde{B}\}^T \tag{11}$$

where $[Q_w]$ is the intensity matrix of the gaussian white noise, $\hat{w}$. The Hessenberg-Schur method[40] is used to solve Eq. 11.

Induced Drag Analysis

Induced drag is calculated for the elastic lift distribution during maneuvers. Drag values assuming either full leading edge suction(fully attached flow) or no leading edge suction (separated flow at the leading edge) or a combination of these[41] are available. The induced drag D_I can be expresssed in quadratic form

$$D_I = \frac{1}{2}\rho U^2 S\{\bar{\bar{q}}\}^T[A_D]\{\bar{\bar{q}}\} \tag{12}$$

where $\frac{1}{2}\rho U^2$ is the dynamic pressure and S is a reference area and $[A_D]$ is an aerodynamic matrix. When the jig shape generalized displacements $\{q^0\}$ and control surface rotations $\{\delta\}$ are small, then (within linearized lifting surface theory) this matrix is fixed and does not depend on either structural or aerodynamic design variables[42]. It is generated once for the set of Ritz polynomials (Eq. 1), control surface rotations and downwash due to pitch rate degrees of freedom in symmetric pull-up maneuvers. $\bar{\bar{q}}$ is the following vector

$$\{\bar{\bar{q}}\} = \begin{Bmatrix} q \\ \delta \\ 0 \end{Bmatrix} + \begin{Bmatrix} q^0 \\ 0 \\ \theta \end{Bmatrix} \tag{13}$$

where q and q^0 are defined in Eqs. 1 and 5. The vector δ contains all control surface rotations and θ is the pitch rate. Thus, D_I depends on the structural and aerodynamic design variables through the generalized deflections $\{q\}$ in maneuver, the jig shape generalized coefficients $\{q^0\}$ and control surface rotations $\{\delta\}$.

Behavior Functions

The following behavior functions can be evaluated with the present capability: elastic displacements; elastic twist; spar/rib cap stresses; skin combined stress failure criteria[43]; natural frequencies; real and imaginary parts of aeroservoelastic poles; RMS of random control surface deflections and rates due to gust; RMS of sensor measurements in gust; total mass; lift and drag coefficients; control surface deflections and hinge moments in maneuvers; roll rate or load factor in maneuvers.

Control surface effectiveness is not addressed directly at this stage. Instead the synthesis focuses on sustaining a desired roll rate or load factor while keeping hinge moments, control surface deflections and stresses within allowable bounds.

Aeroservoelastic stability is gauaranteed by providing enough damping at each flutter critical aeroservoelastic pole throughout the flight envelope[44]. Handling qualities can be addressed via inequality constraints on the aeroservoelastic pole locations (e.g. short period root placement) and pilot seat acceleration due to atmospheric turbulence[45,46]. The control surface deflection needed for trim and overall performance in a given maneuver and its RMS activity due to gusts can be combined in a single constraint to avoid saturation[47,48].

Individual behavior functions or their combinations can serve as objective functions. Possible alternatives are mass, drag(to be minimized), steady roll rate or lift to drag ratio (to be maximized). RMS of aileron rotation or rotation rate due to turbulence or a combination of any of these.

Behavior Sensitivity Analysis

Implicit differentiation of the analysis equations is used here to derive analytical expressions for the derivatives of all behavior functions with respect to all design variables[22,49]. This results in a computer code which is much larger and more complicated than if finite difference derivatives were used. However, analytical sensitivities are free from numerical problems associated with finite difference step size selection and are attractive in the context of multidisciplinary synthesis because of superior computational efficiency.

Approach to Integrated Optimization.

Once the preassigned parameters, design variables, failure modes, load conditions and objective function are selected, the integrated optimization problem can be cast as a nonlinear programming problem of the form

$$\min_{\{X\}} \quad F(\{X\}) \tag{14}$$

$$s.t. \quad \{g(\{X\})\} \le \{0\}$$

$$\{X^L\} \le \{X\} \le \{X^U\}$$

where F is the objective function, $\{X\}$ is the vector of design variables, $\{g\}$ is a vector of inequality constraints and $\{X^L\}$, $\{X^U\}$ are vectors of design variable lower and upper bounds.

The nonlinear programming approach combined with approximation concepts (NLP AC approach) has proven to be an effective method for solving structural synthesis problems[12,13] and here it is adapted to the multidisciplinary design optimization task. In this method relatively few detailed analyses are carried out during optimization. Each analysis and the associated behavior sensitivity analysis serve as a basis for constructing approximations to the objective and constraint functions in terms of the design variables. Thus, a series of explicit approximate optimization problems is solved converging to an optimal design.

The main advantage of this approach is in its generality. No apriori assumptions have to be made about the set of active constraints at the optimum. Given an initial design, a local optimum is sought using mathematical programming techniques. Thus it is especially suitable for multidisciplinary optimization, where the problem is large and complicated and past experience does not provide much intuitive guidance. However, for this approach to be practical it is crucial to avoid too many detailed analyses. Efficient analysis sensitivity calculations and robust, explicit approximations are essential in this context. The CONMIN[50] code is used here for constrained function minimization.

Test Cases

The accuracy, power and computational efficiency of the present capability are discussed in Ref. 22 using a mathematical model of a light weight fighter similar to the YF-16. For the present optimization studies a mathematical model of a small remotely piloted vehicle is used. Its planform geometry is shown in Fig. 3. A 6.8 aspect ratio, biconvex 10% t/c wing is actively controled by a small control surface located at about 80% semi-span towards the tip. The control surface chord is 20% of the local wing chord, and it is driven by an actuator whose transfer function is preassigned

$$\frac{q_{c1}}{\delta_1} = \frac{1.7744728\times10^7}{\{(s+180)(s^2+251s+314^2)\}} \tag{15}$$

The wing control surfaces are only used for active flutter control. The elevators are used for rigid body pitch and roll. The elevator actuator transfer function is

$$\frac{q_{c2}}{\delta_2} = \frac{20}{(s+20)} \tag{16}$$

q_{ci} and δ_i are the actuator actual deflection and its command, respectively.

The RPV structure is modeled as an assembly of four equivalent plates. A flexible wing is attached to a rigid fuselage and rigid control surfaces. The wing is divided into three trapezoids. The two trailing edge extensions, to the left and right of the control surface, are assumed fixed. The main wing box structure, extending from root to tip spanwise and to 80% chordwise, is the structure to be synthesized, and alternative designs can used for the test examples. The weight of fuselage, control surfaces and non-structural wing mass is 308 Kgm for a half airplane. A Dryden gust model with a scale length of 518.16 meters and a vertical gust RMS velocity of 1.06 m/sec is used.

Following Refs. 51,52 an accelerometer is placed on the wing strip containing the control surface. It is located in the middle(spanwise) and 0.65 chord point of the strip. Its measurement serves as an input to a control law which, in turn, generates an input command, δ, to the actuator of the wing control surface.

The set of load conditions for wing stress calculations consists of three 2g symmetric pull-ups at sea level, 10,000 feet and 20,000 feet. In the "maneuver load" calculations (Eq. 6) the airplane is trimmed using the elevator. All stress constraints reflect a 1.5 safety factor. Flutter, gust and aeroservoelastic stability calculations, though, are carried out at sea

level, Mach 0.9 for the cantilevered wing in the examples described herein. This is done intentionally in order to first examine flutter suppression/structural optimization using a realistic but simple example, leaving flight mechanics issues for future studies.

It should be reemphasized that the simplifying assumptions above are made only for illustrative purposes and to facilitate physical interpretation of the design optimization results. The present capability can handle airplane models where multiple equivalent plate elements are synthesized subject to several pull-up or rolling maneuvers. Control systems can contain many control elements and control laws, and aeroservoelastic gust response analyses can be carried out for symmetric/anti-symmetric free free motion in several flight conditions. Using the data manager of Ref. 53, the modeling detail and model size are only limited by available computer memory. The CPU time limits will determine the number of load conditions and flight conditions for aeroservoelastic gust response analysis. However, as shown later, quite complex problems can be handled with reasonable computer resources.

The control law used for this study is the Localized Damping Type Transfer Function (LDTTF) described in Ref. 54. This low order control law provides damping "locally" in the range of frequencies where damping is needed. Its form is

$$\delta = \frac{a_c}{(s^2 + b_c s + c_c)} \ddot{w}_{0.65c} \tag{17}$$

where

$$y_{SL} = \ddot{w}_{0.65c}$$

is the accelerometer measurement and a_c, b_c, c_c are control system design variables. The denominator coefficients can be associated with equivalent damping ζ_c and natural frequency ω_c of the control law

$$c_c = \omega_c^2 \tag{18}$$

$$b_c = 2\zeta_c\omega_c \tag{19}$$

Thus, c_c and b_c determine the center frequency and gain peak width of the control law transfer function while a_c determines the effective gain.

The preassigned accelerometer transfer function is

$$\frac{y_{SL}}{\ddot{w}_{0.65c}} = \frac{314^2}{(s^2 + 376.8s + 314^2)} \tag{20}$$

The LDTTF control law is used here without compensation for sensor and actuator transfer functions[52].

Results

For a first sequence of numerical studies a wing tip pod is added to the wing simulated by two 2.5 Kgm masses at the forward and aft points of the tip. The wing box construction consists of all aluminum cover skins and there are no spars or ribs in order to simplify the model and introduce as few structural design variables as possible. All stress carrying capacity is thus confined to the skins, which are held together mathematically by the plate assumptions and in practice by an array of minimum gage spars/ribs whose stiffness can be neglected. The Von-Mises yield criteria is used. The skin thickness distribution is a nine term polynomial in x and y, whose terms are formed from of the polynomial product $(1, x, x^2)(1, y, y^2)$. There are thus nine structural design variables.

Figure 4 shows skin mass convergence histories for three synthesis cases, all starting with a 1 mm uniform skin distribution. In the first case, mass is minimized subject to stress and minimum gage constraints only. Minimum skin thickness is 0.381 mm (.015 inch), and the Von Mises equivalent stress and minimum gage are constrained at 25 points on the wing box (5 chordwise x 5 spanwise). This is the "stress design" without flutter constraints. In this case the skin mass is reduced in 11 full analyses approximate problem optimization cycles from 4.486 to 1.743 Kgm. The stress design is aeroelastically unstable. It flutters at sea level, Mach 0.9. And thus, a second synthesis is carried out. The same nine structural design variables are used and the same stress and minimum gage limitations are imposed, however dynamic aeroelastic stability constraints are now added to the set of requirements that must be satisfied.

It is required that at sea level, Mach 0.9 there should be at least 4.5% equivalent viscous damping in the two lowest frequency poles, and at least 1.5% damping in the next three. (aerodynamic poles which have very large damping ratios are ignored when the closed loop system poles are ordered by damped frequency). In seven synthesis cycles the optimization process reduces skin mass to 3.094 Kgm. As expected, a stiffer and heavier wing is needed to prevent flutter. The constraint which drives this design is a damping constraint associated with a flutter pole at 14.4 Hz.

We next address an important question: How effective can an active control system be in further reducing the minimum structural weight needed to satisfy stress and flutter constraints? Three control system design variables are now added to the nine structural design variables. Wing skin mass minimization is carried out subject to stress, minimum gage and dynamic aeroelastic stability constraints starting

from a 1 mm thick uniform skin and a control law of the form:

$$\frac{\delta}{y_{SE}} = \frac{2000}{(s^2 + 40s + 10{,}000)}$$

As shown in Fig. 4, the skin mass for this case is reduced to 1.838 Kgm. Examination of the optimization results reveals that the driving constraint is again the damping in a pole. Its frequency is 17.03 Hz, and the final damping ratio is .067, which implies that with tighter convergence criteria for terminating the optimization, additional weight savings could be achieved (1% diminishing return on three consecutive approximate problem optimizations is used as a convergence criterion). In any event, the weight in the third case is brought back almost to the level of the stress design weight. Convergence is slower. It took 27 Cycles and 27 CPU minutes on the UCLA IBM 3090-4. Also, while rapid convergence was achieved for the cases with only structural design variables with move limits of 40%, it was necessary to use 10% move limits when control system design variables were added in order to protect the accuracy of system pole approximations. This explains the slower convergence of the third run.

Minimum mass synthesis of the wing with structural and control system design variables, subject to stress, gage and aeroservoelastic stability constraints was tried again. This time the initial structural design is the unstable stress design of the first case. Initial values for control system design variables are now different. The optimization is started with $1500/(s^2 + 40s + 4000)$. Figure 5 shows the two skin mass convergence histories for the design starting from 1mm uniform skin and the one starting with the stress design. Starting with the 1.743 Kgm skin of the stress design, the mass minimization progresses by first adding mass to stiffen the wing followed by manipulation of the control system design variables to stabilize the wing with the smallest weight penalty possible. In fact, the final skin weighs 1.745 Kgm, practically the same as if there were no flutter constraints at all.

Final skin thickness distributions for the stress, stress + flutter and stress + actively controled flutter designs are shown in Fig. 6.

The final control laws for the two cases shown in Fig. 5 are $1517.7/(s^2 + 51.4s + 15072.9)$ and $1456.7/(s^2 + 40.2s + 15310.4)$ for the 1mm initial design and stress initial design respectively. It is interesting to note that the numerator terms (effective gains) converge from different starting points to values that are within 5% from each other. The constant denominator terms in both final control laws are almost the same indicating that active damping is introduced at a band of frequencies around 19.6 Hz. This is intuitively rewarding since the flutter mechanism seems to involve a wing bending root at 16-17 Hz and a second root at 25-26 Hz. The control law localized damping action is thus tuned so as to be approximately in the middle of this band. The width of the frequency band is controled by the equivalent control law damping parameter ζ_c (Eq. 19) which is 21% and 16% for the two cases in Fig. 5.

The results described so far indicate that, as long as controllability and observability are guaranteed, an active control system of unlimited power can stabilize the wing and avoid essentially all structural weight penalty that would have been needed to achieve this in a passive manner. Even when gust dynamic stresses become critical in the stress design (in addition to the quasi static stresses included here) it is reasonable to believe that a powerful control system can save a substantial amount of structural weight.

The next objective is to study how a limited power control system effects an integrated design and how structural weight and control effort interact in the course of integrated optimization. Gust response constraints are now added to the previous set of constraints. The RMS values of control surface rotation q_c and rotation rate $\dot{q}_c$ serve as measures of control system effort and limitations[51,52].

At the minimum mass control augmented structural design of Fig. 5 (starting with the stress design) these RMS values were 0.35 degrees and 36.6 deg sec. In two additional cases these RMS values were constrained placing limitations of varying severity on the control system. Figure 7 depicts three mass convergence iteration histories all starting with the stress design : a) no bounds on the RMS q_c and $\dot{q}_c$; b) RMS $q_c \leq 0.2°$, $RMS\dot{q}_c \leq 21°$/ sec; c) RMS $q_c \leq 0.1°$, RMS$\dot{q}_c \leq 10.5°$/ sec. Move limits of 10% were used for all three cases. Nine structural and 3 control system design variables are used simultaneously.

As Fig. 7 shows, convergence within 12 cycles is achieved when the gust response constraints are added to the stress, gage and stability constraints. When control surface activity is more restricted, the final skin weight is larger. Thus limited control system resources are traded off against structural resources in a quest for a balanced multidisciplinary optimum design. This interaction takes place dynamically as the synthesis progresses and is hard or impossible to capture in sequential parametric studies.

Figure 8 adds to our understanding of interdisciplinary interactions by following the skin mass history (normalized with respect to the stress design

from a 1 mm thick uniform skin and a control law of the form:

$$\frac{\delta}{y_{SE}} = \frac{2000}{(s^2 + 40s + 10{,}000)}$$

As shown in Fig. 4, the skin mass for this case is reduced to 1.838 Kgm. Examination of the optimization results reveals that the driving constraint is again the damping in a pole. Its frequency is 17.03 Hz, and the final damping ratio is .067, which implies that with tighter convergence criteria for terminating the optimization, additional weight savings could be achieved (1% diminishing return on three consecutive approximate problem optimizations is used as a convergence criterion). In any event, the weight in the third case is brought back almost to the level of the stress design weight. Convergence is slower. It took 27 Cycles and 27 CPU minutes on the UCLA IBM 3090-4. Also, while rapid convergence was achieved for the cases with only structural design variables with move limits of 40%, it was necessary to use 10% move limits when control system design variables were added in order to protect the accuracy of system pole approximations. This explains the slower convergence of the third run.

Minimum mass synthesis of the wing with structural and control system design variables, subject to stress, gage and aeroservoelastic stability constraints was tried again. This time the initial structural design is the unstable stress design of the first case. Initial values for control system design variables are now different. The optimization is started with $1500/(s^2 + 40s + 4000)$. Figure 5 shows the two skin mass convergence histories for the design starting from 1mm uniform skin and the one starting with the stress design. Starting with the 1.743 Kgm skin of the stress design, the mass minimization progresses by first adding mass to stiffen the wing followed by manipulation of the control system design variables to stabilize the wing with the smallest weight penalty possible. In fact, the final skin weighs 1.745 Kgm, practically the same as if there were no flutter constraints at all.

Final skin thickness distributions for the stress, stress + flutter and stress + actively controled flutter designs are shown in Fig. 6.

The final control laws for the two cases shown in Fig. 5 are $1517.7/(s^2 + 51.4s + 15072.9)$ and $1456.7/(s^2 + 40.2s + 15310.4)$ for the 1mm initial design and stress initial design respectively. It is interesting to note that the numerator terms (effective gains) converge from different starting points to values that are within 5% from each other. The constant denominator terms in both final control laws are almost the same indicating that active damping is introduced at a band of frequencies around 19.6 Hz. This is intuitively rewarding since the flutter mechanism seems to involve a wing bending root at 16-17 Hz and a second root at 25-26 Hz. The control law localized damping action is thus tuned so as to be approximately in the middle of this band. The width of the frequency band is controled by the equivalent control law damping parameter ζ_c (Eq. 19) which is 21% and 16% for the two cases in Fig. 5.

The results described so far indicate that, as long as controllability and observability are guaranteed, an active control system of unlimited power can stabilize the wing and avoid essentially all structural weight penalty that would have been needed to achieve this in a passive manner. Even when gust dynamic stresses become critical in the stress design (in addition to the quasi static stresses included here) it is reasonable to believe that a powerful control system can save a substantial amount of structural weight.

The next objective is to study how a limited power control system effects an integrated design and how structural weight and control effort interact in the course of integrated optimization. Gust response constraints are now added to the previous set of constraints. The RMS values of control surface rotation q_c and rotation rate $\dot{q}_c$ serve as measures of control system effort and limitations[51,52].

At the minimum mass control augmented structural design of Fig. 5 (starting with the stress design) these RMS values were 0.35 degrees and 36.6 deg sec. In two additional cases these RMS values were constrained placing limitations of varying severity on the control system. Figure 7 depicts three mass convergence iteration histories all starting with the stress design : a) no bounds on the RMS q_c and $\dot{q}_c$; b) RMS $q_c \leq 0.2°$, $RMS\dot{q}_c \leq 21°/\text{sec}$; c) RMS $q_c \leq 0.1°$, $RMS\dot{q}_c \leq 10.5°/\text{sec}$. Move limits of 10% were used for all three cases. Nine structural and 3 control system design variables are used simultaneously.

As Fig. 7 shows, convergence within 12 cycles is achieved when the gust response constraints are added to the stress, gage and stability constraints. When control surface activity is more restricted, the final skin weight is larger. Thus limited control system resources are traded off against structural resources in a quest for a balanced multidisciplinary optimum design. This interaction takes place dynamically as the synthesis progresses and is hard or impossible to capture in sequential parametric studies.

Figure 8 adds to our understanding of interdisciplinary interactions by following the skin mass history (normalized with respect to the stress design

Gallagher, R.H., Ragsdell, K.M., and Zienkiewicz, O.C., John Wiley and Sons, 1984.

14. Lynch,R.W., and Rogers, W.A., "Aeroelastic Tailoring of Composite Materials to improve Performance," Proceedings of the 16th AIAA Structures,Structural Dynamics and Materials Conference, 1975.

15. Haftka, R.T., "Optimization of Flexible Wing Structures Subject to Strength and Induced Drag Constraints," AIAA Journal, Vol. 15, pp. 1101-1106, 1977.

16. Wilkinson, K., Markowitz, J., Lerner, E., George, D., and Batill, S.M., "TASTOP - A Flutter and Strength Optimization Program for Lifting Surface Structures," Journal of Aircraft, Vol.14, No 6, June 1977.

17. Lecina, G. and Petiau, C., "Advances in Optimal Design with Composite Materials,"

in: Computer Aided Optimal Design: Structural and Mechanical Systems, C.A.Mota Soares (ed.), Springer-Verlag, 1987.

18. Neill, D.J, Johnson, E.H. and Canfield, R., "ASTROS - A Multidisciplinary Automated Structural Design Tool," AIAA Paper no. 87-0713 presented at the 28th AIAA ASME ASCE AHS Structures,Structural Dynamics and Materials Conference, Monterey, California, April 1987.

19. Zeiler, T.A., and Weisshaar, T.A., "Integrated Aeroservoelasic Tailoring of Lifting Surfaces," Journal of Aircraft, Vol. 25, No. 1, January 1988, pp. 76-83.

20. Morris, S., and Kroo, I., "Aircraft Design Optimization with Multidisciplinary Performance Criteria", AIAA Paper 89-1265, in Proceedings of the AIAA ASME ASCE AHS ASC 30th Structures,Structural Dynamics and Materials Conference, Mobile, Alabama, April 1989.

21. Dracopoulos, T.N., and Oz, H., "Integrated Aeroelastic Control Optimization", 7th VPISU AIAA Symposium on Dynamics and Control of Large Structures, Virginia, May 1989.

22. Livne, E., Schmit, L.A., and Friedmann, P.P., "Towards an Integrated Approach to the Optimum Design of Actively Controlled Composite Wings", (submitted for publication in the Journal of Aircraft special issue on Multidisciplinary Optimization of Aeronautical Systems, to be published in 1990).

23. Livne, E., Schmit, L.A., and Friedmann, P., Design Oriented Structural Analysis for Fiber Composite Wings, UCLA Report UCLA-ENG-88-36, November 1988.

24. Giles, G.L., "Equivalent Plate Analysis of Aircraft Wing Box Structures with General Planform Geometry," Journal of Aircraft, Vol 23, No 11 November 1986, pp.859-864.

25. Lottati, I., and Nissim, E., "Three Dimensional Oscillatory Piecewise Continuous Kernel Function Method",(in three parts), Journal of Aircraft Vol 18, No. 5, May 1981, pp.346-363.

26. Lottati, I. and Nissim,E., "Nonplanar,Subsonic Three Dimensional Oscillatory Piecewise Continuous Kernel Function Method", Journal of Aircraft, Vol. 22,No. 12,December 1985, pp 1043-1048.

27. Nissim, E., and Lottati, I., "Supersonic Three Dimensional Oscillatory Piecewise Continuous Kernel Function Method," Journal of Aircraft Vol 20, No. 8, August 1983, pp.674-681.

28. Lottati, I., "Induced Drag and Lift of Wing by the Piecewise Continuous Kernel Function Method", Journal of Aircraft, Vol. 21, No. 11, November 1984, pp. 833-834.

29. Roger, K.L., "Airplane Math Modeling Methods for Active Control Design", Structural Aspects of Active Controls, AGARD CP-228, August 1977, pp 4-11.

30. Karpel, M., "Design for Active Flutter Suppression and Gust Alleviation using State Space Aeroelastic Modeling," Journal of Aircraft, Vol 19 No. 3, March 1982, pp. 221-227.

31. Tiffany, S.H., and Adams, W.M., "Nonlinear Programming Extensions to Rational Function Approximations of Unsteady Aerodynamics" Proceedings of the 28th Structures,Structural Dynamics and Materials Conference, Monterey,California,1987.

32. Rowe, W.S., "Comparison of Analysis Methods used in Lifting Surface Theory," in Computational Methods in Potential Aerodynamics, edited by T Morino, Springer Verlag, 1985.

33. Schmidt,W., "Advanced Numerical Methods for Analysis and Design in Aircraft Aerodynamics" International Journal of Vehicle Design Vol ? No 3/4, 1986, pp. 415-440.

34. Rogers, W.A., Brayman, W.W., and Shirk M.H., "Design, Analysis, and Model Tests of an Aeroelastically Tailored Lifting Surface," Journal of Aircraft, Vol. 20, No. 3, March 1983, pp. 208-215

Gallagher, R.H., Ragsdell, K.M., and Zienkiewicz, O.C., John Wiley and Sons, 1984.

14. Lynch,R.W., and Rogers, W.A., "Aeroelastic Tailoring of Composite Materials to improve Performance," Proceedings of the 16th AIAA Structures,Structural Dynamics and Materials Conference, 1975.

15. Haftka, R.T., "Optimization of Flexible Wing Structures Subject to Strength and Induced Drag Constraints," AIAA Journal, Vol. 15, pp. 1101-1106, 1977.

16. Wilkinson, K., Markowitz, J., Lerner, E., George, D., and Batill, S.M., "TASTOP - A Flutter and Strength Optimization Program for Lifting Surface Structures," Journal of Aircraft, Vol.14, No 6, June 1977.

17. Lecina, G. and Petiau, C., "Advances in Optimal Design with Composite Materials,"

in: Computer Aided Optimal Design: Structural and Mechanical Systems, C.A.Mota Soares (ed.), Springer-Verlag, 1987.

18. Neill, D.J, Johnson, E.H. and Canfield, R., "ASTROS - A Multidisciplinary Automated Structural Design Tool," AIAA Paper no. 87-0713 presented at the 28th AIAA/ASME/ASCE/AHS Structures,Structural Dynamics and Materials Conference, Monterey, California, April 1987.

19. Zeiler, T.A., and Weisshaar, T.A., "Integrated Aeroservoelasic Tailoring of Lifting Surfaces," Journal of Aircraft, Vol. 25, No. 1, January 1988, pp. 76-83.

20. Morris, S., and Kroo, I., "Aircraft Design Optimization with Multidisciplinary Performance Criteria", AIAA Paper 89-1265, in Proceedings of the AIAA/ASME/ASCE/AHS/ASC 30th Structures,Structural Dynamics and Materials Conference, Mobile, Alabama, April 1989.

21. Dracopoulos, T.N., and Oz, H., "Integrated Aeroelastic Control Optimization", 7th VPISU/AIAA Symposium on Dynamics and Control of Large Structures, Virginia, May 1989.

22. Livne, E., Schmit, L.A., and Friedmann, P.P., "Towards an Integrated Approach to the Optimum Design of Actively Controlled Composite Wings", (submitted for publication in the Journal of Aircraft special issue on Multidisciplinary Optimization of Aeronautical Systems, to be published in 1990).

23. Livne, E., Schmit, L.A., and Friedmann, P., Design Oriented Structural Analysis for Fiber Composite Wings, UCLA Report UCLA-ENG-88-36, November 1988.

24. Giles, G.L., "Equivalent Plate Analysis of Aircraft Wing Box Structures with General Planform Geometry," Journal of Aircraft, Vol 23, No 11 November 1986. pp.859-864.

25. Lottati, I., and Nissim, E., "Three Dimensional Oscillatory Piecewise Continuous Kernel Function Method",(in three parts), Journal of Aircraft Vol 18, No. 5, May 1981, pp.346-363.

26. Lottati, I. and Nissim,E., "Nonplanar,Subsonic,Three Dimensional Oscillatory Piecewise Continuous Kernel Function Method", Journal of Aircraft, Vol. 22,No. 12,December 1985. pp 1043-1048.

27. Nissim, E., and Lottati, I., "Supersonic Three Dimensional Oscillatory Piecewise Continuous-Kernel Function Method," Journal of Aircraft Vol 20, No. 8, August 1983, pp.674-681.

28. Lottati, I., "Induced Drag and Lift of Wing by the Piecewise Continuous Kernel Function Method", Journal of Aircraft, Vol. 21, No. 11, November 1984, pp. 833-834.

29. Roger, K.L., "Airplane Math Modeling Methods for Active Control Design", Structural Aspects of Active Controls, AGARD CP-228, August 19[illegible], pp 4-11.

30. Karpel, M., "Design for Active Flutter Suppression and Gust Alleviation using State Space Aeroelastic Modeling," Journal of Aircraft, Vol 19 No. 3, March 1982, pp. 221-227.

31. Tiffany, S.H., and Adams, W.M., "Nonlinear Programming Extensions to Rational Function Approximations of Unsteady Aerodynamics," Proceedings of the 28th Structures,Structural Dynamics and Materials Conference, Monterey,California,1987.

32. Rowe, W.S., "Comparison of Analysis Methods used in Lifting Surface Theory," in Computational Methods in Potential Aerodynamics, edited by J Morino, Springer Verlag, 1985.

33. Schmidt,W., "Advanced Numerical Methods for Analysis and Design in Aircraft Aerodynamics" International Journal of Vehicle Design Vol [illegible] No 3/4, 1986, pp. 415-440.

34. Rogers, W.A., Brayman, W.W., and Shirk M.H., "Design, Analysis, and Model Tests of an Aeroelastically Tailored Lifting Surface," Journal of Aircraft, Vol. 20, No 3, March 1983, pp. 205-215

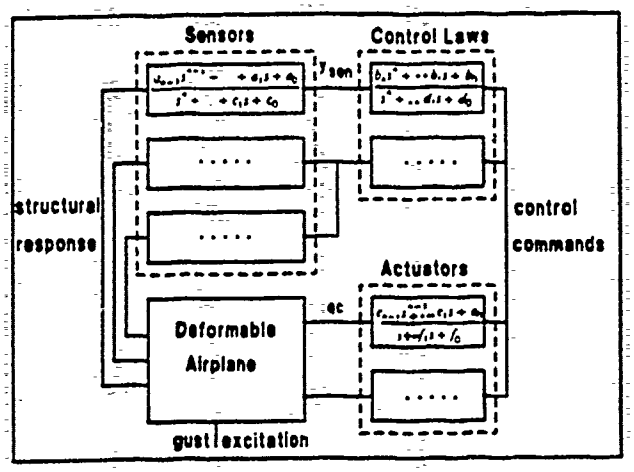

Figure 1: Control system block diagram

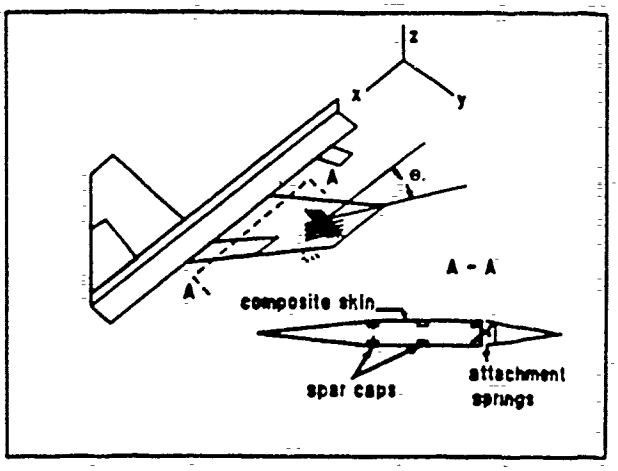

Figure 2: Equivalent plate structural model

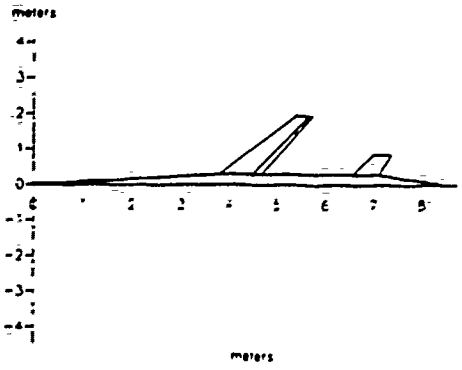

Figure 3 RPV geometric layout

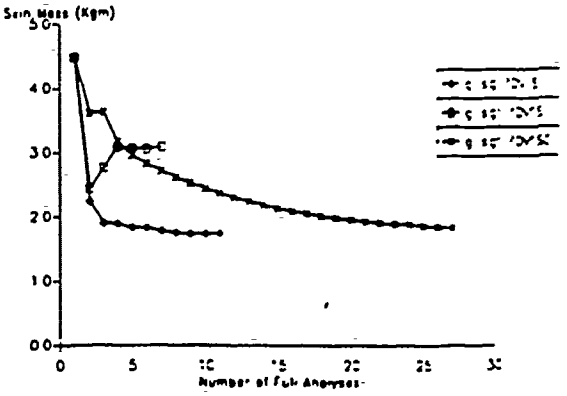

Figure 4: Skin mass convergence histories with different constraints and design variables

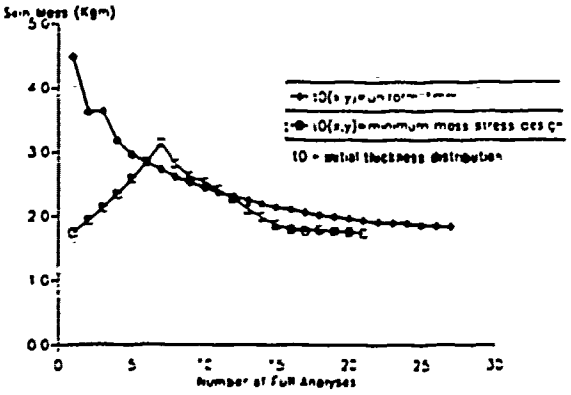

Figure 6 Control/structure synthesis mass convergence histories (different initial designs)

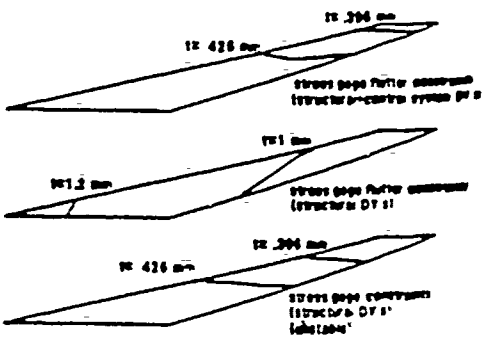

Figure 8: Final minimum mass skin thickness distributions

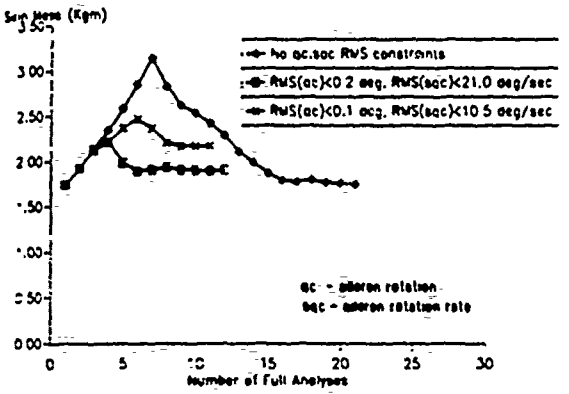

Figure 7. Convergence histories for control/structure mass minimization

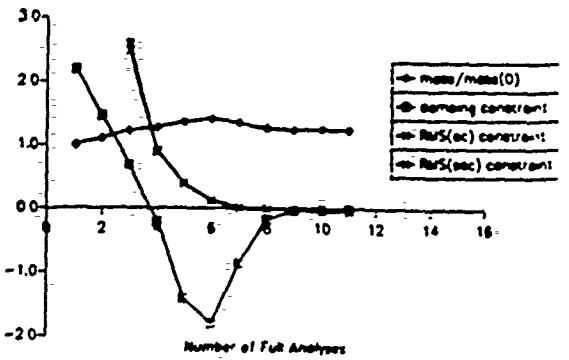

Figure 8: Min mass design histories s.t. torsion,flutter and gust response constraints

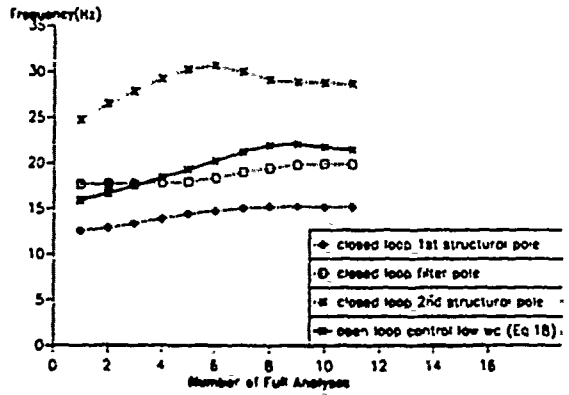

Figure 9: Closed loop damped frequency design histories

AIAA-91-1098

Studies in Integrated Aeroservoelastic Optimization of Actively Controlled Composite Wings

E. Livne, Dept. of Aeronautics and Astronautics, The University of Washington, Seattle, WA
P.P. Friedmann and L.A. Schmit, Mechanical, Aerospace and Nuclear Engineering Dept., University of California, Los Angeles, CA

AIAA 32nd Structures, Structural Dynamics, and Materials Conference
April 8 - 10, 1991 / Baltimore, MD

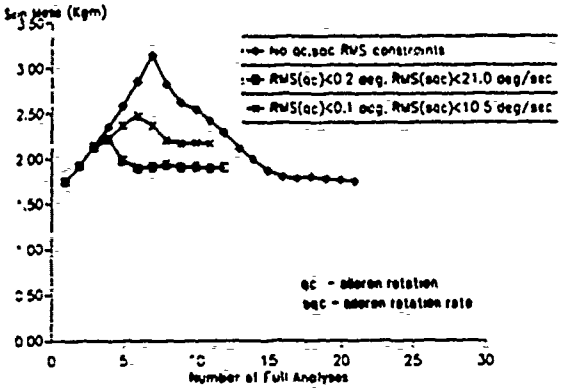

Figure 7: Convergence histories for control/structure mass minimization

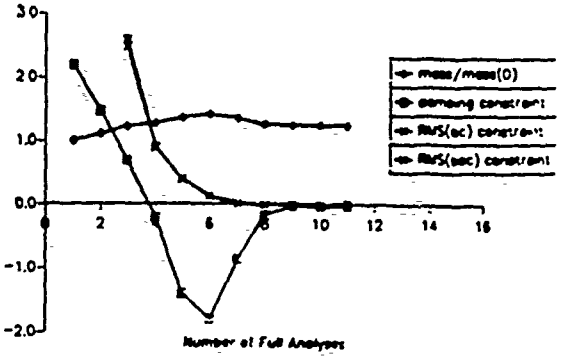

Figure 8: Min mass design histories s.t. stress,flutter and gust response constraints

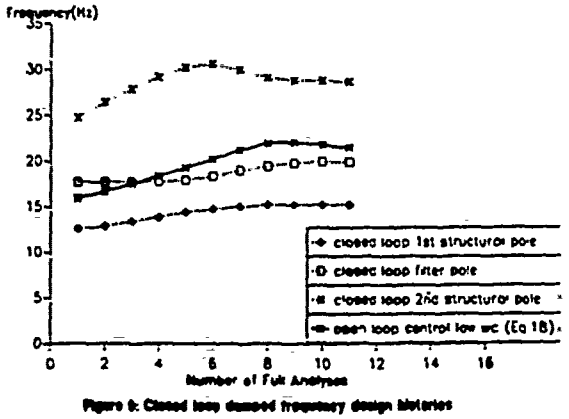

Figure 9: Closed loop damped frequency design histories

Thus the design space spanned three disciplines, namely, structures, control and aerodynamics and the blend of behavior constraints covered strength, minimum gage, flutter, gust response and performance (induced drag). The same RPV model as used in Ref. 17 served as a test case.

The design studies in Refs. 17-19 contribute to the state of the art in design optimization by developing and gaining experience with synthesis techniques for multidisciplinary complex problems involving a very rich blend of constraints. They also offer better understanding and a fresh insight into the interactions between the various disciplines in wing design as well as numerical results that may serve as a basis for design tradeoffs.

The purpose of the present paper is to add to the growing experience in aeroservoelastic wing optimization. The design space for the numerical examples reported here is made up of sizing type structural and control system design variables (Ref. 16). The present capability can handle aerodynamic design variables as well but they are not used in the present studies. The RPV (Refs. 17-19) is used to study optimal designs achieved with different control law structures and the resulting robustness of these control augmented composite wings. The performance of different complex eigenvalue approximations is also examined. The new multidisciplinary wing synthesis capability is then applied to the aeroservoelastic synthesis of realistic F16 and X29 type airplanes in order to demonstrate its power and generality and assess computational efficiency in dealing with more complex aeroelastic and control system configurations. Simplified handling qualities requirements are added to the set of constraints.

Analytical Modeling Techniques

A unique integration of analytical modeling techniques makes it possible to bridge the gap between those that are over simplified and the detailed techniques that require too much computer time. In the structures area, an equivalent plate analysis is used (Refs. 20,21). It is integrated with the PCKFM (Piecewise Continuous Kernel Function Method) for lifting surface unsteady aerodynamics (Ref. 22). The method of Roger (Ref. 23) is used to generate finite dimensional state space approximations for the unsteady aerodynamic loads. The integrated aeroservoelastic system is modeled as a Linear Time Invariant (LTI) system. The control system is completely described by the location of sensors and control surfaces and by the transfer functions of the sensors.control laws and actuators. Behavior sensitivity analysis is based on analytical derivatives of all behavior functions with respect to all design variables.

Multidisciplinary Synthesis Methodology

Approach to Optimization

Following its success in structural synthesis, the nonlinear programming approach combined with approximation concepts (NLP,AC) is used for the multidisciplinary optimization task (Ref. 24). In this method only a small number of detailed analyses are carried out during optimization. Each analysis serves as a basis for constructing approximations to the objective and constraint functions in terms of the design variables. Then, a series of approximate optimization problems is solved converging to the optimal design. For this approach to be practical it is crucial to avoid too many detailed analyses for function evaluation and derivative calculations. This depends on making the approximations accurate yet simple enough for efficient solution.

Design Variables

Preassigned parameters for the optimization include wing planform and depth distribution, material properties and structural layout of the wing (number of spars and ribs and their locations) Control system structure is also preassigned. Thus the number of sensors and actuators and their locations are given along with the number of control laws transforming given combinations of sensor outputs into control commands. It is also assumed that the general form of the transfer functions of sensors and actuators are given and cannot be changed during optimization.

To take advantage of multidisciplinary interactions, the design space is opened up to include structural design variables, control system and aerodynamic design variables simultaneously. Structural design variables then include polynomial coefficients in the series describing skin layer thickness distribution over the wing

$$t(x,y) = \sum_{i}^{I} T_i \, x^{m_i} \, y^{n_i}$$

Additional structural design variables include spar rib cap areas, concentrated masses and spring constants (for the springs representing stiffness of actuator and backup structure connecting control surfaces to the wing box or canard to the fuselage). Control system design variables include polynomial coefficients in the transfer functions representing control laws. Aerodynamic design variables include coefficients in the polynomial series for wing initial (jig) shape.

$$w_0(x,y) = \sum_i^I W_i x^{r_i} y^{s_i}$$

With the structural, control and aerodynamic configurations preassigned (following the hierarchy of design variables in Ref. 16) the control augmented structural synthesis problem formulated in this work is a sizing problem for the three disciplines. Thus the balanced treatment of these disciplines (controls, aerodynamics and structures) is also retained in formulating the optimization problem.

Objective Functions and Behavior Constraints

The wing can be synthesized to minimize mass or gust response or maximize performance with constraints on stresses, aeroservoelastic stability, aircraft performance in terms of roll rate, drag or drag polar specifications and control system performance in terms of activity in gusts and limits on control surface travel and hinge moment. The objective function can be chosen to be mass, drag, RMS value of any response to atmospheric turbulence (to be minimized) or steady roll rate or lift to drag ratio (to be maximized) or a combination of these. Constraints are imposed to meet a combined stress criterion for composite skin layers and a unidirectional stress criterion for spar/rib caps. The aeroservoelastic system poles are forced to reside in the left hand half of the complex plane to guarantee dynamic stability. If not included as part of the objective function, the drag, lift/drag, mass or roll rate can be constrained to ensure acceptable performance. Static load conditions include sets of given loads acting on the wing or definition of airplane maneuvers. In the second case, static deformation and stresses are calculated to take trim and aeroelastic load redistribution into account.

The nonlinear programming algorithm used for constrained function minimization throughout this work is the method of feasible directions as implemented in the CONMIN code (Refs. 25 and 26).

The RPV Wing

Description

Optimization studies presented here deal first with a small RPV similar to the NASA DAST research vehicle. Its planform geometry is shown in Fig. 1. A 6.8 aspect ratio, biconvex 10% t/c wing is actively controlled by a small control surface located at about 80% semi-span towards the tip. The control surface chord is 20% of the local wing chord, and it is driven by an actuator whose transfer function is preassigned as follows (Ref. 27)

$$\frac{q_{c1}}{\delta_1} = \frac{1.7744728 \times 10^7}{((s+180)(s^2+251s+314^2))}$$

The wing control surfaces are used only for active flutter control. The elevators are used for rigid body pitch and roll. The elevator actuator transfer function is

$$\frac{q_{c2}}{\delta_2} = \frac{20}{(s+20)}$$

q_{ci} and δ_i are the actuator actual deflection and its command, respectively.

An accelerometer is placed on the wing strip containing the control surface. It is located in the middle(spanwise) and at the 0.65 chord point of the strip. Its measurement, y_{SE}, serves as an input to a control law which, in turn, generates an input command, δ_1, to the actuator of the wing control surface. The preassigned accelerometer transfer function is

$$\frac{y_{SE}}{\ddot{w}_{0.65c}} = \frac{314^2}{(s^2+376.8s+314^2)}$$

$w_{0.65c}$ is the actual vertical acceleration at the measurement point.

The RPV structure is modeled as an assembly of four equivalent plates. A flexible wing is attached to a rigid fuselage and rigid control surfaces. The main wing box structure, extending from root to tip spanwise and to 80% chordwise, is the structure to be synthesized. The weight of fuselage, control surfaces and non-structural wing mass is 308 Kgm for a half airplane. A Dryden gust model with a scale length of 518.16 meters and a vertical gust RMS velocity of 1.06 m/sec is used.

The set of three load conditions for wing stress calculations consists of 3g symmetric pull-ups at sea level, 10,000 feet and 20,000 feet. In the "maneuver load" calculations the airplane is trimmed using the elevator. All stress constraints reflect a 1.5 safety factor. Flutter, gust and aeroservoelastic stability calculations, though, are carried out at sea level, Mach 0.9 for the cantilevered wing. This is done intentionally in order to first examine flutter suppression structural optimization using a realistic but simple example without flight mechanics interactions.

The RPV wing box skins are made of glass epoxy laminates (Ref. 28). Fiber directions are 0, 90, +45 and -45 degrees relative to a line passing through the midchord points of the wing box. The skin is then modeled as made of four unidirectional lamina. The thickness distribution of each of these

lamina is described by a nine term polynomial in x and y as in Fig. 1. Thus, there are 36 structural design variables.

Structural Designs.

Minimum weight designs with structural design variables only subject to minimum gage and stress constraints ("stress design") or gage,stress and flutter constraints ("flutter design") are synthesized first (Fig. 2). The stress design is unstable. The flutter constraints are in the form of a 2% lower bound on viscous damping in five modes corresponding to the lowest frequencies. Move limits of 40% were used and convergence was achieved within 15 optimization cycles.

Structure Control Designs.

The control system is now incorporated and wing mass is minimized subject to gage,stress and flutter constraints while the design space includes both structural and control system design variables.

Following its successful application to the all Aluminum wing studied in Ref. 17, the first control law used for this study is the Localized Damping Type Transfer Function (LDTTF) described in Ref. 29. This second order control law provides damping "locally" in the range of frequencies where damping is needed. Its form is

$$\delta = \frac{a_c}{(s^2 + b_c\, s + c_c)}\, y_{SE}$$

where y_{SE} is the accelerometer measurement and a_c, b_c, c_c are control system design variables The denominator coefficients can be associated with equivalent damping ζ_c and natural frequency ω_c of the control law

$$c_c = \omega_c^2$$

$$b_c = 2\zeta_c\omega_c$$

Thus, c_c and b_c determine the center frequency and gain peak width of the control law transfer function while a_c determines the effective gain.

The LDTTF control law is used here without compensation for sensor and actuator transfer functions (Ref. 30). The active control system is assumed to have no weight in the calculations performed in this study.

In the case of the all Aluminum wing (Ref. 17), when the second order control system was added to the the problem and design synthesis started with the stress gage constrained (unstable) design, aeroservoelastic mass minimization made it possible to reduce the structural mass to its stress design value while the active control system prevented flutter. In the case of the composite wing, however, when the design space was opened up to include the three control system design variables as well as the 36 structural design variables, convergence could not be achieved when starting with the stress design.

When synthesis starts with the feasible flutter design, convergence is achieved with 10% move limits, but only about 60% of the weight penalty needed for flutter prevention is recovered by the addition of the control system (Fig. 3).

Limiting the control system power by including constraints on the aileron activity in atmospheric turbulence yields the same trend that was found for the Aluminum wing: The more limited the control system is, the higher the structural weight penalty needed for aeroservoelastic stability. But the fact that when the control system is unlimited in power, it could not take care of the flutter problem (without structural penalty) was disturbing and intriguing. This called for further study.

Careful examination of the iteration histories starting with the stress design revealed complex eigenvalue approximations that were extremely sensitive to design changes. The accuracy of these approximations is evaluated when constraint values via a full analysis at a new design point are compared to their values at the same point based on approximations constructed from full analysis (and sensitivity analysis) at the previous base design point. In the design synthesis cases that failed to converge approximation accuracy for complex eigenvalues could change dramatically from iteration to iteration yielding very good approximations in some instances and substantial errors in others.

The Rayleigh Quotient Approximations (RQA), (Ref. 31) improved approximation accuracy but did not solve the convergence problem. It seems that for the given structure of the control system it is impossible to regain all the weight penalty associated with flutter stabilization. Indeed a close look at the poles of the stress design composite wing reveals two flutter mechanisms (Fig. 4). It appears that the second order control law cannot stabilize both simultaneously because of the narrow range of frequencies for which it is effective. Indeed, the design does not converge since it fluctuates between these two instabilities. When one is stabilized, the other may become unstable.

The control law was subsequently changed to a first order low pass filter of the form

$$\delta = \frac{a}{s + b}\, y_{SE}$$

This control law is expected to have a wider bandwidth and thus be more effective in controlling the two instabilities. Design iteration histories with gust response constraints of varying severity are shown in Fig. 5. The first order control law makes it possible to regain most (85%) of the flutter weight penalty. The RMS of control surface rotation and rotation rate, however, are much higher compared with the second order control law (Figs. 3,5) and this is not surprising given the wider bandwidth of the first order control law.

A third control law was also studied. It is a fourth order law made up from the sum of two second order filters. This control law is expected to be more effective than the single second order law in suppressing the flutter of the stress design. This is because the form of this control law offers the freedom to tune a second order filter to each of the two instabilities.

$$\delta = \left[\frac{a_c}{(s^2 + b_c\, s + c_c)} + \frac{d_c}{(s^2 + e_c\, s + f_c)} \right] y_{SE}$$

where y_{SE} is the accelerometer measurement and $a_c, b_c, c_c, d_c, e_c, f_c$ are control system design variables. The denominator coefficients can be associated with equivalent damping ζ_c and natural frequency ω_c of the control law for each filter

$$c_c = \omega_{1c}^2$$

$$f_c = \omega_{2c}^2$$

$$b_c = 2\zeta_{1c}\omega_{1c}$$

$$e_c = 2\zeta_{2c}\omega_{2c}$$

Thus, c_c, f_c, b_c and e_c determine the center frequencies and gain peak widths of the control law transfer function while a_c, d_c determine the effective gains.

The performance of the three control laws when no gust constraints are imposed on the control system is compared in Fig. 6. Indeed, the fourth order control law makes it possible to stabilize the wing without any mass penalty over the stress design. Actually, it even reduces the mass slightly with respect to the stress design, but this is associated with the convergence criteria used. The stress design mass could be slightly reduced by tightening the percent change in objective function used in a diminishing return convergence criterion (1% was used in the examples shown).

The initial fourth order law is

$$1400./(s^2 + 20.s + 14000.) +$$

$$22000./(s^2 + 100.s + 20000.)$$

The final fourth order law is

$$1421.7/(s^2 + 20.6s + 9596.8) +$$

$$21224.6/(s^2 + 120.1s + 20752.3)$$

The double quadratic control law is thus tuned to frequencies of 15.6 and 23.0 cps with equivalent damping ratios of 10.5% and 41.7% in theses two frequencies, respectively.

Freezing the stress design of the composite RPV wing and looking for the "best" control system to stabilize it using a fourth order control law leads to the design history in Figure 7. Six control system design variables are now used in an effort to minimize the RMS of aileron rotation due to atmospheric gusts. 10% move limits are used to converge to a control law

$$2289./(s^2 + 17.2s + 9209.7) +$$

$$50900./(s^2 + 305.s + 23380.)$$

yielding a minimum RMS rotation of 1.9 degrees and associated RMS of rotation rate of 249. deg sec. When, during the optimization, stability is lost, the gust response calculation is bypassed. This shows up as gaps in the design history of Figure 7 Imposing more severe gust response constraints on the control system, makes it necessary to trade in some weight as shown in Fig. 8.

Of course, it might be argued that control system power translates in the end to added mass, and that for the tradeoff studies to be more realistic, we need to include the weight of the control system in the objective function. The current capability can take this into account by linking the values of certain concentrated masses to the RMS aileron rotation and rotation rate needed. This was not carried out, however, in the examples given here because of lack of appropriate data that will make such a linking meaningful. In any case, as with the Aluminum wing, the complex tradeoff between structural weight and control system power (or the resulting weight of the control system) is evident.

Another issue of extreme importance in control system synthesis is that of robustness (Refs. 30.32). Although robustness is not included directly in the set of behavior functions in this study, it is interesting to examine robustness of the control systems synthesized in light of the fact that control system synthesis here is carried out for a plant that is changing during the synthesis process.

All the examples up to this point involve a single input single output control system. Robustness of this control system can be studied by examining the

Nyquist plots of the open loop system. These are shown in Figs. 9-12.

Figures 9-12 show Nyquist plots for control augmented wing designs subject to gage,stress and flutter constraints for the quadratic, first order and fourth order control laws, respectively. In studying them it should be remembered that they reflect control laws synthesized for different final plants (wing structure). The most robust is the second order control law (with the highest penalty in terms of wing weight). The first and fourth order laws show poor robustness (small gain and phase margins) as a result of the increased bandwidth. Considerable improvement in gain margins is achieved by subjecting the system to gust response constraints (Fig. 12). This results in a higher weight and corresponds to higher damping in the resulting aeroservoelastic poles.

Before concluding this section, it is interesting to examine the effect of different complex eigenvalue approximations on synthesis results. Composite wing skin mass histories for a structural design subject to stress, minimum gage and flutter constraints are shown in Fig. 13. The hybrid approximations lead to a slightly heavier design while RQA and direct Taylor series approximations lead to essentialy the same result.

The F16 Type Airplane Model

The studies presented thus far focused on a very simple airplane configuration (the RPV) and a simple single input single output control system. In order to demonstrate the power of the present capability in synthesizing more complex configurations with more complex control systems two more realistic models are considered.

The first is similar to an F16 fighter airplane and is shown in Fig. 14. A flexible wing/flaperon combination is attached to a rigid fuselage,elevator combination. The wing box skin thickness distribution is to be synthesized. The airplane is initially statically stable and weighs 4234 Kgm per half airplane (not including the skin mass). Minimum gage and stress constraints are imposed on an array of 5 x 5 grid points over the skin. The two maneuver conditions considered for stress calculations are a 7.33g symmetric pullup and a steady 160 deg/sec roll, both at sea level, M = 0.9. Stress (stress + gage constraints) and flutter (stress + gage + flutter) design histories are shown in Fig. 15 for an all Aluminum wing and a composite Graphite,Epoxy wing. Minimum gage is 0.508mm (0.02 inch) for the Aluminum skin and 0.0127mm (0.005 inch) for each laminate (0, 90, + 45, -45 deg.) in the Gr,Ep skin. Aeroelastic stability is examined for symmetric and anti symmetric vibrations of the free free airplane at sea level. M = 0.9. A minimum of 5% damping (ζ) is required in the first four symmetric and three anti-symmetric poles (the first symmetric pole is a short period pole). Damping of 1% is required for higher frequency poles.

As Fig. 15 shows, convergence of the design process is achieved within 15 full analysis,optimization cycles. When only structural design variables were considered, move limits of 40% were used. The big penalty in terms of weight paid for meeting the flutter constraints is clearly evident as well as the weight savings possible with composite construction.

A multi input multi output (MIMO) control system is now added to the model (Fig. 16). It is structured after the actual F16 control system (Ref. 33) with an addition for flutter suppression. Angle of attack, pitch rate and normal acceleration are measured at the center fuselage and used by control laws that take care of static stability and handling qualities of the airplane in symmetric motion. Roll rate measurement at the fuselage is used for the roll channel to control rolling performance. Wing tip accelerometers (at the tip leading edge) of each wing are used for flutter suppression in combination with the fuselage normal acceleration reading. The sum of the tip accelerations is used for flutter suppression in symmetric motion. Their difference is used for anti symmetric vibration stabilization.

Assuming perfect sensors and using the transfer functions of the actual F16 actuators (Ref. 33), six control laws are synthesized simultaneously to ensure 5% damping (ζ) in poles associated with elastic modes in symmetric and anti symmetric motion. A 35% minimum damping constraint and constraints on short period frequency that limit it to the range of 0.25 - 1.00 cps (Ref. 10) as well as a 35% minimum damping requirement on the control augmented roll pole are a simple way to introduce handling quality considerations. The interactions between a flight control system and an active flutter suppression system can thus be taken into acount in the early design stages.

Figure 17 shows a skin mass design iteration history for the control augmented F16 type airplane model. A total of 36 design variables are used for the thickness distribution of a wing box skin consisting of 4 composite laminates and 14 design variables are used in the control system. Gage, stress, flutter and handling quality constraints are included. The design converges to the stress design weight in 11 full analysis,optimization cycles. The initial and final control systems are shown in Figs. 18 and 19. Move limits of 10% were used.

Nyquist plots of the open loop system. These are shown in Figs. 9-12.

Figures 9-12 show Nyquist plots for control augmented wing designs subject to gage,stress and flutter constraints for the quadratic, first order and fourth order control laws, respectively. In studying them it should be remembered that they reflect control laws synthesized for different final plants (wing structure). The most robust is the second order control law (with the highest penalty in terms of wing weight). The first and fourth order laws show poor robustness (small gain and phase margins) as a result of the increased bandwidth. Considerable improvement in gain margins is achieved by subjecting the system to gust response constraints (Fig. 12). This results in a higher weight and corresponds to higher damping in the resulting aeroservoelastic poles.

Before concluding this section, it is interesting to examine the effect of different complex eigenvalue approximations on synthesis results. Composite wing skin mass histories for a structural design subject to stress, minimum gage and flutter constraints are shown in Fig. 13. The hybrid approximations lead to a slightly heavier design while RQA and direct Taylor series approximations lead to essentialy the same result.

The F16 Type Airplane Model

The studies presented thus far focused on a very simple airplane configuration (the RPV) and a simple single input single output control system. In order to demonstrate the power of the present capability in synthesizing more complex configurations with more complex control systems two more realistic models are considered.

The first is similar to an F16 fighter airplane and is shown in Fig. 14. A flexible wing/flaperon combination is attached to a rigid fuselage/elevator combination. The wing box skin thickness distribution is to be synthesized. The airplane is initially statically stable and weighs 4234 Kgm per half airplane (not including the skin mass). Minimum gage and stress constraints are imposed on an array of 5 x 5 grid points over the skin. The two maneuver conditions considered for stress calculations are a 7.33g symmetric pullup and a steady 160 deg/sec roll, both at sea level, M = 0.9. Stress (stress + gage constraints) and flutter (stress + gage + flutter) design histories are shown in Fig. 15 for an all Aluminum wing and a composite Graphite/Epoxy wing. Minimum gage is 0.508mm (0.02 inch) for the Aluminum skin and 0.0127mm (0.005 inch) for each laminate (0, 90, +45, -45 deg.) in the Gr/Ep skin. Aeroelastic stability is examined for symmetric and anti symmetric vibrations of the free free airplane at sea level, M = 0.9. A minimum of 5% damping (ζ) is required in the first four symmetric and three anti-symmetric poles (the first symmetric pole is a short period pole). Damping of 1% is required for higher frequency poles.

As Fig. 15 shows, convergence of the design process is achieved within 15 full analysis/optimization cycles. When only structural design variables were considered, move limits of 40% were used. The big penalty in terms of weight paid for meeting the flutter constraints is clearly evident as well as the weight savings possible with composite construction.

A multi input multi output (MIMO) control system is now added to the model (Fig. 16). It is structured after the actual F16 control system (Ref. 33) with an addition for flutter suppression. Angle of attack, pitch rate and normal acceleration are measured at the center fuselage and used by control laws that take care of static stability and handling qualities of the airplane in symmetric motion. Roll rate measurement at the fuselage is used for the roll channel to control rolling performance. Wing tip accelerometers (at the tip leading edge) of each wing are used for flutter suppression in combination with the fuselage normal acceleration reading. The sum of the tip accelerations is used for flutter suppression in symmetric motion. Their difference is used for anti symmetric vibration stabilization.

Assuming perfect sensors and using the transfer functions of the actual F16 actuators (Ref. 33), six control laws are synthesized simultaneously to ensure 5% damping (ζ) in poles associated with elastic modes in symmetric and anti symmetric motion. A 35% minimum damping constraint and constraints on short period frequency that limit it to the range of 0.25 - 1.00 cps (Ref. 10) as well as a 35% minimum damping requirement on the control augmented roll pole are a simple way to introduce handling quality considerations. The interactions between a flight control system and an active flutter suppression system can thus be taken into acount in the early design stages.

Figure 17 shows a skin mass design iteration history for the control augmented F16 type airplane model. A total of 36 design variables are used for the thickness distribution of a wing box skin consisting of 4 composite laminates and 14 design variables are used in the control system. Gage, stress, flutter and handling quality constraints are included. The design converges to the stress design weight in 11 full analysis/optimization cycles. The initial and final control systems are shown in Figs. 18 and 19. Move limits of 10% were used.

It is interesting to notice the change in sign in the anti symmetric flutter suppression control law, the bandwidth increase in the two flutter suppression laws and the practical elimination of the symmetric flutter suppression law in the final control system compared with the initial design. Locations of the complex poles of the symmetric control augmented F16 type model are shown in Fig. 20 (actuator poles, aerodynamic poles, integrator poles are not shown). The damping measure is defined as

$$\zeta = \frac{\sigma}{\sqrt{\sigma^2 + \omega^2}}$$

where σ and ω are the real and imaginary parts of the complex poles. A positive damping measure, thus, indicates instability.

The synthesis of the control augmented F16 type model wing involved 1080 constraints and 50 design variables. It took 18. minutes of CPU time on the UCLA IBM 3090 Model 600J.

The X29 Type Airplane Model

The X29 type airplane model was selected for study because of the potential Body Freedom Flutter (BFF) instability typical of forward swept wings (Ref. 10). This instability is a result of the interaction between a wing bending mode whose frequency drops as effective stiffness (structural + aerodynamic) is lost and the short period mode. The strong interaction between rigid body and elastic degrees of freedom presents a serious challenge to the control system designer. A control system must now be designed that will ensure proper handling qualities and flutter margins simultaneously.

The X29 type model is shown in Fig. 21. A canard surface is used for symmetric trim. The outer aileron is used for roll control. Tip missiles are introduced so that first wing bending frequency is lowered compared with the clean wing with the intention of creating a BFF instability and providing an interesting test case for the present studies.

Stresses are calculated in 7.33g symmetric pullup and a 160 deg/sec steady roll at sea level, M = 0.9. The skin of the wing box is made of four layers of Graphite/Epoxy material (0, 90, +45, -45 deg. with repect to a line connecting the mid chord point of the root and tip of the wing). The same gage and stress constraints are used as in the F16 type model case. Flutter constraints are applied to symmetric and antisymmetric vibrations at sea level, M = 0.9. A minimum of 3% damping (ζ) is required in the first three poles associated with elastic modes and 1% for higher frequency poles. Six modes are used in the stability analysis.

Figure 22 shows skin mass design histories for the stress (stress + gage) and flutter (flutter + stress + gage) designs with structural design variables only. Nine term second order polynomials are used for the thickness distribution of each layer (as in the RPV composite wing case) for a total of 36 design variables. The optimization is started with uniform thicknesses and uses 40% move limits. Convergence is achieved in 10 full analysis/optimization cycles.

Figure 23 shows a speed root locus plot of the resulting stress design. As can be seen, the stress design is unstable and the instability is of a BFF type. The frequency of the first wing symmetric bending drops and the short period root becomes unstable as the speed is increased.

A control system identical to the one used for the F16 studies is now added and used as the starting point for the control system optimization. Skin mass of the control augmented X29 type airplane is minimized subject to gage, stress, flutter and simplified handling quality constraints and the design history is shown in Fig. 24. Again, as with the F16, the control system takes care of the dynamic instabilities and guarantees proper handling qualities and flutter margins while the structural mass is reduced so as to take care of gage and stress only. Figure 25 shows the final pole structure of the control augmented X29 in symmetric motion (aerodynamic poles, integrator poles and actuator poles are not shown). 1096 constraints and 50 design variables were included and the optimization took 58 CPU minutes on the UCLA IBM Model 600J.

Examination of the initial (Fig. 18) and final (Fig. 26) control systems reveals major changes introduced during design optimization including changes of sign and elimination of some design variables. The power and applicability of the present technology to complex configurations is clearly demonstrated.

Conclusions

The present paper and Refs. 14-19 that preceded it clearly show that using current supercomputers, ingenious integration of analysis techniques, analytic sensitivities and approximation concept based optimization methodology, the single level multidisciplinary synthesis of realistic actively controlled composite wings is both practical and feasible. One of the important lessons of this research is that the introduction of control system design variables in addition to structural design variables presents a challenge to current state of the art approximation techniques used for approximate optimization problem generation. Smaller move limits are necessary

AIAA-91-0986

Transonic Adaptive Flutter Suppression Using Approximate Unsteady Time Domain Aerodynamics

Chan-Gi Pak and Peretz P. Friedmann
Mechanical, Aerospace, and Nuclear Engineering Department, University of California, Los Angeles, CA
Eli Livne, Dept. of Aeronautics and Astronautics, University of Washington, Seattle, WA

AIAA 32nd Structures, Structural Dynamics, and Materials Conference
April 8 - 10, 1991 / Baltimore, MD

AIAA-91-0986-CP

TRANSONIC ADAPTIVE FLUTTER SUPPRESSION USING APPROXIMATE UNSTEADY TIME DOMAIN AERODYNAMICS

Chan-Gi Pak , Peretz P. Friedmann†*

Mechanical, Aerospace, and Nuclear Engineering Department
University of California, Los Angeles, CA 90024-1597

and Eli Livne‡

Department of Aeronautics and Astronautics, FS-10
University of Washington, Seattle, WA 98195

Abstract

A digital adaptive controller is applied to the active flutter suppression problem of a wing under time varying flight conditions in subsonic and transonic flow. Linear quadratic controller gain at each time step is obtained using an iterative Riccati solver. The digital adaptive optimal controller is robust with respect to the unknown external loads. Flutter and divergence instabilities are simultaneously suppressed using a trailing-edge control surface and displacement sensing. A new transonic unsteady aerodynamic approximation methodology is developed which enables one to carry out the rapid calculation required for transonic aeroservoelastic applications. This approximation is based on a combination of unsteady subsonic aerodynamics combined with a transonic correction procedure. Aeroservoelastic transient time response is obtained using Roger's approximation, state transition matrices and an iterative time marching algorithm. The aeroservoelastic system in the time domain is modelled using a deterministic ARMA model together with a parameter estimator. Transonic flutter boundaries of a wing structure are computed, in the time domain, using an estimated aeroelastic system matrix and are in good agreement with experimental data for the low transonic Mach number range.

Nomenclature

General notation

(t)	Denotes value at time t.
(∞)	Denotes steady state value at $t=\infty$.
$\{x\}_k$	Denotes $\{x\}$ at discrete time k.

Scalar Symbols

$A_{gi}(\infty)$	The i-th element of the vector $\{A_g(\infty)\}$
$\tilde{A}_{gi}(\infty)$	The i-th element of the vector $\{\tilde{A}_g(\infty)\}$
a_i	AR coefficient
b_i	MA coefficient
c	Chord length
c_j	Real part of the j-th eigenvalue
d_j	Imaginary part of the j-th eigenvalue
f_{max}	Nyquist frequency
J	Performance index for the digital adaptive optimal controller
$2M$	Order of ARMA model
M_∞	Free stream Mach number
m	Order of generalized displacement vector $\{\eta(t)\}$
N_s	Number of discrete frequencies at which subsonic aerodynamic influence coefficient matrices are computed
NG	Number of aerodynamic lag terms
NM	Order of aeroelastic system matrices obtained from the Roger's approximation
n	Order of displacement vector $\{q(t)\}$

* Graduate Research Assistant, Student Member AIAA

† Professor and Chairman, Member AHS, ASME, Fellow AIAA

‡ Assistant Professor, Member AIAA

P_∞	Free stream pressure
q_D	Free stream dynamic pressure ($\equiv\frac{1}{2}\gamma P_\infty M_\infty^2$)
r_i	The i-th element of the vector $\{r(t)\}$
r_w	Weighting factor for the control surface deflection angle δ_k
s	Laplace variable
T_a	Time step for the iterative time-marching algorithm
T_s	Sampling time for the parameter estimator
$T_{\delta ii}(\infty)$	The i-th diagonal element of the matrix $[T_\delta(\infty)]$
y_k	Wing response at sensor
γ	Ratio of specific heats (=1.4)
$\delta_k, \delta(t)$	Control surface deflection angle
$\bar{\delta}(s)$	Laplace transform of $\delta(t)$
λ_k	Forgetting factor
σ_i	The i-th modal damping of the wing structure
Ω_i	The i-th aerodynamic lag term
ω_i	The i-th undamped natural circular frequency of the wing structure
ω_{di}	The i-th damped natural circular frequency of the wing structure
ζ_i	The i-th modal damping factor of the wing structure

Vector Symbols

$\{A_{ei}(t)\}$	The i-th column vector of the matrix $[A_e(t)]$
$\{A_\delta(t)\}$	Generalized transonic aerodynamic influence coefficient vector corresponding to the unsteady control surface motion
$\{\bar{A}_\delta(t)\}$	Generalized subsonic aerodynamic influence coefficient vector corresponding to the unsteady control surface motion
$\{\bar{A}_\delta(s)\}$	Laplace transform of the vector $\{\bar{A}_\delta(t)\}$
$\{e_i\}$	Unit vector whose i-th element is 1
$\{G\}_k$	Controller gain vector at time $t=kT_s$
$\{L\}_k$	Estimator gain vector at time $t=kT_s$
$\{q(t)\}$	Displacement vector
$\{Q(t)\}$	Transonic aerodynamic force vector
$\{R(t)\}$	Generalized transonic aerodynamic force vector
$\{R_s\}$	Generalized transonic aerodynamic force vector at steady state
$\{R_e(t)\}$	Generalized transonic aerodynamic force vector corresponding to the unsteady elastic wing motion
$\{\bar{R}_e(t)\}$	Generalized subsonic aerodynamic force vector corresponding to the unsteady elastic wing motion
$\{\bar{R}_e(s)\}$	Laplace transform of $\{\bar{R}_e(t)\}$
$\{R_\delta(t)\}$	Generalized transonic aerodynamic force vector corresponding to the unsteady control surface motion
$\{\bar{R}_\delta(t)\}$	Generalized subsonic aerodynamic force vector corresponding to the unsteady control surface motion
$\{\bar{R}_\delta(s)\}$	Laplace transform of $\{\bar{R}_\delta(t)\}$
$\{r(t)\}$	Unsteady component of the generalized displacement vector
$\{X_p\}_k$	Aeroservoelastic state vector associated with the estimated system parameters
$\{X_r(t)\}$	Aerodynamic state vector corresponding to the elastic wing deformation
$\{X_s(t)\}$	Structural State vector
$\{X_\delta(t)\}$	Aerodynamic state vector corresponding to the control surface deflection
$\{Y(t)\}$	Aeroservoelastic output vector
$\{\eta(t)\}$	Generalized displacement vector
$\{\eta_s\}$	Generalized displacement vector at steady state
$\{\theta\}_k$	Parameter vector at time $t=kT_s$
$\{\phi\}_k$	Regression vector at time $t=kT_s$

Matrix Symbols

$[A_p], [B_p], [C_p]$	Estimated aeroservoelastic system matrices
$[A_r], [B_{0r}], [B_{1r}],$ $[C_r], [D_{0r}], [D_{1r}]$	Aerodynamic system matrices corresponding to the elastic wing deformation
$[A_s], [B_s], [C_s]$	Structural system matrices
$[A_\delta], [B_{0\delta}], [B_{1\delta}],$ $[C_\delta], [D_{0\delta}], [D_{1\delta}]$	Aerodynamic system matrices corresponding to the control surface deflection
$[A_e(t)]$	Generalized transonic aerodynamic influence coefficient matrix corresponding to the unsteady elastic wing motion

$[\tilde{A}_e(t)]$	Generalized subsonic aerodynamic influence coefficient matrix corresponding to the unsteady elastic wing motion
$[\bar{A}_e(s)]$	Laplace transform of the matrix $[\tilde{A}_e(t)]$
[C]	Damping matrix
[I]	Identity matrix
[K]	Stiffness matrix
[M]	Mass matrix
[P]	Steady state Riccati matrix
$[P]_k$	Riccati matrix at time $t=kT_a$
[Q]	Weighting matrix for the state vector $\{X_p\}_k$
$[T_e(t)]$	Transonic correction matrix due to elastic wing deformation
$[T_\delta(t)]$	Transonic correction matrix due to control surface deflection
[U]	Eigenmatrix of order $n \times m$
$[V]_k$	Covariance matrix at time $t=kT_a$
$2[\zeta\omega]$	Generalized damping matrix
$[\omega^2]$	Generalized stiffness matrix
$[\Phi_r]$	State transition matrix $(\equiv e^{[A_r]T_a})$
$[\Phi_s]$	State transition matrix $(\equiv e^{[A_s]T_a})$
$[\Phi_\delta]$	State transition matrix $(\equiv e^{[A_\delta]T_a})$
$[\Theta_r]$	Time integration of state transition matrix $[\Phi_r]$ $(\equiv \int_0^{T_a} e^{[A_r]kT_a-\sigma)} d\sigma)$
$[\Theta_s]$	Time integration of state transition matrix $[\Phi_s]$ $(\equiv \int_0^{T_a} e^{[A_s]kT_a-\sigma)} d\sigma)$
$[\Theta_\delta]$	Time integration of state transition matrix $[\Phi_\delta]$ $(\equiv \int_0^{T_a} e^{[A_\delta]kT_a-\sigma)} d\sigma)$

1. Introduction

1.1 Background

The active flutter suppression problem of advanced aircraft configurations is a multidisciplinary design task which combines several disciplines such as structural dynamics, unsteady aerodynamics, control, and flight mechanics. During the past decade active flutter suppression systems for the subsonic and supersonic flight regimes have been studied extensively. However, the transonic flight regime has received only very limited attention. A considerable amount of effort has been spent on the development of active flutter suppression systems at NASA Langley Research Center under the Drones for Aerodynamic and Structural Testing (DAST) program.[1,2,3] The majority of flutter suppression studies related to the DAST wing model are based on the time invariant subsonic aeroservoelasticity.

Flutter suppression in the transonic flight regime using active controls presents a challenging problem due to the nonlinear nature of the transonic aeroelastic problem. Simple proportional, integral, and derivative (PID) type controllers combined with detailed unsteady transonic aerodynamics based on computational fluid dynamics (CFD) have been applied to the transonic flutter suppression problem.[4] In a recent research activity, industry, the Air Force research laboratories, and the NASA have joined efforts on the Active Flexible Wing (AFW) program.[5] A low-order real time digital flutter suppression system for the AFW model was actually built and tested in subsonic flight conditions.[6] For the transonic regime a simple PID controller for the AFW was studied using a computational aerodynamics based simulation.[7,8]

In recent years an extensive body of research aimed at computing the three-dimensional unsteady transonic aerodynamic loads using computational aerodynamics has been developed.[9,10,11] Excellent computer codes based on the transonic small disturbance equation or the full potential equation were developed and tested with various wing geometries.[12,13,14] Detailed CFD techniques for the three-dimensional unsteady transonic aerodynamics promise accurate prediction of the aerodynamic forces for structural optimization applications. However, these techniques are often difficult to use in aeroservoelastic studies, because computing time can become excessive. Furthermore, frequently the aerodynamic loads are obtained in a form which is not convenient for inclusion in studies aimed at flutter suppression.

1.2 Motivation

The inherently nonlinear nature of the transonic aeroelasticity combined with the high computational cost associated with computational aerodynamic codes has limited the number of aeroservoelastic studies dealing with this flight regime.[4,7,8] To reduce computational cost for the three-dimensional unsteady transonic computations, approximation methods have been developed by a number of authors.[15,16,17] Approximation techniques developed to date were based on the frequency domain approach. The need for effective on-line active flutter suppression systems has led to the recognition that time domain aerodynamics are needed for aeroservoelasticity. A number of authors have developed time domain aeroelastic analyses suitable for the subsonic or supersonic flow regime.[18,19]

The majority of aeroservoelastic studies conducted to date have emphasized a linear time invariant system approach, because this approach has been found to be successful in the subsonic and supersonic flight regimes. In the transonic flight regime, which is inherently nonlinear, the validity of this linear approach is questionable. Furthermore, under actual flight conditions one can have variations in flight speed, thermal loads due to aerodynamic heating, varying amounts of fuel in the wing structure, and different external store configurations. Under such conditions the time invariant assumption may limit the validity of the aeroservoelastic model used in the design of an active flutter suppression system. Digital adaptive control methodology is an attractive candidate for real time active flutter suppression, because the control law parameters can be adjusted to follow the changes in the aeroelastic system.

Discrete time, digital, adaptive control is a well established methodology. The most attractive feature of this approach is its ability to handle mildly time varying nonlinear system, such as encountered in transonic aeroelasticity. Adaptive control has been applied successfully to the control of robotic manipulators by a number of authors.[20,21] Application of an adaptive controller to subsonic active flutter suppression has been described by Slater and Livneh[22] using the model-reference adaptive system. The main drawback of the model-reference adaptive system is that the adaptive flutter suppression system did not work for a non-minimum-phase system which can occur in aeroelastic problems.[22]

The efficient computer modelling and simulation studies of a digital adaptive, real time, active flutter suppression system for time varying flight conditions in transonic flow require the treatment of three specific items. The first item required is an approximate method for computing the three-dimensional unsteady transonic aerodynamic loads to reduce the computational cost of the aeroservoelastic studies. Secondly, the approximate three-dimensional unsteady transonic aerodynamic loads should be calculated in the time domain. This is an essential requirement for the real time computer simulation of the adaptive digital flutter suppression system. The third ingredient is the ability to change the free stream Mach number during the computer simulation, so as to be able to test the adaptive flutter suppression system under time varying flight conditions. This last ingredient is quite difficult to implement because the unsteady aerodynamic load calculations are usually based on the assumption of a fixed free steam Mach number. Finally, it should be emphasized that a fast, approximate transonic aeroservoelastic simulation capability can play a useful role in preliminary design and structural optimization of actively controlled composite wings.

1.3 Research Goals

The primary objective of this study is to study the application of a digital adaptive optimal controller to transonic active flutter suppression. This is achieved by introducing on-line estimation for the aeroelastic state space model combined with an iterative Riccati solver for the control law synthesis procedure. On-line estimation of the aeroservoelastic state space model is based on a deterministic Auto-Regressive Moving Average (ARMA) model and an on-line parameter estimation technique. Wing response information at a selected sensor location is used for on-line parameter estimation.

The major advantage of this technique is that the same flutter suppression system can be used for the subsonic, transonic, or supersonic flight regimes, since the adaptive control technique is based only on the time history of wing motion. The on-line estimation of the aeroelastic state space model yields additional benefits. Until now the least squares curve fitting method[23] and the moving-block analysis[24] have been used to identify aeroelastic system damping and frequencies in time domain.[25,26,27] However, because of excellent convergence of the parameter estimator used in the present research, the time domain flutter boundary identification procedure can be carried out with a relatively small number of aeroelastic transient time history calculations. Simple eigenanalysis can be applied to the estimated state space equations to obtain the aeroelastic system damping and frequencies.

The second objective of this study is to develop a simple methodology for approximating the three-dimensional unsteady transonic aerodynamic loads in the time domain for the aeroservoelastic applications. The approximation procedure for obtaining these unsteady transonic loads is based on using relevant information from time domain unsteady subsonic aerodynamics. Methods developed for subsonic aerodynamic load calculations such as frequency domain lifting surface theories[28,29] and the finite state approximations[30,31,32] are utilized in this approximation method. The transonic approximation method developed here requires only the computation of a transonic correction matrix which is used in conjunction with a time domain subsonic code.

The well known transonic bucket effect can be captured. Thus, transonic aeroelastic computations can be carried out with low computational cost while retaining the important physical transonic aeroelastic characteristics. Divergence analysis can also be carried out with considerable ease. Another important feature of the approximate transonic aerodynamic load representation used in this study is the ability to vary the free stream Mach number during the simulation. This enables one to test the adaptive optimal controller under time varying flight conditions.

2. Mathematical Model for the Aeroelastic System in Transonic Flow

2.1 Structural Modelling

The small perturbation equations of motion for a wing structure have the following form

$$[M]\{\ddot{q}(t)\} + [C]\{\dot{q}(t)\} + [K]\{q(t)\} = \{Q(t)\} \quad . \tag{1}$$

Mass and stiffness matrices, [M] and [K], in Eq.(1) are obtained using the LIfting Surface Structural Analysis (LISSA) computer code.[33] This code is based on wing equivalent plate analysis.[34] In this wing equivalent plate analysis wing deflections and mode shapes are accurately predicted using a relatively small number of polynomial terms. It was reported[34] that wing equivalent plate analysis is 30 and 60 times faster than the finite element method in static and free vibration analysis, respectively. The LISSA code is particulary efficient for the multidsciplinary optimization of composite wings[35,36] with a rich variety of practical constraints.

Solving the free vibration problem represented by Eq.(1) using an orthonormal coordinate transformation $\{q(t)\} = [U]\{\eta(t)\}$ together with an assumed modal damping yields:

$$\{\ddot{\eta}(t)\} + 2[\zeta\omega]\{\dot{\eta}(t)\} + [\omega^2]\{\eta(t)\} = \{R(t)\} \tag{2}$$

The orthonormalized equations of motion, Eq.(2), can be rearranged to obtain the structural state-differential equation and structural measurement equation. The structural state-differential equation in the first order state variable form is given by:

$$\{\dot{X}_s(t)\} = [A_s]\{X_s(t)\} + [B_s]\{R(t)\} \tag{3}$$

and the structural measurement equation can be written as:

$$\{Y(t)\} = [C_s]\{X_s(t)\} \tag{4}$$

2.2 Time Domain Unsteady Transonic Aerodynamics

Since the steady state transonic aerodynamics of the wing is essentially nonlinear, the airfoil shape of the wing determines both the position and strength of the steady state shock. The perturbed unsteady aerodynamics, due to wing motion, is strongly affected by the steady state shock waves. To obtain a good approximation to the unsteady aerodynamic loads, the correct computation of the steady state pressure on the wing surface is a basic requirement.[37] In some cases steady state pressure distribution from the wind tunnel test or computations based on CFD codes were used to obtain the nonlinear steady state aerodynamics for the approximate methods.[16,17,37] The second assumption frequently used in approximate transonic aerodynamic load calculations is that the perturbed unsteady wing motion around the steady state position can be treated as linear when sufficiently small wing motions occur.[38]

In this study, we adopt the assumption that for a small dynamic motion of the wing, the unsteady transonic aeroelastic model is a dynamically linear model.[38] Using this assumption for the perturbed wing motion the following vector equation can be written for the generalized transonic aerodynamic force vector $\{R(t)\}$.

$$\{R(t)\} = \{R_s\} + \{R_\epsilon(t)\} + \{R_\delta(t)\} \tag{5}$$

The vector $\{R_s\}$ in Eq.(5) represents the generalized steady state transonic aerodynamic force vector. $\{R_\epsilon(t)\}$ and $\{R_\delta(t)\}$ are generalized unsteady transonic aerodynamic force vectors due to elastic deformations of the wing around the steady state position and control surface motion, respectively.

The approximate method for calculating the three-dimensional unsteady transonic aerodynamic loads employed in this research consists of three steps.

1) Steady state transonic aerodynamic influence coefficient matrices are computed using detailed three-dimensional full potential transonic CFD code.
2) Transonic correction matrices are obtained from the steady state subsonic and transonic aerodynamic influence coefficient matrices.
3) Three-dimensional unsteady transonic aerodynamic loads are obtained from the three-dimensional unsteady subsonic aerodynamic loads corrected by the using transonic correction matrices.

The first step is the computation of the steady state transonic aerodynamic force vector $\{R_s\}$. The vector $\{R_s\}$ is a generalized nonlinear steady state transonic aerodynamic force vector. The full potential code developed by Shankar et al.[13] is used to obtain $\{R_s\}$ and $\{\eta_s\}$. Here, the generalized displacement vector $\{\eta_s\}$ of order m corresponds to the steady state position of the wing structure.

The unsteady components $\{R_\epsilon(t)\}$ and $\{R_\delta(t)\}$ in Eq.(5) are computed as follows. A perturbed generalized displacement vector for the dynamic motion of the wing can be defined by

$$\{r(t)\} \equiv \{\eta(t)\} - \{\eta_s\} \quad .$$

Since $\{r(t)\}$ and the control surface deflection $\delta(t)$ are small, it is assumed that vectors $\{R_\epsilon(t)\}$ and $\{R_\delta(t)\}$ in Eq.(5) can be calculated using the transonic aerodynamic influence coefficient matrices given by

$$\{R_\epsilon(t)\} \equiv [A_\epsilon(t)]\{r(t)\} \tag{6}$$

and

$$\{R_\delta(t)\} \equiv \{A_\delta(t)\}\delta(t) \tag{7}$$

$[A_\epsilon(t)]$ and $\{A_\delta(t)\}$ are assumed constant and are calculated by perturbing the generalized displacements about

the steady state reference position of the wing and calculating the resulting perturbations in transonic aerodynamic forces. Thus,

$$\{A_{ri}(t)\} = \frac{\partial}{\partial r_i}\{R_r(t)\} \tag{8}$$

and

$$A_{\delta i}(t) = \frac{\partial}{\partial \delta}\{R_\delta(t)\} \tag{9}$$

and since there is no dependency on time we denote them $[A_r(\infty)]$ and $\{A_\delta(\infty)\}$. Now, corresponding influence coefficient matrices due to small steady displacement and control surface perturbations in subsonic flow are calculated by the Piecewise Continuous Kernel Function Method[29] (PCKFM) and denoted $[\bar{A}_r(\infty)]$ and $\{\bar{A}_\delta(\infty)\}$. A correction matrix is now constructed to transform the subsonic steady generalized load matrix to its transonic small perturbation equivalent.

$$[A_r(\infty)] = [T_r(\infty)][\bar{A}_r(\infty)] \tag{10}$$

leading to:

$$[T_r(\infty)] = [A_r(\infty)][\bar{A}_r(\infty)]^{-1}$$

Similarly, the i-th element of the other transonic correction matrix $[T_\delta(\infty)]$, which is a diagonal matrix, is assumed to be

$$T_{\delta i}(\infty) = \frac{A_{\delta i}(\infty)}{\bar{A}_{\delta i}(\infty)}$$

This correction is applied at each time t to unsteady aerodynamic forces calculated by the PCKFM.

$$\{A_r(t)\} = [T_r(\infty)][\bar{A}_r(t)]$$

$$\{A_\delta(t)\} = \{T_\delta(\infty)\}\{\bar{A}_\delta(t)\}$$

leading (Eqs.(6) and (7)) to

$$\{R_r(t)\} = [T_r(\infty)]\{\bar{R}_r(t)\}$$

$$\{R_\delta(t)\} = [T_\delta(\infty)]\{\bar{R}_\delta(t)\}$$

The second step in obtaining the approximate aerodynamic loads used in this study resembles the quasisteady correction method suggested by Zwaan.[16]

The third step required for the computation of the approximate aerodynamic loads consists of the computations of the generalized subsonic aerodynamic force vectors $\{\bar{R}_r(t)\}$ and $\{\bar{R}_\delta(t)\}$ in the time domain. The generalized subsonic aerodynamic force vectors $\{\bar{R}_r(t)\}$ and $\{\bar{R}_\delta(t)\}$ in the time domain are obtained from the subsonic aerodynamic state space descriptions. Using the Roger's approximation to the Laplace transformed subsonic generalized aerodynamic influence coefficient matrices leads to

$$[\bar{A}_r(s)] = [D_{0r}] + s[D_{1r}] + \sum_{i=1}^{NG}[C_i]\frac{s}{s+\Omega_i} \quad . \tag{12}$$

Since for subsonic unsteady flow

$$\{\bar{R}_r(s)\} = [\bar{A}_r(s)]\{r(s)\} \quad . \tag{13}$$

we substitute Eq.(13) into (12) to get

$$\{\bar{R}_r(s)\} = [D_{0r}]\{r(s)\} + [D_{1r}]s\{r(s)\} + \sum_{i=1}^{NG}[C_i]\frac{s}{s+\Omega_i}\{r(s)\}. \tag{14}$$

Aerodynamic states are defined as

$$\{\bar{X}_{ri}(s)\} = \{\bar{r}(s)\}\frac{s}{s+\Omega_i}$$

$$s\{\bar{X}_{ri}(s)\} = -\Omega_i[I]\{\bar{X}_{ri}(s)\} + s[I]\{\bar{r}(s)\} \quad i=1,2,\cdots NG$$

Thus:

$$s\{\bar{X}_r(s)\} = [A_r]\{\bar{X}_r(s)\} + [B_{1r}]s\{\bar{r}(s)\} \quad . \tag{15}$$

where $\{\bar{X}_r(s)\}^T = \left[\{\bar{X}_{r1}(s)\}^T\{\bar{X}_{r2}(s)\}^T \cdots \{\bar{X}_{rNG}(s)\}^T\right]$.

Transforming Eqs.(14) and (15) back to the time domain leads to

$$\{\bar{R}_r(t)\} = [C_r]\{X_r(t)\} + [D_{0r}]\{r(t)\} + [D_{1r}]\{\dot{r}(t)\} \quad . \tag{16}$$

where $[C_r] = [[C_1][C_2]\cdots[C_{NG}]]$,

and to

$$\{\dot{X}_r(t)\} = [A_r]\{X_r(t)\} + [B_{1r}]\{\dot{r}(t)\} \quad . \tag{17}$$

Similarly, for the control surface subsonic unsteady aerodynamic forces:

$$\{\bar{R}_\delta(t)\} = [C_\delta]\{X_\delta(t)\} + [D_{0\delta}]\delta(t) + [D_{1\delta}]\dot{\delta}(t) \tag{18}$$

$$\{\dot{X}_\delta(t)\} = [A_\delta]\{X_\delta(t)\} + [B_{1\delta}]\dot{\delta}(t) \tag{19}$$

To complete this section a brief discussion of the limitations of the present approximations to the unsteady transonic aerodynamic loads is presented. Three possible cases can be encountered during the simulations. The first case corresponds to a subsonic free stream Mach number, which is sufficiently low so that the local shock has not developed yet over the wing surface. For this case the subsonic assumption for representing the unsteady aerodynamic effects is appropriate. The second flight condition corresponds to the development of a local shock over the wing surface, however its position is still far upstream of the trailing edge. In this case the wing trailing edge is still in subsonic flow. However, due to the local supersonic subregion on the wing, the unsteady subsonic assumption is violated in this, fairly small region. The third condition corresponds to a strong shock which is in the vicinity of the trailing edge. Under such conditions wing motions will produce chordwise motion and oscillations of the local shock wave. When the local shock wave moves aft of the trailing edge, the wing trailing edge will be in the local supersonic flow. Obviously this condition will represent the most severe violation of the subsonic assumption, used to generate the unsteady transonic aerodynamic loads, employed in this

study.

Another limitation of the present approximate method is due to the quasisteady correction for transonic effects. Due to this limitation the approximate method gives more accurate results in the low reduced frequency range.

2.3 Iterative Time Marching Structure/Aerodynamic Integration

Structural and aerodynamic state-differential equations are integrated simultaneously using an iterative time-marching algorithm and state transition matrices. It is assumed that vectors $\{R(t)\}$, $\{r(t)\}$, and $\{\dot{r}(t)\}$ are linear in time interval $kT_a \le t \le (k+1)T_a$. In this time interval, these vectors are assumed to be equal to average of their value over the interval. Where, T_a represents the time step of the iterative time-marching algorithm. Thus, time integration of state-differential equations in the first order state variable form yields the following state-difference equations.[25]

$$\{X_s\}_{k+1} = [\Phi_s]\{X_s\}_k + [\Theta_s][B_s]\frac{\{R\}_k + \{R\}_{k+1}}{2} \quad . \qquad (20)$$

Similarly the aerodynamic state-difference equations can be written as:

$$\{X_r\}_{k+1} = [\Phi_r]\{X_r\}_k + [\Theta_r][B_{1r}]\frac{\{\dot{r}\}_k + \{\dot{r}\}_{k+1}}{2} \qquad (21)$$

$$\{X_\delta\}_{k+1} = [\Phi_\delta]\{X_\delta\}_k + [\Theta_\delta]\{B_{1\delta}\}\frac{\dot{\delta}_k + \dot{\delta}_{k+1}}{2} \qquad (22)$$

Structural and aerodynamic measurement equations at a discrete time $k+1$ lend themselves to simple representations. The structural measurement equation given in Eq.(4) can be written in the discrete time as

$$\{Y\}_{k+1} = [C_s]\{X_s\}_{k+1} \qquad (23)$$

and aerodynamic measurement equations become

$$\{\bar{R}_e\}_{k+1} = [C_r]\{X_r\}_{k+1} + [D_{0r}]\{r\}_{k+1} + [D_{1r}]\{\dot{r}\}_{k+1} \qquad (24)$$

and

$$\{\bar{R}_\delta\}_{k+1} = [C_\delta]\{X_\delta\}_{k+1} + \{D_{0\delta}\}\delta_{k+1} + \{D_{1\delta}\}\dot{\delta}_{k+1} \qquad (25)$$

In Eq.(20) the structural state vector $\{X_s\}_{k+1}$ is a function of the structural state vector $\{X_s\}_k$ and the generalized transonic aerodynamic force vectors $\{R\}_k$ and $\{R\}_{k+1}$. However, the generalized transonic aerodynamic force vector $\{R\}_{k+1}$ is not available at the beginning of time step $k+1$. At time $k+1$, the generalized subsonic aerodynamic force vectors can be written as

$$\{\bar{R}_e\}_{k+1} \simeq 2\{\bar{R}_e\}_k - \{\bar{R}_e\}_{k-1} \qquad (26)$$

$$\{\bar{R}_\delta\}_{k+1} \simeq 2\{\bar{R}_\delta\}_k - \{\bar{R}_\delta\}_{k-1} \qquad (27)$$

Thus, Eqs.(20) through (25) can be solved iteratively at time step $k+1$, and the iterative time-marching algorithm can be summarized as follows:

1) Predict $\{\bar{R}_e\}_{k+1}$ and $\{\bar{R}_\delta\}_{k+1}$ using Eqs.(26) and (27).
2) Calculate the generalized transonic aerodynamic force vector at time $k+1$.

   $$\{R\}_{k+1} = \{R_s\} + [T_e(\infty)]\{\bar{R}_e\}_{k+1} + [T_\delta(\infty)]\{\bar{R}_\delta\}_{k+1}$$

3) The structural state vector $\{X_s\}_{k+1}$ and aeroservoelastic output vector $\{Y\}_{k+1}$ can be obtained from Eqs.(20) and (23), respectively.
4) Determine the control surface deflection angle δ_{k+1} and construct generalized displacement vectors $\{r\}_{k+1}$ and $\{\dot{r}\}_{k+1}$. The control surface deflection angle δ_{k+1} can be calculated using information associated with the controller, which will be described in the next section.
5) Calculate aerodynamic state vectors $\{X_r\}_{k+1}$ and $\{X_\delta\}_{k+1}$ from Eqs.(21) and (22), respectively, and update generalized subsonic aerodynamic force vectors $\{\bar{R}_e\}_{k+1}$ and $\{\bar{R}_\delta\}_{k+1}$ at time $k+1$ using Eqs.(24) and (25). If the iteration number is larger than the assigned value, go to step 1. Otherwise, return to step 2.

It should be noted that one iteration in the this iterative scheme corresponds to the time-marching algorithm developed by Edwards et al.[25] Two consecutive iterations in this iterative algorithm correspond to the predictor-corrector scheme used by Robinson et al.[39] The main drawback of the above iterative scheme is that the time consuming control law design procedure is inside the iterative scheme. Therefore for better computational efficiency control surface deflection angle δ_{k+1} is not updated during these iterative computations.

3. Adaptive Controller

3.1 Input-Output and State-Space Descriptions of the Aeroservoelastic System

In this study single-input single-output deterministic ARMA model with $2M$ Auto-Regressive (AR) and $2M$ Moving Average (MA) coefficients[40] is used to describe the input-output relation for the aeroservoelastic system.

$$y_k + \sum_{i=1}^{2M} a_i y_{k-i} = \sum_{i=1}^{2M} b_i \delta_{k-i} \quad ,$$

In vector form,

$$y_k = \{\theta\}_k^T\{\phi\}_k \quad , \qquad (28)$$

where

$$\{\theta\}_k^T \equiv \left\lfloor -a_1 \; -a_2 \; \cdots \; -a_{2M} \; b_1 \; b_2 \; \cdots \; b_{2M} \right\rfloor$$

$$\{\phi\}_k^T \equiv \left\lfloor y_{k-1} \; y_{k-2} \; \cdots \; y_{k-2M} \; \delta_{k-1} \; \delta_{k-2} \; \cdots \; \delta_{k-2M} \right\rfloor .$$

In Eq.(28) y_k and δ_k are the wing response and control surface deflection angle at discete time k, respectively. The input-output description given by Eq.(28) is equivalent to a state-space description which can be written as

$$\{X_p\}_{k-1} = [A_p]\{X_p\}_k + \{B_p\}\delta_k \tag{29}$$

$$y_k = [C_p]\{X_p\}_k \ , \tag{30}$$

where

$$[A_p]=\begin{bmatrix} -a_1 & 1 & 0 & \cdots & 0 \\ -a_2 & 0 & 1 & \cdots & 0 \\ \cdots & \cdots & \cdots & \cdots & \cdots \\ -a_{2M-1} & 0 & 0 & \cdots & 1 \\ -a_{2M} & 0 & 0 & \cdots & 0 \end{bmatrix} \quad \{B_p\}=\begin{Bmatrix} b_1 \\ b_2 \\ \cdots \\ b_{2M-1} \\ b_{2M} \end{Bmatrix}$$

and

$$[C_p] = \begin{bmatrix} 1 & 0 & 0 & \cdots & 0 \end{bmatrix} .$$

The state vector $\{X_p\}_k$ is defined

$$\{X_p\}_k \equiv \begin{Bmatrix} y_k \\ h_1(k) \\ \cdots \\ h_{2M-1}(k) \end{Bmatrix} \tag{31}$$

with

$$\begin{aligned} y_k &= -a_1 y_{k-1} + b_1\delta_{k-1} + h_1(k-1) \\ h_1(k) &= -a_2 y_{k-1} + b_2\delta_{k-1} + h_2(k-1) \\ &\cdots \\ h_{2M-2}(k) &= -a_{2M-1} y_{k-1} + b_{2M-1}\delta_{k-1} + h_{2M-1}(k-1) \\ h_{2M-1}(k) &= -a_{2M} y_{k-1} + b_{2M}\delta_{k-1} \ . \end{aligned} \tag{32}$$

The state space description in Eqs.(29) and (30) is in *observer form* and is completely observable.[41] Thus, each element of the state vector given in Eq.(31) can be observed completely.

3.2 On-Line Parameter Estimation

Identification of structural dynamic properties using parameter estimation techniques has been studied by many authors.[20,21,42,43] Parameter estimation techniques have been also applied to the stability and control studies of flight vehicles.[44,45,46] Application of parameter estimation techniques to aeroservoelastic systems is introduced in this study. The AR and MA coefficients in matrices $[A_p]$ and $\{B_p\}$ are estimated using the Bierman's U-D (BUD) algorithm[47] given as

$$\{\theta\}_k = \{\theta\}_{k-1} + \{L\}_k(y_k - \{\theta\}_{k-1}^T\{\phi\}_k)$$

$$\{L\}_k = \frac{[V]_{k-1}\{\phi\}_k}{\lambda_k + \{\phi\}_k^T[V]_{k-1}\{\phi\}_k} \tag{33}$$

$$[V]_k = \frac{[V]_{k-1}}{\lambda_k} - \frac{[V]_{k-1}\{\phi\}_k\{\phi\}_k^T[V]_{k-1}}{\lambda_k(\lambda_k + \{\phi\}_k^T[V]_{k-1}\{\phi\}_k)} \ ,$$

where a covariance matrix $[V]_k$ is defined as $[V]_k \equiv [U]_k[D]_k[U]_k^T$. Detailed descriptions of the calculations of a diagonal matrix $[D]_k$ and an upper triangular matrix $[U]_k$, whose diagonal elements equal to 1, are presented in reference 47. The BUD algorithm is a modified version of the recursive least squares algorithm which ensures the positive definiteness of the covariance matrix in the recursive estimation procedure.

The main advantage of the parameter estimator is that the additional state estimator is not required to estimate system states. Once the AR and MA coefficients in matrices $[A_p]$ and $\{B_p\}$ are estimated, then the state vector $\{X_p\}_k$ can be calculated using Eq.(32).

3.3 On-Line Control Law Design

The unknown aeroservoelastic system parameters are estimated using an on-line recursive estimation method. The next step is an on-line control law design procedure using the estimated aeroservoelastic system parameters. The estimated aeroservoelastic system parameters are treated as if they are true; i.e. the uncertainties of the estimation are not considered.

The adaptive optimal control law is designed to minimize approximately the following linear quadratic performance index J.

$$J = \sum_{k=0}^{\infty} (\{X_p\}_k^T[Q]\{X_p\}_k + r_w\delta_k^2) \ .$$

where $[Q]$ is a positive semidefinite symmetric matrix and r_w is a positive constant. The following control law would be optimal for J.[20]

$$\delta_k = -\{G\}_k^T\{X_p\}_k \ , \tag{34}$$

where a controller gain vector $\{G\}_k$ is based on

$$\{G\}_k^T = \frac{\{B_p\}^T[P]_k[A_p]}{r_w + \{B_p\}^T[P]_k\{B_p\}}$$

and the Riccati matrix $[P]_k$ is obtained using

$$[P]_k=[A_p]^T\left([P]_{k-1}-\frac{[P]_{k-1}\{B_p\}\{B_p\}^T[P]_{k-1}}{r_w+\{B_p\}^T[P]_{k-1}\{B_p\}}\right)[A_p]+[Q] \tag{35}$$

The Riccati matrix $[P]_k$ will converge to a constant nonnegative symmetric matric $[P]$, which satisfies the discrete-time algebraic Riccati equation

$$[P] = [A_p]^T\left([P] - \frac{[P]\{B_p\}\{B_p\}^T[P]}{r_w + \{B_p\}^T[P]\{B_p\}}\right)[A_p] + [Q] \tag{36}$$

, if the aeroservoelastic system is stabilizable. At time k the Riccati matrix $[P]_k$ in Eq.(35) can be iterated as follows:

1) Calculate $[P]_k$ based on Eq.(35).

2) If the Riccati matrix $[P]_k$ is converged, go to the next time step. Otherwise, assign $[P]_{k-1} = [P]_k$ and return to step 1).

Only one iteration is recommended at each discrete time step to save the computation time for the control law design procedure.[40] The adaptive optimal control law given in Eq.(34) is thus obtained using estimated aeroservoelastic system matrices $[A_p]$ and $\{B_p\}$ together with one iteration of Eq.(35).

3.4 Special Features of the Computer Simulation

Covariance Matrix Resetting Technique. When diagonal elements, which corresponds to AR coefficients, of the covariance matrix $[V]_k$ in the parameter estimator given in Eq.(33) converge to very small values while other elements, which corresponds to MA coefficients, remain large, then additional recursive computations can not improve the convergence of AR and MA coefficients. A covariance matrix resetting technique is essential in order to increase the convergence rate and robustness of the parameter estimator.[41] In such a technique the covariance matrix is periodically changed to a diagonal matrix $\alpha[I]$. In this study, the average of the maximum and minimum diagonal elements of the covariance matrix is used

$$[D]_j = \alpha[I]$$

$$[U]_j = [I] \ .$$

where

$$\alpha = \frac{MAX(D_{ii}(j-1)) + MIN(D_{ii}(j-1))}{2}.$$

The subscript j and $D_{ii}(j-1)$ represent the resetting time and the i-th diagonal element of the matrix $[D]_{j-1}$, respectively.

Order of the ARMA Model. It is possible to estimate the order of the ARMA model from input and output data if a lattice filter is used as a parameter estimator.[21,43,48] The BUD algorithm for parameter estimation in this study does not have the ability to estimate the order of the ARMA model. Thus, it is assumed that the order of the ARMA model, $2M$, is known. The order of aeroelastic system matrices obtained from the Roger's approximation can be calculated from the following equation.[49]

$$NM = 2m + m \times NG \ .$$

Here, m and NG represent the order of the generalized displacement vector and the number of aerodynamic lag terms in the Roger's approximation, respectively. Theoretically, the order of a deterministic ARMA model, $2M$, should be equal to NM. However, the full state-feedback control law and the small sampling time T_s for a digital controller can not be used because of practical limitations. Therefore, the reduced order feedback controller is used in this study. It is assumed that the order of the deterministic ARMA model is less than or equal to the order of the generalized displacement vector.

$$M \le m \ .$$

The reduced order ARMA model ($2M<NM$) faces a potential problem since unmodeled high frequency components can cause a frequency aliasing in the parameter estimation and control law design procedures. Using an anti-aliasing filter is one possible approach for reducing the sensitivity of the estimator.

Since the contribution of lightly damped modes dominates the dynamic response of an aeroservoelsuc system, and since our interest is focused on these lightly damped modes, relatively small M and m are selected for the reduced order ARMA model and the order of the generalized displacement vector, respectively. In this study, most of the numerical examples use $m = 3$ and $NG = 8$. Therefore, NM becomes 30. However, the order of the ARMA model $2M$ is equal to 6. Hence, 24 frequency components are neglected in the adaptive optimal control law design procedure.

In order to study potential problems due to unmodelled dynamics a large order aeroservoelastic system is also used. A tenth order sine Butterworth low-pass filter[50] is used as the anti-aliasing filter in the present study. The number of structural natural frequencies which are smaller than the cutoff frequency of the anti-aliasing filter is assigned to the value of M. For this example with the unknown random external loads, 8, 16, and 3 are assigned to values of m, NG, and M, respectively. Thus, eight modes are included in the time histories computed with three modes in the previous case.

Learning Period. A short learning period, $t = 8 \times M \times T_s$, is used for obtaining the initial estimates of the ARMA coefficients which are needed for initializing the Riccati matrix $[P]_k$ in Eq.(34). During this period, the control surface is excited by small-amplitude white noise. At the end of the learning period, the initial condition of the the Riccati matrix, $[P]_0$, is calculated from the discrete-time algebraic Riccati equation, Eq.(36), using Potter's method.[51]

Caution should be exercised when the computer simulation is started under the unstable flight condition because wing response in this case can become excessively large during the learning period.

Forgetting Factor. A fundamental property of the adaptive controller for an active flutter suppression system is its ability to track variations in the aeroelastic system. To follow changes in the aeroelastic system it

is necessary to discard old time history of the aeroelastic response information in the parameter estimator. It should be emphasized that tracking a system with rapidly varying parameters is not possible. However, a slow time varying system can be tracked reasonably well. It is assumed in this study that aeroelastic system parameters change slowly.

Old time history data of the aeroelastic response is discarded exponentially in this study.[40] When the forgetting factor λ_i, given in Eq.(33), is equal to one, all data have the same weighting. This forgetting factor is used for the time invariant aeroelastic system. When the forgetting factor is less than one, recent data are given more weight than old data. Thus, a forgetting factor of less than one is used for the time varying aeroelastic system.

From this brief discussion it is evident that the forgetting factor is linked to the rate of change of the system parameters. In practical implemetation, changes in the properties of an aeroelastic system can be associated with changes in air temperature, pressure, and speed of flight. The proper forgetting factor for different rates of parameter changes can be determined accordingly.

Computational Delay. The on-line computation of the aeroelastic system parameter estimation and control law design will produce a computational delay between measurement and control command. In this study a computational delay is not taken into account. It should be noted that in order to have feasible practical implementation, the computational delay should be less than or equal to the sampling time T_ϵ.

4. The Wing Model Used for Computer Simulations

The structural modelling in this study can handle practical wings with composite skins.[36] However for the computations carried out in this study, an aluminum/plastic foam wing model was selected, because the results of the computed flutter boundaries could be compared with experimental results. This cantilevered rectangular wind tunnel model wing with 6% circular-arc cross sections and an aspect-ratio of 5.0 was actually built and tested in 1959.[52] It has an aluminum insert covered with flexible plastic foam. Experimental flutter boundaries and natural frequencies for this wing are available.

Natural frequencies and flutter boundaries for this wing model were computed by Guruswamy et al. using XTRAN3S[53] and XTRAN3S-AMES[54] codes. The planform geometry of this wing has been modified in the flutter suppression studies by Guruswamy et al.[4] A trailing edge control surface as shown in Figure 1 was introduced in Ref. 4. Five translational and five rotational springs are used in this study to physically connect the wing and control surfaces. These springs are equally spaced along the hinge line between the wing and trailing-edge control surfaces as shown in Figure 1. The material properties of the model wing and the additional spring constants defined in this study are given in Table 1.

Three wing rectangular sections as shown in Figure 1 are used for the LISSA and PCKFM computer representation. The full potential CFD code developed by Shankar et al.[13] with 88x12x18 grid is used to obtain the transonic correction matrices. Steady state transonic pressure distribution on the wing surface for different Mach numbers are shown in Figure 2.

5. Results

5.1 Flutter and Divergence Boundaries

Before comparing the flutter and divergence boundaries, natural frequncies of the cantilevered rectangular wing obtained from the on-line parameter estimation technique are compared with the experimental and other computational results. In this example structural transient time response was calculated using the iterative time marching structure/aerodynamic integration scheme with the assumption $\{R\}_i = \{0\}$ and $[\zeta\omega] = [0]$. Natural frequencies from the experiment[52], a finite element analysis[53], the LISSA code with eigenanalysis, and the LISSA code with the on-line parameter estimation technique are presented in Table 2. The results in Table 2 are calculated for $T_\epsilon = 0.001656$sec; 24 AR coefficients were used together with 45 sampling points. The on-line estimation of structural frequencies and the assumed structural modal damping factors for the cantilevered rectangular wing without aerodynamic loads is presented in Table 3. The results in Table 3 are calculated for the same values of T_ϵ, AR coefficients and sampling points as used in Table 2. It was also assumed that the modal damping ratio was $\zeta_i = .0200$, $i=1,2,\cdots,5$. It is evident from Tables 2 and 3 that the on-line estimation can yield system frequencies and values of modal damping correctly. In Table 2 the difference between the present analysis and the finite element analysis of Ref. 53 is that mass and stiffness properties of the plastic foam were not included in Ref. 53 analysis. In our analysis, the stiffness and mass properties of the flexible plastic foam are included in the calculation. It is evident from the results shown in Table 2 that the stiffness and mass properties of the flexible plastic foam need to be included in order to obtain the better agreement with experiment.

Flutter Boundaries. In the estimation of the open-loop flutter boundaries the MA coefficients in the ARMA model are neglected. Aeroelastic stability of the wing is determined from the eigenvalues of the estimated matrix $[A_p]$ in Eq.(29). It should be noted that the ARMA model in Eq.(28) is based on the discrete time system. Aeroelastic modal dampings and

damped frequencies, σ_j and ω_{dj}, for the continuous time system can be obtained by using the following equations.

$$\sigma_j = \frac{1}{2T_s}\log_e(c_j^2 + d_j^2)$$

$$\omega_{dj} = \frac{1}{T_s}\tan^{-1}\frac{d_j}{c_j}$$

Here, c_j and d_j are the real and imaginary part of the eigenvalues obtained from the estimated matrix $[A_p]$. Flutter boundaries for the aeroelastic system are determined from the aeroelastic modal dampings σ_j. When $\sigma_j < 0$ the system is stable and when $\sigma_j = 0$, it is on the flutter boundary. When $\sigma_j > 0$ the system is unstable.

The effectiveness of the parameter estimation technique based on the ARMA model to identify the flutter boundary is demonstrated in Table 4. The results in Table 4 are calculated for the same values of T_s and AR coefficient as used in Tables 2 and 3; $q_D = 9.439\ kPa$ and 10 iterations are used for the iterative time marching structure/aerodynamic integration scheme. Flutter boundaries obtained from eigenanalysis of the aeroelastic system equation in first order state variable form, V-g method in frequency domain, and the on-line parameter estimation technique applied to the aeroelastic transient time responses are compared in Table 4. In this table subsonic aerodynamics are used to check the accuracy of the iterative time marching structure/aerodynamic integration scheme. The agreement between these three sets of results is quite good. Small discrepancies between the eigenanalysis and on-line parameter estimation observed in Table 4 are mainly due to the linear assumptions for $\{R(t)\}$,$\{r(t)\}$, and $\{\dot{r}(t)\}$ vectors in time interval $kT_a \le t \le (k+1)T_a$.

Transonic flutter boundaries for the cantilevered wing, obtained from the on-line parameter estimation technique developed in this study, are compared with experimental and other computational results in Figures 3 and 4. Steady state pressure distributions for various Mach number (Figure 2) show that transonic shock effects start to appear near $M_\infty = 0.84$. Thus, the transonic approximation, shown in Figures 3 and 4, is in reasonable agreement with experimental results up to $M_\infty = 0.84$. Between Mach number 0.84 to 0.90, the shock is well developed on the wing surface. Some discrepancies in this Mach number range in Figure 3 and 4 may be due to the mixed subsonic and supersonic sub-regions. When the Mach number exceeds 0.90, the shock will reach the wing trailing edge and supersonic sub-region will become much wider than the subsonic sub-region, as indicated in Figure 2. Therefore, the subsonic assumption used for generating the unsteady transonic aerodynamics is violated and it can not be used for Mach numbers greater than 0.90.

Flutter boundaries with the steady transonic aerodynamic load are also presented in Figures 3 and 4 to check the quasisteady assumption for the transonic correction matrix. It is evident from Figures 3 and 4 that the quasisteady assumption for the transonic correction matrix gives good agreement with the experimental and CFD results in the low transonic Mach number range.

Divergence Boundaries. A transonic divergence boundary for the wing can be obtained using the transonic aerodynamic influence coefficient matrix given in Eq.(6). From Eqs.(2), (5), and (6), the following equation can be derived to include only structural stiffness and aerodynamic stiffness of the wing.

$$([\omega^2] - [A_s(t)])\{\eta(t)\} = \{0\}$$

Divergence boundaries are a function of dynamic pressure q_D, and it can be obtained from the determinant of the matrix $([\omega^2] - [A_s(t)])$ using a root finder.

Divergence boundaries for the cantilevered rectangular wing using subsonic or transonic aerodynamics are shown in Figure 5. Comparing Figures 2 and 5 a transonic bucket (evident also in the flutter boundary) occurs at a lower Mach number for the divergence boundaries. In the present case the transonic bucket in the flutter boundaries could be directly associated with the steady transonic aerodynamic loads.

5.2 Adaptive Subsonic Flutter Suppression

The effectiveness and versatility of the adaptive optimal controller is studied by applying it in two flight regimes: subsonic and transonic. The subsonic flutter suppression studies are used to learn about input parameters for the digital adaptive optimal controller.

Random External Loads. Robustness of the digital adaptive controller was tested using random loads. The computer simulation was carried out using subsonic aerodynamic loads obtained from assuming that $[T_s(\infty)] = [T_\delta(\infty)] = [I]$. The random loads are generated by introducing appropriate random changes in the angle of attack. Maximum change in the angle of attack is determined by using a suitable combination of gust and free stream velocities. A gust velocity of 39.37 *inch/sec* at $M_\infty = 0.714$ and $q_D = 9.763\ kPa$ produces approximately one *inch* deflection at a sensor position indicated in Figure 1.

The generalized equations of motion are based on 8 structural modes which are obtained from the LISSA code with 24 degrees of freedom. The aerodynamic influence coefficients evaluated by the PCKFM are based on the same number of degrees of freedom used in the LISSA model. Aerodynamic influence coefficient matrices are tabulated for 21 frequencies, where the highest frequency is 95.49 *Hz*. Tabulated generalized aerodynamic influence coefficient matrices are fitted in Laplace domain using Roger's approxima-

tion with 16 aerodynamic lag terms which are equally spaced between 0 and 95.49 Hz.

A sine Butterworth lowpass filter of order 10 is used as an anti-aliasing filter. Note that the high frequency aliasing effects can not be perfectly removed with the anti-aliasing filter. It should be emphasized that the parameter estimator (BUD algorithm combined with covariance resetting technique) which we use is very powerful so that the high frequency components can be identified whether the anti-aliasing filter is used or not. When the anti-aliasing filter is used, estimated damping in the high frequency components are much larger than for low frequency components. In this research one anti-aliasing filter is used since it can remove most high frequency components in the filtered aeroelastic transient time responses, in an adequate manner.

The time step of T_a = 0.000414 sec is used in the iterative time marching structure/aerodynamic integration procedure. For the parameter estimator the sampling time is taken as T_t = 0.00414 sec. The sampling time T_t should satisfy the Shannon's sampling theorem.[55] Therefore, the Nyquist frequency, f_{max}, becomes 120.8 Hz, and the first three aeroelastic modes can be identified using the parameter estimator. The ARMA model consisting of 6 AR and 6 MA coefficients is used to obtain the aeroservoelastic state space description. Covariance matrix resetting interval for the parameter estimator is equal to 12 sampling steps (= 0.05 sec).

Weighting factors [Q] and r_w in the performance index J, given in Eq.(24), are assumed as [I] and 30, respectively. In this study maximum amplitude of the allowable control surface deflection angle is constrained to be less than 4 degrees.

The following computer simulation lasting 10 seconds is made of four important time periods. The first 24 sampling steps constitute the learning period. During this period the control surface is activated randomly to get the initial estimation of the aeroservoelastic system matrices. A maximum amplitude of random control surface deflection angle is limited to 0.8°. At the end of the learning period the controller is engaged and the initial condition for the Riccati matrix is obtained using the Potter's method. In the second period, from 0.1 sec to 2.0 sec, the active flutter suppression system controls the acceleration at the sensor position, caused by the random control surface deflection angle in the learning period. During the third period, from 2.0 sec to 8.0 sec, random variation in the wing angle of attack is introduced. The robustness of the active flutter suppression system with respect to the unknown external disturbance can be verified by examing the time histories of the controller gain vector. This unknown external disturbance is removed during the fourth time period, from 8.0 sec to 10.0 sec. A constant forgetting factor of 0.9999 for the parameter estimator is used throughout the computer simulation procedure.

Time histories of acceleration at the sensor position and the first element of the controller gain vector are shown in Figures 6 and 7. In Figure 6 accelerations at the beginning of the second period are relatively large. It should be mentioned that estimated aeroservoelastic parameters at the beginning of the second period may not be completely converged after 24 time steps. It is evident in Figure 7 that the controller gain vector is robust with respect to the unknown external disturbance. During the third period the controller gain does not change significantly, and when the unknown external disturbance is removed, the controller gain converges again to the constant value. Small variations in controller gain can be observed before and after the third period, these small variations can be eliminated if the longer learning period is used.

Computation times required for the parameter estimator and the on-line control law design procedure are shown in Table 5. The computational delay of 0.002436 sec, for the ARMA model of order 6 on SUN3/280 computer with a floating point accelerator is smaller than the sampling time T_t = 0.00414 sec. Therefore, the digital adaptive optimal controller in this study is a feasible for practical active flutter suppression.

Time Varying Aerodynamic Loads. Time varying subsonic aerodynamics are obtained from the table of subsonic aerodynamic influence coefficient matrices as follows:

1) Subsonic aerodynamic influence coefficient matrices are computed at different Mach numbers and frequencies.
2) At each Mach number tabulated subsonic aerodynamic influence coefficient matrices are fitted with respect to frequency, using Roger's approximation.
3) Continuously fitted aerodynamic influence coefficient matrices obtained in step 2) are fitted with respect to Mach number. Between two adjacent Mach numbers, linear interpolation is used for simplicity.

It is evident from Figure 6 that high frequency components do not affect the performance of the controller. Therefore, the first three structural modes without the anti-aliasing filter will be used in the computer simulations which follow. Aerodynamic influence coefficient matrices are tabulated at 11 frequencies between 0 and 47.75 Hz. Twelve Mach numbers between M_∞ = 0.714 and M_∞ = 0.920 are selected to generate the time varying subsonic aerodynamic loads. The Roger's approximation with 8 aerodynamic lag terms, which are equally spaced between 0 and 47.75 Hz, are used to fit the aerodynamic influence coefficient matrices at each Mach number.

A computer simulation lasting 10 seconds, which is similar to that described in the previous section is shown in Figure 8. The main difference between the previous and the current simulation is in the third period, extending from 2.0 sec to 8.0 sec. During this time period the free stream Mach number is increased gradually from $M_\infty = 0.714$ to $M_\infty = 0.870$, and therefore this period is denoted as the varying parameter time period. During this period, the forgetting factor of 0.9999 is changed to 0.85 to follow the aeroservoelastic system changes. The flight path at $P_\infty = 20.27\ kPa$ together with the flutter and divergence boundaries are presented in Figure 9. All the other input data are identical to the previous computer simulation.

Time histories of acceleration at the sensor position and the first element of the controller gain vector are shown in Figures 10 and 11. In Figure 11 controller gain follows the aeroservoelastic system changes successfully. It should be noted that the robustness of the controller gain in time varying interval depends on the forgetting factor, [Q], and r_w.

Free stream pressure, P_∞, for the second flight path in Figure 9 is assumed to be $27.36\ kPa$. In this case free stream Mach number is increased gradually from $M_\infty = 0.714$ to $M_\infty = 0.916$. Time histories of acceleration at the sensor position and the first element of the controller gain vector are shown in Figures 12 and 13. In Figure 12 the adaptive flutter suppression system fails around time $t = 4.5$ sec. The corresponding Mach number can be obtained from Figure 8, and is approximately equal to $M_\infty = 0.8$. In Figure 9 the second flight path and the divergence boundary intersect around $M_\infty = 0.8$. This is another example of the failure of acceleration based control in stabilizing divergence type instabilities. To suppress both the flutter and divergence instabilities, displacement sensing is used along the second flight path, and results are presented in Figures 14 and 15. It is evident that both instabilities are now suppressed. Similar results have been reported by a number of authors.[56,57]

5.3 Adaptive Transonic Flutter Suppression

Time varying transonic aerodynamics are obtained from tables of steady transonic and unsteady subsonic aerodynamic influence coefficient matrices. In addition to the three steps described in section 5.2.2, the tabulated steady transonic aerodynamic influence coefficient matrices are also fitted linearly between two adjacent input Mach numbers. Thus, the time varying transonic aerodynamic loads can be obtained with relative ease.

Transonic flutter boundaries, transonic divergence boundaries, and two flight paths are shown in Figure 16. Transonic aerodynamic influence coefficient matrices are computed at $M_\infty = 0.714$, 0.850, 0.873, 0.895, and 0.916. The same input data given in section 5.2.2 are used for all other variables.

Aeroservoelastic response with acceleration sensing is shown in Figures 17 and 18. In Figure 18 the controller gain is increased from $t = 2.0$ sec to $t = 6.5$ sec However, from $t = 6.5$ sec to $t = 8.0$ sec the controller gain decreases. In Figure 8, time $t = 6.5$ sec corresponds to $M_\infty = 0.87$, and this Mach number is approximately the center of the transonic bucket in Figure 16. It is evident from Figure 18 that the controller gain is increased when the aircraft penetrates further into the flutter region. On the other hand, if the aircraft leaves the flutter region, then controller gain will decrease.

Aeroservoelastic response with the acceleration sensing along the second flight path is shown in Figures 19 and 20. In Figure 20 the parameter estimator can not follow the aeroelstic system change around $t = 5.5$ sec. Here, time $t = 5.5$ sec corresponds to $M_\infty = 0.83$ in Figure 8. In Figure 16 the second flight path and transonic divergence boundaries intersect each other around $M_\infty = 0.81$. Thus, again it is evident that divergence type instabilities can not be suppressed using the acceleration sensing. The aeroservoelastic response with displacement sensing along the second flight path are presented in Figures 21 and 22. The change of controller gain in Figure 22 is similar to that in Figure 18. Thus, one may conclude that the digital adaptive optimal controller used in this study does follow system changes correctly.

6. Concluding Remarks

A new adaptive optimal control methodology for active flutter suppression is studied for a number of aeroelastic systems. This controller is robust with respect to the unknown external disturbances and can be applied to time varying flight conditions. The same adaptive optimal control algorithm is applied in both subsonic and transonic flight conditions.

It is also shown in this study that the divergence type instability can not be adaptively controlled with the acceleration sensing. Since the controller performance with the acceleration sensing strongly depends on the relative positions of flutter and divergence boundaries, it is important to design the controller and the structure simultaneously in an integrated manner so as to avoid such difficulty.

The ARMA model with a parameter estimation technique is successfully implemented to yield transonic flutter boundaries of the wing structure. This methodology yields flutter boundaries very efficiently in time domain, and thus only a small number of aeroelastic transient time responses are needed in order to obtain reasonable results.

A simple methodology for obtaining three-dimensional unsteady transonic aerodynamics in the time domain is presented. The transonic bucket is successfully reproduced and predicted by this simple approximate method. Since the unsteady computations

are based on unsteady subsonic aerodynamics, transonic aeroelastic responses in the time domain can be obtained at low computational cost. The most time consuming ingredient in this approximate method is the computation of transonic aerodynamic influence coefficient matrices.

Acknowledgment

This research was supported by NASA grant NCC 2-374 and in part by AFOSR Contract F49620-87-K0003. The grant monitor from NASA Dryden Research Center is Dr. K. Gupta.

References

1. Newsom, J.R., "Control Law Synthesis for Active Flutter Suppression Using Optimal Control Theory," *Journal of Guidance and Control*, vol. 2, no. 5, pp. 388-394, Sept.-Oct., 1979.
2. Abel, I. and Newsom, J.R., "Langley Research Center Contributions in Advancing Active Control Technology," NASA-CP-2172, Oct., 1980.
3. Mukhopadhyay, V., Newsom, J.R. and Abel, I., "A Method for Obtaining Reduced-Order Control Laws for High-Order Systems Using Optimization Techniques," NASA-TP-1876, 1981.
4. Guruswamy, G.P., Tu, E.L. and Goorjian, P.M., "Transonic Aeroelasticity of Wings with Active Control Surfaces," AIAA Paper 87-0709, Proceedings of AIAA/ASME/ASCE/AHS 28th Structures, Structural Dynamics and Materials Conference, pp. 16-30, Monterey, CA, April 6-8, 1987.
5. Noll, T.E., "Aeroservoelasticity," AIAA Paper 90-1073, Proceedings of AIAA/ASME/ASCE /AHS/ASC 31st Structures, Structural Dynamics and Materials Conference, pp. 1560-1570, Long Beach, CA, April 2-4, 1990.
6. Perry III, B., Mukhopadhyay, V., Hoadley, S.T., Cole, S.R., Buttrill, C.S., and Houck, J.A., "Digital-Flutter-Suppression-System Investigations for the Active Flexible Wing Wind-Tunnel Model," AIAA Paper 90-1074, Proceedings of AIAA/ASME/ASCE/AHS/ASC 31st Structures, Structural Dynamics and Materials Conference, pp. 1571-1581, Long Beach, CA, April 2-4, 1990.
7. Ominsky, D. and Ide, H., "An Effective Flutter Control Method Using Fast, Time-Accurate CFD Codes," AIAA Paper 89-3468, AIAA Guidance, Navigation and Control Conference, pp. 365-375, Boston, MA, Aug., 1989.
8. Ide, H. and Ominsky, D., "Simulation of Static and Dynamic Aeroelastic Behavior of a Flexible Wing with Multiple Control Surface," AIAA Paper 90-1075, Proceedings of AIAA/ASME /ASCE/AHS/ASC 31st Structures, Structural Dynamics and Materials Conference, pp. 1582-1588, Long Beach, CA, April 2-4, 1990.
9. Borland, C.J., Rizzetta, D.P. and Yoshihara, H., "Numerical Solution of Three-Dimensional Unsteady Transonic Flow over Swept Wings," *AIAA Journal*, vol. 20, no. 3, pp. 340-347, Mar. 1982.
10. Guruswamy, P. and Goorjian, P.M., "Computations and Aeroelastic Applications of Unsteady Transonic Aerodynamics About Wings," *Journal of Aircraft*, vol. 21, no. 1, pp. 37-43, Jan., 1984.
11. Isogai, K. and Suetsugu, K., "Numerical Calculation of Unsteady Transonic Potential Flow over Three-Dimensional Wings with Oscillating Control Surfaces," *AIAA Journal*, vol. 22, no. 4, pp. 478-485, April, 1984.
12. Borland, C.J., "XTRAN3S - Transonic Steady and Unsteady Aerodynamics for Aeroelastic Applications - Vol I : Technical Development Summary," AFWAL-TR-85-3124, Jan. 1986.
13. Shankar, V., Ide, H., Gorski, J., and Osher, S., "A Fast, Time-Accurate, Unsteady Full Potential Scheme," *AIAA Journal*, vol. 25, no. 2, pp. 230-238, Feb. 1987.
14. Batina, J.T., Seidel, D.A., Bland, S.R., and Bennett, R.M., "Unsteady Transonic Flow Calculations for Realistic Aircraft Configuration," AIAA Paper 87-0850, Proceedings of AIAA/ASME /ASCE/AHS 28th Structures, Structural Dynamics and Materials Conference, pp. 344-362, Monterey, CA, April 6-8, 1987.
15. Carson Yates Jr., E., Wynne, E.C., Farmer, M.G. and Desmarais, R.N., "Prediction of Transonic Flutter for a Supercritical Wing by Modified Strip Analysis," *Journal of Aircraft*, vol. 19, no. 11, pp. 999-1004, Nov. 1982.
16. Zwaan, R.J., "Verification of Calculation Methods for Unsteady Airloads in the Prediction of Transonic Flutter," *Journal of Aircraft*, vol. 22, no. 10, pp. 833-839, Oct. 1985.
17. Liu, D.D., Kao, Y.F. and Fung, K.Y., "An Efficient Method for Computing Unsteady Transonic Aerodynamics of Swept Wings with Control Surfaces," *Journal of Aircraft*, vol. 25, no. 1, pp. 25-31, Jan. 1988.
18. Blair, M. and Williams, M.H., "A Time Domain Panel Method for Wings," AIAA Paper 89-1323, Proceedings of AIAA/ASME/ASCE/AHS/ASC 30th Structures, Structural Dynamics and Materials Conference, Mobile, AL, April, 1989.
19. Woods, J.A. and Gilbert, M.G., "Direct Use of Linear Time-Domain Aerodynamics in Aeroservoelastic Analysis: Aerodynamic Model," NASA-CP-3064, April 1990.

20. Kim, S.M., "Adaptive LQ Tracking of MIMO Systems and its Application to Robotic Manipulators with Flexible Joints," Ph.D. thesis, University of California, Los Angeles, 1990.

21. Kim, Y.K., "Adaptive Control of a Robotic Manipulator with a Sliding Flexible Link," Ph.D. thesis, University of California, Los Angeles, 1988.

22. Slater, G.L. and Livneh, R., "A Second Order Adaptive Controller for Wing Flutter Control," AIAA Guidance, Navigation and Control Conference, pp. 679-687, Snowmass, Colorado, Aug., 1985.

23. Bennett, R.M. and Desmarais, R.N., "Curve Fitting of Aeroelastic Transient Response Data with Exponential Functions," NASA-SP-415, pp. 43-58, Oct. 1975.

24. Bousman, W.G. and Winkler, D.J., "Application of the Moving-Block Analysis," AIAA Paper 81-0653, Proceedings of AIAA/ASME/ASCE/AHS 22nd Structures, Structural Dynamics and Materials Conference, pp. 755-763, 1981.

25. Edwards, J.W., Bennett, R.M., Whitlow, W. and Seidel, D.A., "Time-Marching Transonic Flutter Solutions Including Angle-of-Attack Effects," *Journal of Aircraft*, vol. 20, no. 11, pp. 899-906, Nov. 1983.

26. Cunningham, H.J., Batina, J.T., and Bennett, R.M., "Modern Wing Flutter Analysis by Computational Fluid Dynamics Methods," *Journal of Aircraft*, vol. 25, no. 10, pp. 962-968, Oct. 1988.

27. Blair, M., Williams, M.H. and Weisshaar, T.A., "Time Domain Simulations of a Flexible Wing in Subsonic, Compressible Flow," AIAA Paper 90-1153, Proceedings of AIAA/ASME/ASCE /AHS/ASC 31st Structures, Structural Dynamics and Materials Conference, pp. 1395-1404, Long Beach, CA, April 2-4, 1990.

28. Albano, E. and Rodden, W.P., "A Doublet Lattice Method for Calculating Lift Distributions of Oscillating Surfaces in Subsonic Flow," *AIAA Journal*, vol. 7, no. 2, pp. 279-285, Feb. 1969.

29. Lottati, I. and Nissim, E., "Three-Dimensional Oscillatory Piecewise Continuous-Kernel Function Method," *Journal of Aircraft*, vol. 18, no. 5, pp. 346-363, May 1981.

30. Roger, K.L., "Airplane Math Modeling Methods for Active Control Design," AGARD-CP-228, pp. 4-11, Aug. 1977.

31. Vepa, R., "Finite State Modeling of Aeroelastic System," NASA-CR-2779, Feb. 1977.

32. Karpel, M., "Design for Active Flutter Suppression and Gust Alleviation Using State-Space Aeroelastic Modeling," *Journal of Aircraft*, vol. 19, no. 3, pp. 221-227, Mar. 1982.

33. Livne, E., Schmit, L.A. and Friedmann, P., "Design Oriented Structural Analysis for Fiber Composite Wings," UCLA Report UCLA-ENG-88-36, Nov. 1988.

34. Giles, G.L., "Equivalent Plate Analysis of Aircraft Wing Box Structures with General Planform Geometry," *Journal of Aircraft*, vol. 23, no. 11, pp. 859-864, Nov. 1986.

35. Livne, E., Schmit, L.A. and Friedmann, P., "An Integrated Approach to the Optimum Design of Actively Controlled Composite Wings," AIAA Paper 89-1268, Proceedings of AIAA/ASME /ASCE/AHS/ASC 30st Structures, Structural Dynamics and Materials Conference, Mobile, AL, April 1989.

36. Livne, E., Schmit, L.A. and Friedmann, P., "Exploratory Design Studies Using an Integrated Multidisciplinary Synthesis Capability for Actively Controlled Composite Wings," AIAA Paper 90-0953, Proceedings of AIAA/ASME /ASCE/AHS/ASC 31st Structures, Structural Dynamics and Materials Conference, pp. 97-109, Long Beach, CA, April 2-4, 1990.

37. Rodman, L.C., Nixon, D., and Huttsell, L.J., "Modifications to Transonic Flow Codes for Unsteady Perturbations Around an Experimental Mean," *Journal of Aircraft*, vol. 26, no. 8, Aug., 1989.

38. Dowell, E.H. and Ilgamov, M., *Studies in Nonlinear Aeroelasticity*, pp. 243-248, Springer-Verlag, New York, 1988.

39. Robinson, B.A., Batina, J.T., and Yang, H.T.Y., "Aeroelastic Analysis of Wings using the Euler Equations with a Deforming Mesh," AIAA Paper 90-1032, Proceedings of AIAA/ASME/ASCE /AHS/ASC 31st Structures, Structural Dynamics and Materials Conference, pp. 1510-1518, Long Beach, CA, April 2-4, 1990.

40. Åström, K.R. and Wittenmark, B., *Adaptive Control*, Addison Wesley, 1989.

41. Goodwin, G.C. and Sin, K.S., *Adaptive Filtering Prediction and Control*, Prentice-Hall, Inc., Englewood Cliffs, New Jersey, 1984.

42. Wiberg, D.M., "Frequencies of Vibration Estimated by Lattice," *Journal of the Astronautical Sciences*, vol. 33, pp. 48-60, 1985.

43. Jabbari, F. and Gibson, J.S., "Vector-Channel Lattice Filters and Identification of Flexible Structures," *IEEE Trans. on Automatic Control*, vol. 33, no. 5, pp. 448-456, May, 1988.

44. Bryson Jr., A.E., "New Concepts in Control Theory, 1959-1984," *Journal of Guidance, Control, and Dynamics*, vol. 8, no. 4, pp. 417-425, July-Aug., 1985.

45. Maine, R.E. and Iliff, K.M., "Application of Parameter Estimation to Aircraft Stability and Control," NASA-RP-1168, June, 1986.

46. Iliff, K.M., "Parameter Estimation for Flight Vehicles," *Journal of Guidance, Control, and Dynamics*, vol. 12, no. 5, Sept.-Oct., 1989.

47. Ljung, L. and Söderström, T., *Theory and Practice of Recursive Identification*, The MIT Press, Cambridge, Massachusetts, 1987.

48. Jabbari, F. and Gibson, J.S., "Adaptive Identification of a Flexible Structure by Lattice Filters," *Journal of Guidance, Control, and Dynamics*, vol. 12, pp. 548-554, July-Aug., 1989.

49. Tiffany, S.H. and Adams, W.M., "Nonlinear Programming Extensions to Rational Function Approximations of Unsteady Aerodynamics," AIAA Paper 87-0854, Proceedings of AIAA /ASME/ASCE/AHS the 28th Structures, Structural Dynamics and Materials Conference, pp. 406-420, Monterey, CA, April 6-8, 1987.

50. Otnes, R.K. and Enochson, L., *Applied Time Series Analysis*, pp. 137-144, John Wiley & Sons, Inc., 1978.

51. Potter, J.E., "Matrix Quadratic Solutions," *SIAM Journal of Applied Mathematics*, vol. 14, no. 3, pp. 496-501, 1964.

52. Doggett Jr., R.V., Rainey, G.A. and Morgan, H.G., "An Experimental Investigation of Aerodynamic Effects of Airfoil Thickness on Transonic Flutter Characteristics," NASA-TMX-79, Nov., 1959.

53. Guruswamy, G.P., Goorjian, P.M. and Tu, E.L., "Transonic Aeroelasticity of Wings with Tip Stores," *Journal of Aircraft*, vol. 24, no. 10, pp. 688-695, Oct., 1987.

54. Guruswamy, G.P. and Goorjian, P.M., "Unsteady Transonic Aerodynamics and Aeroelastic Calculations at Low-Supersonic Freestreams," *Journal of Aircraft*, vol. 25, no. 10, pp. 955-961, Oct., 1988.

55. Phillips, C.L. and Nagle, H.T., *Digital Control System Analysis and Design*, Prentice-Hall, Inc., Englewood Cliffs, New Jersey, 1984.

56. Griffin, K.E. and Eastep, F.E., "Active Control of Forward-Swept Wings with Divergence and Flutter Aeroelastic Instabilities," *Journal of Aircraft*, pp. 885-891, Oct., 1982.

57. Chipman, R.R., Zislin, A.M., and Waters, C., "Control of Aeroelastic Divergence," *Journal of Aircraft*, vol. 20, no. 12, pp. 1007-1013, Dec., 1983.

Table 1. Material Properties of the Cantilevered Rectangular Wing Model

Material Properties	
Young's Modulus	9847878.6 psi
Poisson's Ratio	0.3528521
Density	0.1116599 lbm/in^3
Translational Spring Constant	1.e9 lbf/in
Rotational Spring Constant	1.e1 $lbf-in/rad$

Table 2. Natural Frequencies (Hz) of the Cantilevered Rectangular Wing

Mode	Experiment•	FEM••	LISSA	LISSA†	LISSA†‡
1-st	14.29	13.21	15.18	15.18	15.20
2-nd	80.41	67.32	78.04	78.04	75.94
3-rd	89.80	76.97	94.46	94.46	96 58
4-th	----	203.6	250.5	250.5	225.8
5-th	----	203.9	266.0	266.0	274 7

• Ref.52; •• Ref.53; † On-line parameter estimation technique is applied to the free vibration of the wing; ‡ Cantilevered wing with control surface.

Table 3. Natural Frequencies (Hz) and Modal Damping Factors of the Cantilevered Rectangular Wing with Control Surface

Mode	Eigen†	Estimated ω_i •	Estimated ζ_i •
1-st	15.20	15.20	.0200
2-nd	75.94	75.94	.0200
3-rd	96.58	96.58	.0200
4-th	225.8	225.8	.0200
5-th	274.7	274.7	.0200

† Obtained from the LISSA code using eigenanalysis; • Calculated using $\omega_i = \frac{\omega_d}{\sqrt{1-\zeta_i^2}}$ and $\zeta_i = \frac{\sigma_i}{\omega_i}$. Here, ω_d and σ_i are estimated from the on-line parameter estimation with the AR model.

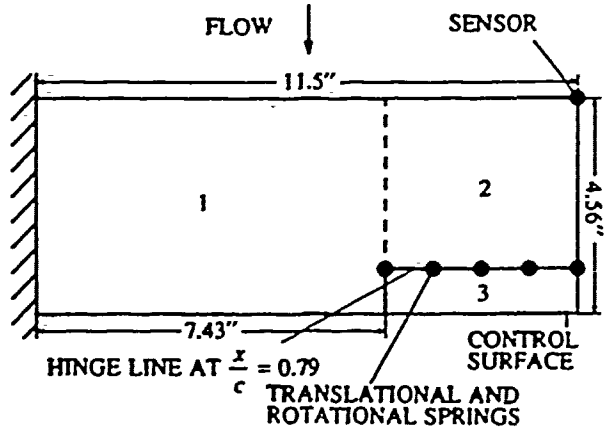

Fig.1 Cantilevered Rectangular Wing with Trailing-Edge Control Surface

Table 4. Flutter Boundaries of the Cantilevered Rectangular Wing at $M_\infty = 0.714$ from the Eigenanalysis, V-g Method, and On-Line Parameter Estimation Technique

A) Flutter Speed and Frequency			
	V-g	Eigen	On-Line
Speed(m/sec)	243.0	243.0	243.0
Frequency(Hz)	35.40	35.40	35.49
B) Frequencies(Hz) at Flutter Condition			
Mode	V-g	Eigen	On-Line
1-st	12.17	13.64	13.66
2-nd	35.40	35.40	35.49
3-rd	95.99	95.98	95.96
4-th	243.2	243.2	243.7
5-th	266.3	266.3	266.2
C) Aerodynamic Damping(σ) at Flutter Condition			
Mode	V-g	Eigen	On-Line
1-st	-----	-64.88	-64.80
2-nd	-----	-.2123e-5	-.1520
3-rd	-----	-7.528	-7.468
4-th	-----	-21.39	-20.01
5-th	-----	-3.158	-2.918

Table 5. Execution Time (seconds) for the On-Line Computations on SUN3/280 Computer with Floating Point Accelerator

Order of the ARMA Model	Iterative Riccati Solver†	BUD Algorithm†	Computational Delay
4	.000773	.000522	.001295
6	.001542	.000894	.002436
8	.002517	.001382	.003899
10	.003681	.002004	.005685
12	.005221	.002710	.007931

† Computed from 10000 iterations by the use of FUNCTION DTIME in SUN FORTRAN77 run-time library routines

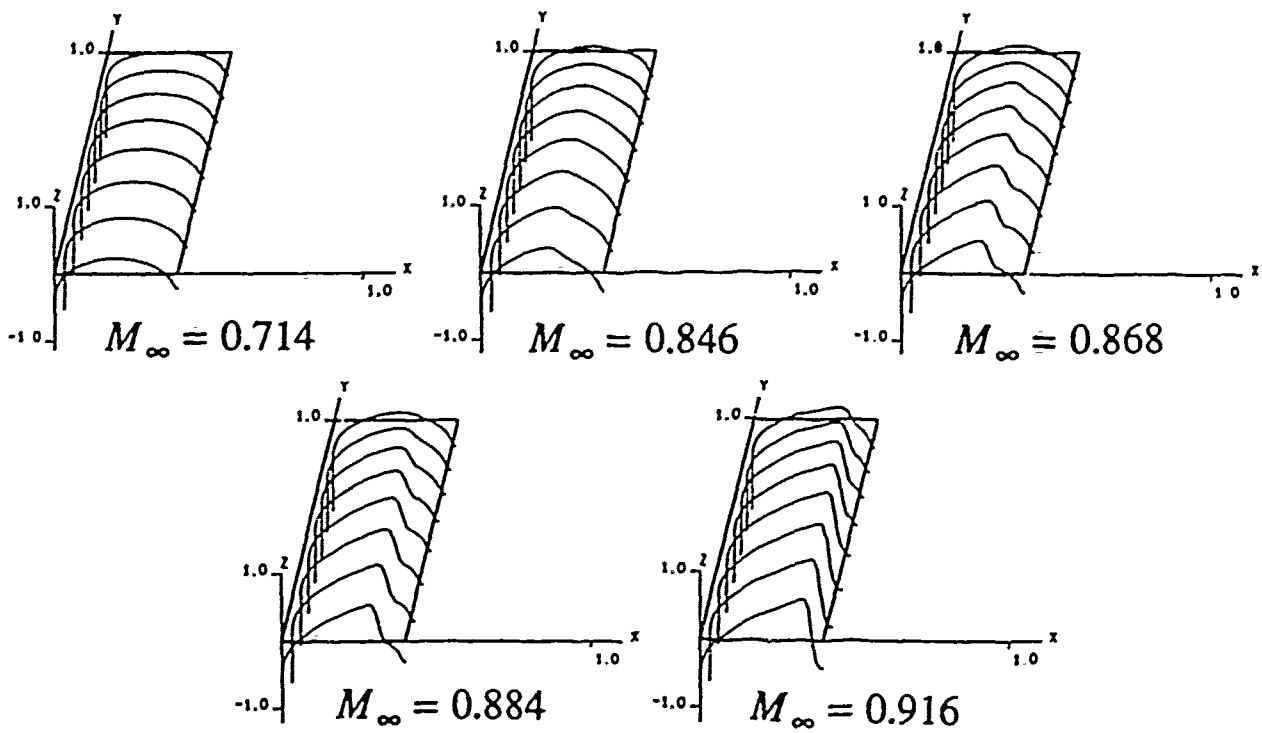

Fig.2 Steady State Pressure Distribution on the Wing Surface

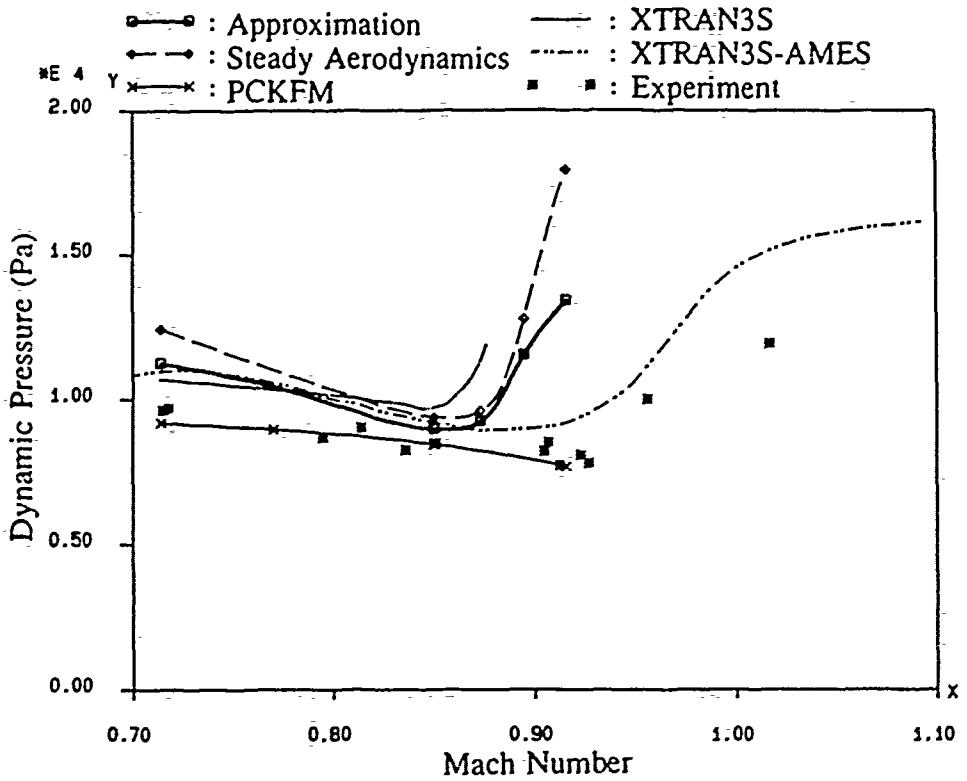

Fig.3 Comparisons of Flutter Boundaries, M_∞ vs. q_D

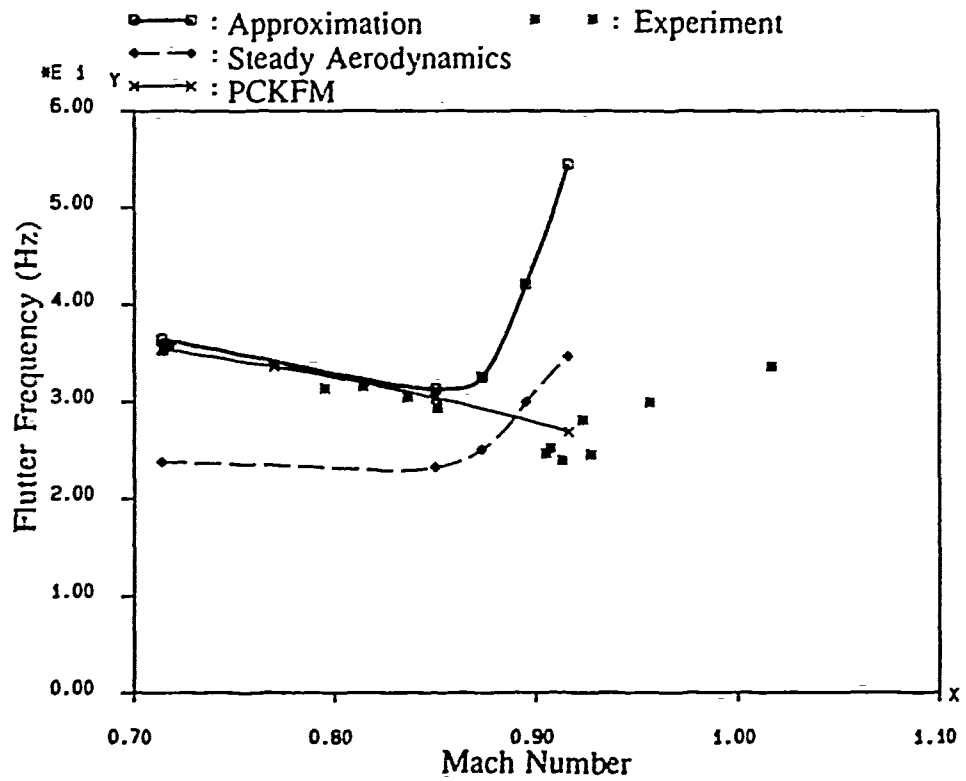

Fig.4 Comparisons of Flutter Boundaries, M_∞ vs. ω_F

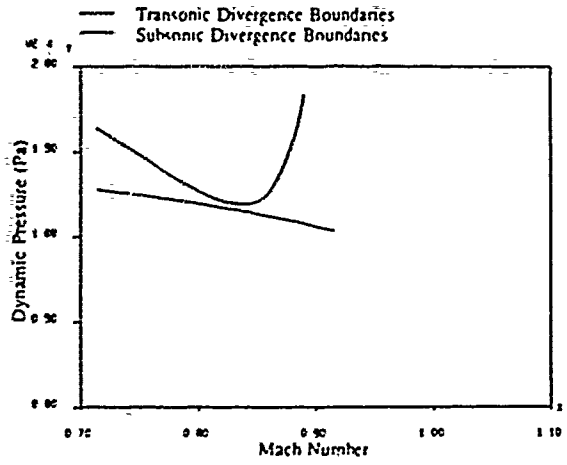

Fig.5 Comparisons of Subsonic and Transonic Divergence Boundaries

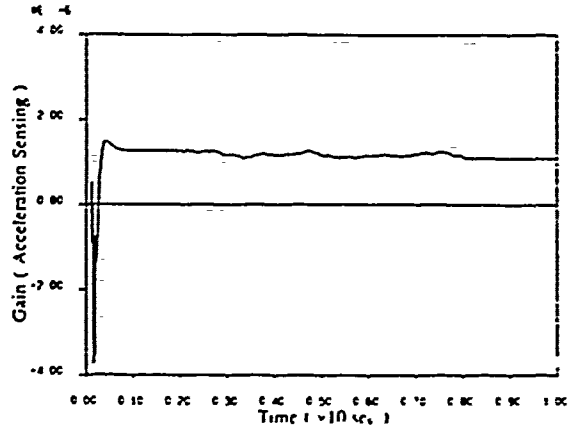

Fig.7 Controller Gain for the Random External Loads

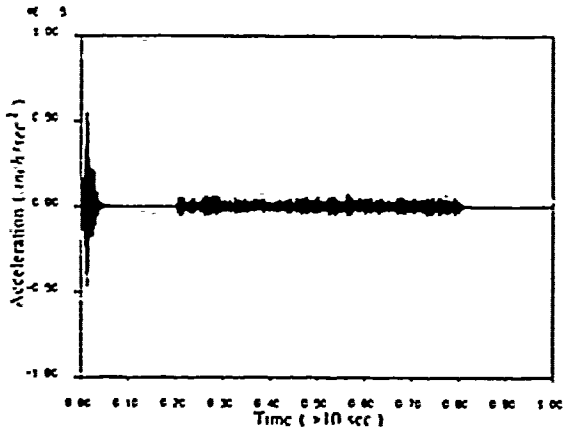

Fig.6 Aeroservoelastic Response under Random External Loads

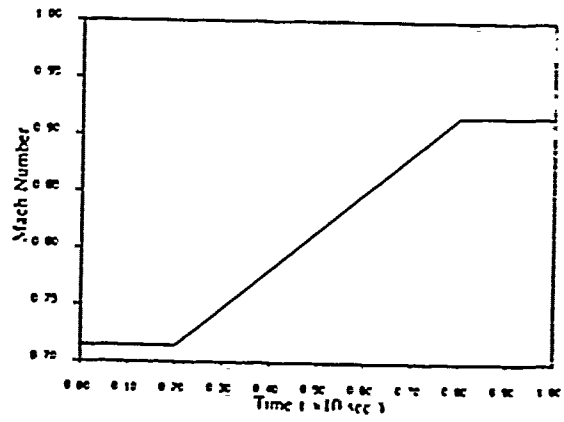

Fig.8 Computer Simulation Scenario

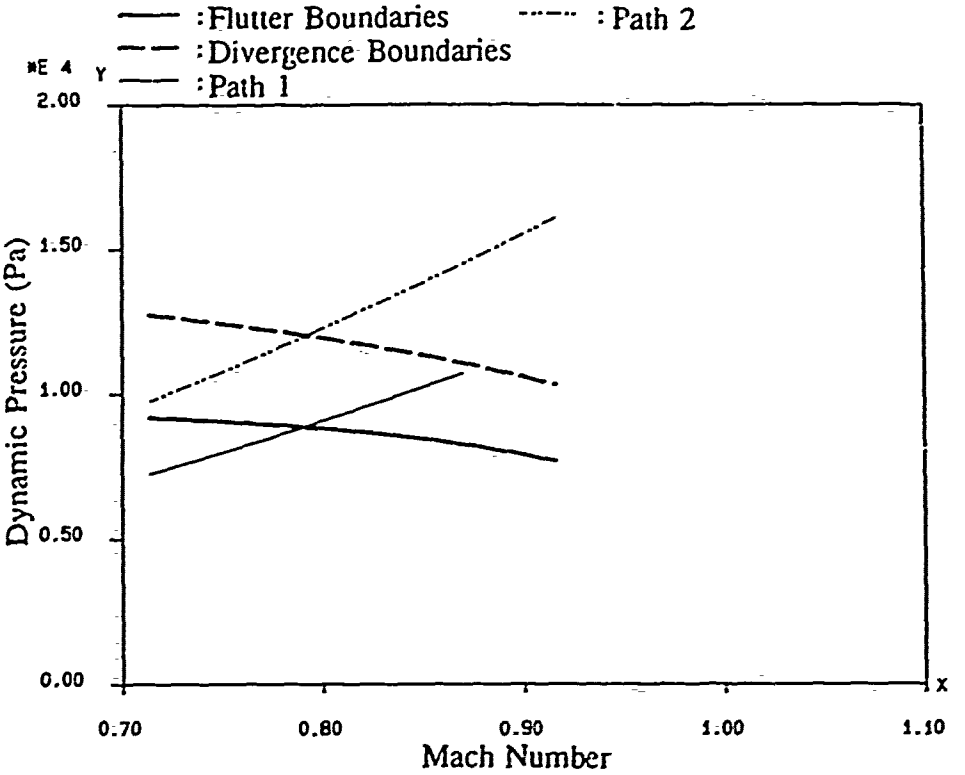

Fig.9 Computer Simulation Paths for Subsonic Aeroservoelasticity

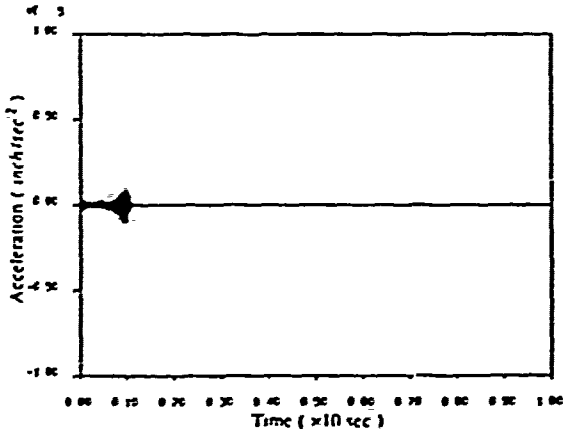

Fig.10 Subsonic Aeroservoelastic Response along Path 1

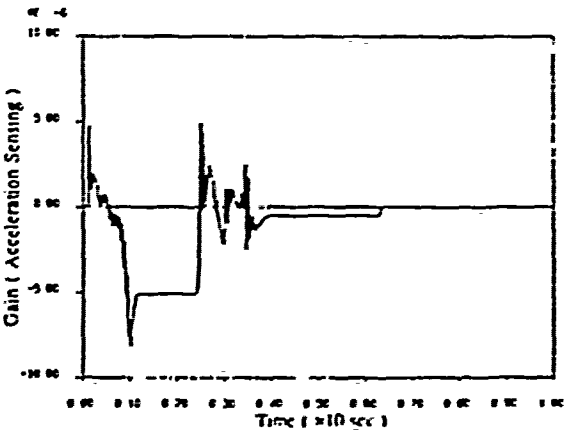

Fig.11 Controller Gain for Subsonic Aeroservoelasticity along Path 1

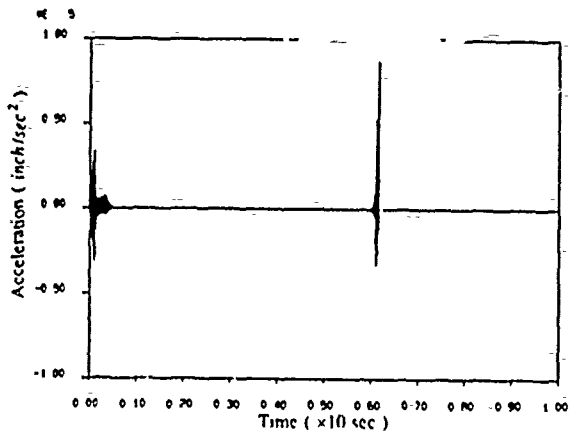

Fig.12 Subsonic Aeroservoelastic Response along Path 2

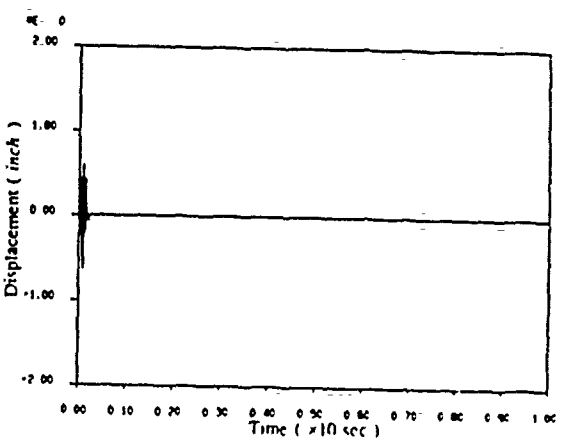

Fig.14 Subsonic Aeroservoelastic Response along Path 2

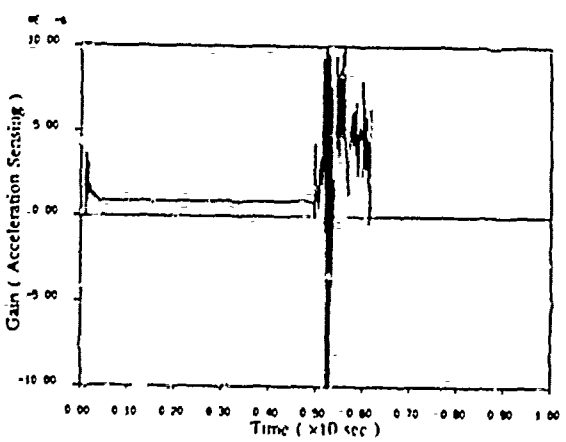

Fig.13 Controller Gain for Subsonic Aeroservoelasticity along Path 2

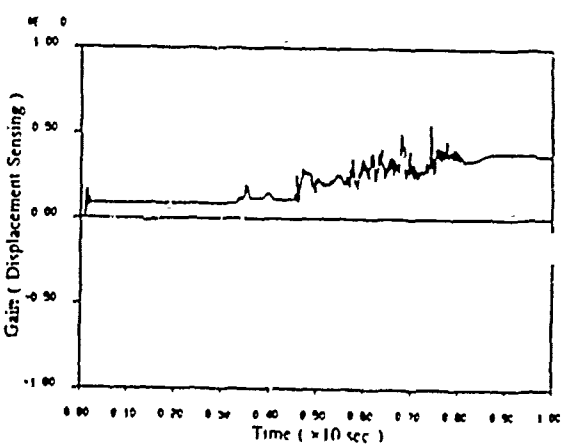

Fig.15 Controller Gain for Subsonic Aeroservoelasticity along Path 2

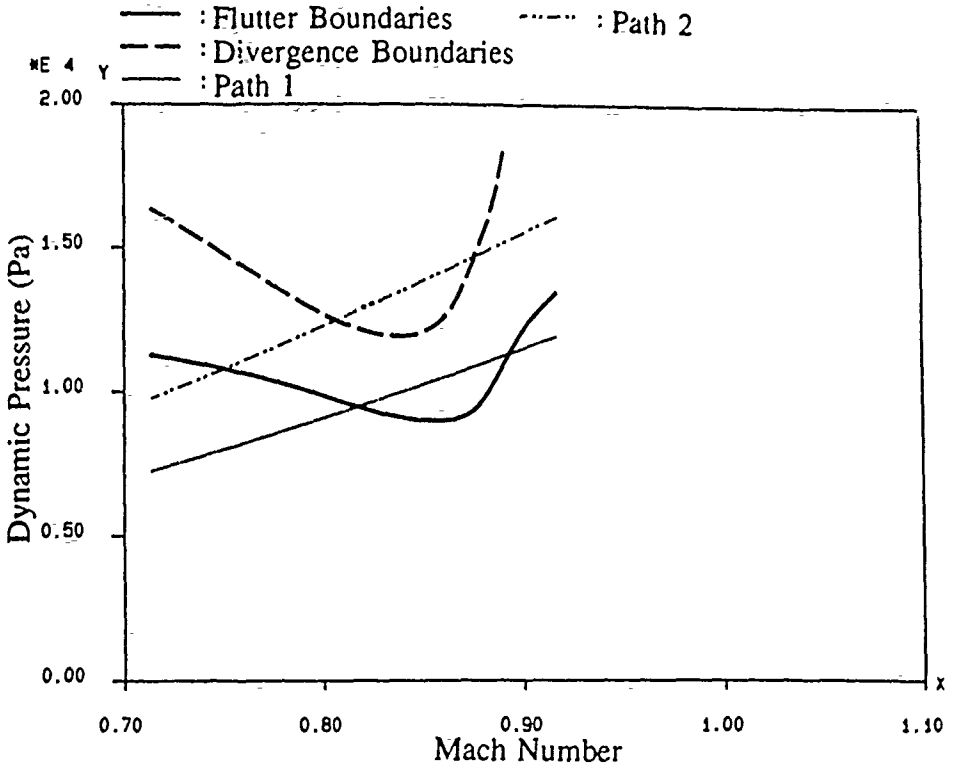

Fig.16 Computer Simulation Paths for Transonic Acroservoelasticity

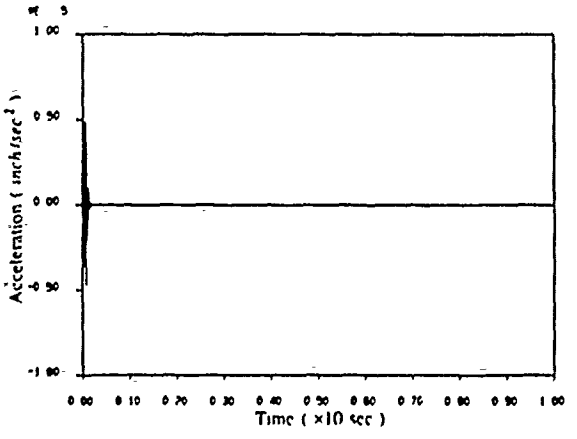

Fig.17 Transonic Aeroservoelastic Response along Path 1

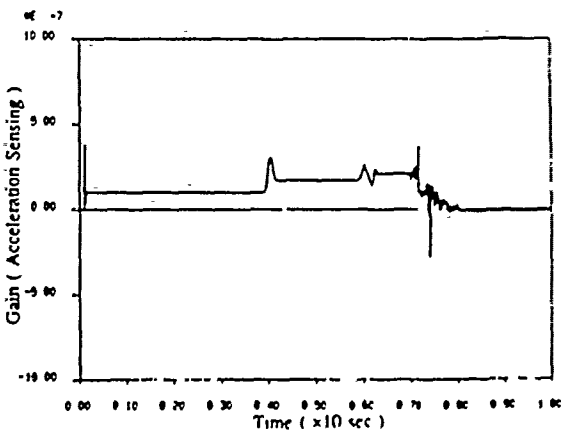

Fig.18 Controller Gain for Transonic Aeroservoelasticity along Path 1

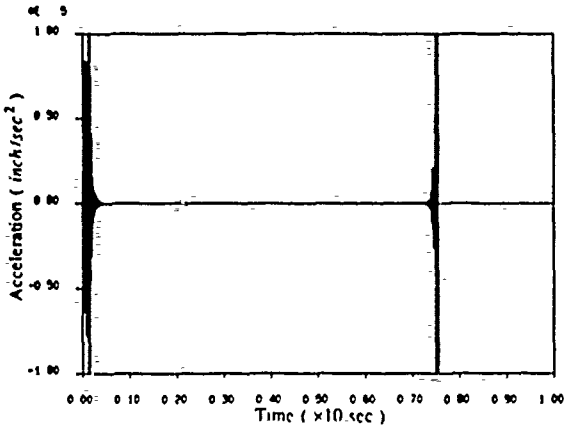

Fig.19 Transonic Aeroservoelastic Response along Path 2

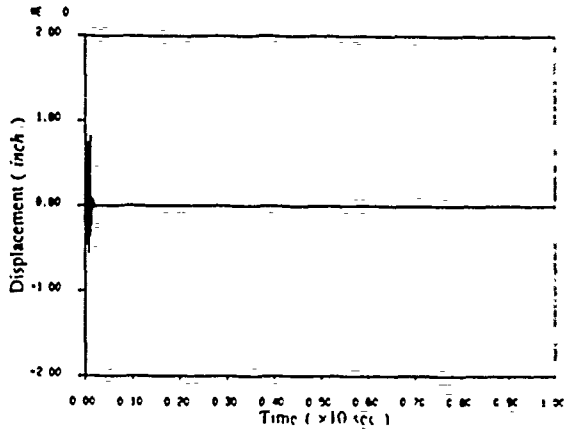

Fig.21 Transonic Aeroservoelastic Response along Path 2

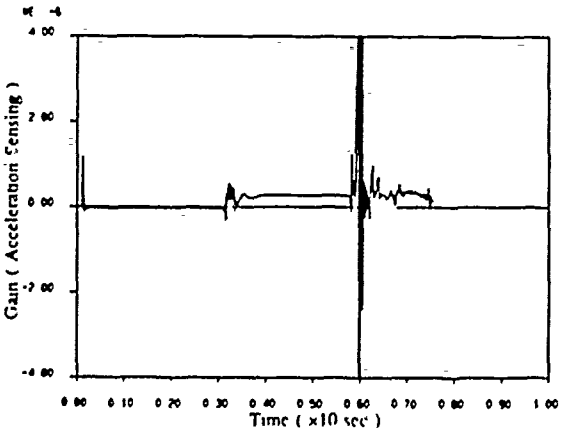

Fig.20 Controller Gain for Transonic Aeroservoelasticity along Path 2

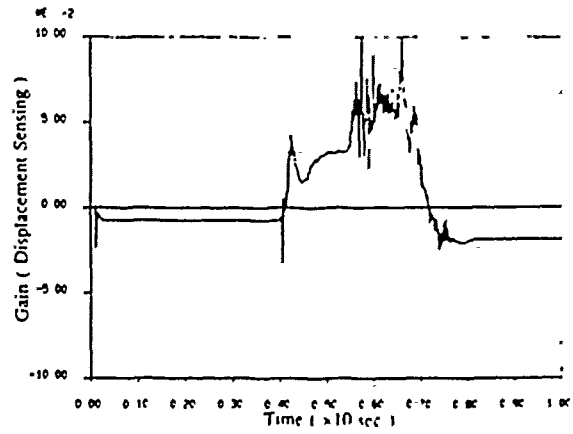

Fig.22 Controller Gain for Transonic Aeroservoelasticity along Path 2